Dissertation
submitted to the
Combined Faculties of the Natural Sciences and Mathematics
of the Ruperto-Carola-University of Heidelberg, Germany
for the degree of
Doctor of Natural Sciences

Put forward by
Andreas Hohenegger
Born in Munich
Oral examination: 8 February 2010

Finite Density Aspects of Leptogenesis

Referees: Prof. Dr. Manfred Lindner
Prof. Dr. Manfred Salmhofer

...Zuerst entwickeln sich majestätisch die Variationen der Geschwindigkeiten, dann setzen von der einen Seite die Zustands-Gleichungen, von der anderen die Gleichungen der Centralbewegung ein, immer höher wogt das Chaos der Formeln; plötzlich ertönen die vier Worte: "Put $n = 5$." Der böse Dämon V verschwindet, wie in der Musik eine wilde, bisher alles unterwühlende Figur der Bässe plötzlich verstummt; wie mit einem Zauberschlage ordnet sich, was früher unbezwingbar schien...
(Ludwig Boltzmann, 1887)

Aspekte der Leptogenese bei endlichen Dichten

Leptogenese ist ein Modell zur dynamischen Erklärung der Materie-Antimaterie Asymmetrie. Dieser Prozess findet im frühen Universum bei hohen Temperaturen statt und eine Abweichung vom Gleichgewicht ist fundamentale Voraussetzung für die Erzeugung der Asymmetrie. Die Beschreibung dieses Prozesses basiert auf klassischen Boltzmann Gleichungen (BGn). Diese wurden durch die Verwendung thermaler Propagatoren verfeinert. In Anbetracht der grundlegenden Beschränkungen dieser Gleichungen erscheint es wünschenswert einen systematischen Ansatz zu entwickeln der auf Nicht-Gleichgewichts QFT beruht. In dieser Arbeit werden modifizierte BGn verwendet die aus ersten Prinzipien innerhalb des Kadanoff–Baym Formalismus hergeleitet werden. Dies wird für ein einfaches Toy-Modell durchgeführt welches ausreichend komplex ist um populäre Szenarien wie das der thermalen Leptogenese in Analogie untersuchen zu können. Dieser Ansatz legt die Struktur der korrigierten BGn offen und führt zu einem neuen Ergebnis für die thermalen Beiträge zum CP-verletzenden Parameter, sodass die gängige Form überdacht werden muss. Es stellt sich heraus, dass die verschiedenen Ansätze in Einklang gebracht werden können. Die neuen Ergebnisse sagen eine Verstärkung der Asymmetrie vorher. Die Grösse der Korrekturen innerhalb des Toy-Modells wird durch numerische Lösung der vollen BGn bestimmt.

Finite Density Aspects of Leptogenesis

Leptogenesis is a model for the dynamical generation of the matter-antimatter asymmetry. This process takes place in the early universe at very high temperatures and a deviation from equilibrium is a fundamental requirement for the formation of the asymmetry. The equations used for its description originate from classical Boltzmann equations (BEs), which were refined using thermal propagators. In view of the basic restrictions of BEs, it is desirable to develop a systematic approach which uses non-equilibrium QFT as starting point. In this thesis modified BEs are used which are derived from first principles in the Kadanoff–Baym formalism. This is done for a simple toy model which is sufficiently intricate to study popular scenarios such as thermal leptogenesis in analogy to the phenomenological theory. This approach uncovers the structure of the corrected BEs and leads to a new result for the form of the thermal contributions to the CP-violating parameter, so that the established one must be reconsidered. It turns out that the different approaches can be reconciled. The new form predicts an enhancement of the asymmetry. The quantitative implications of the medium corrections within the toy model are studied numerically in terms of the full BEs.

Contents

Chapter 1

Introduction

1.1 Overview

While the standard model of particle physics combined with the big-bang theory for the formation of the universe predicts an approximate symmetry between matter and antimatter, the latter is almost completely absent on earth and in the solar system. The obvious conclusion that the universe is baryonically asymmetric is confirmed by experimental data on the abundances of the light elements predicted by primordial nucleosynthesis [5–7] and precise measurements of the cosmic microwave background anisotropies [8, 9] by the WMAP satellite experiment. As it is somewhat unsatisfactory and insufficient to assume that this asymmetry comes as an initial condition of the universe, many possible mechanisms have been proposed to generate the asymmetry in a dynamic way. It has been shown that this possibility exists if three conditions are met. Two of these directly address extensions of the standard model and since 1967, when Sakharov found these requirements [10], numerous possible scenarios have been invented which can rather satisfactorily fulfill them. Some of these became disfavoured or were ruled out later.

A viable class of models which has attracted a lot of attention in recent years is known as leptogenesis [11]. Here the asymmetry is initially produced in the lepton sector and (partially) converted to the baryon sector subsequently [12, 13]. The success of this scenario is partly due to the fact that the required extension of the standard model, through the implementation of Majorana mass terms, is relatively moderate and tightly linked to a favored mechanism for the generation of the neutrino masses. Another advantage is that a non-vanishing $B - L$ asymmetry is produced which survives the conversion process to baryons, in contrast to a B and L asymmetry with $B - L = 0$. Many aspects of leptogenesis have been extensively investigated. In particular, it has been studied in the context of supersymmetry and it has been shown that the CP-violating parameter and the efficiency of leptogenesis are affected by the flavor structure of the neutrino Yukawa couplings [14–20]. It has also been shown that the creation of the asymmetry may be resonantly enhanced if the Majorana neutrino masses are quasi-degenerate [21–24].

Comparatively few progress has been made towards a better understanding of the underlying kinetic equations which are needed to implement the third Sakharov condition, namely the necessity of a deviation from thermal equilibrium. In most of the models it is realized with help of a standard out-of-equilibrium decay scenario. This scenario is based on the fact that, because of the rapid expansion of the universe, a relatively weakly interacting massive particle species (heavy Majorana neutrinos in the case of leptogenesis) may fail to follow its equilibrium abundance while it decays.

This process takes place at high temperatures which approximately correspond to the mass of the heavy Majorana neutrinos, in the simplest case of thermal leptogenesis above $T \gtrsim 10^9\,\mathrm{GeV}$. In practice, the detailed time evolution of the abundances of the different species in this scenario is investigated by solving rate equations, as in many cases in cosmology. These phenomenological equations are usually constructed from generalized *Boltzmann equations* [25–29] in a *bottom-up approach*. This means that the standard form of the Boltzmann equation, with amplitudes computed from perturbation theory in the usual in-out formalism in vacuum, is used as starting point. In the case of leptogenesis and baryogenesis one then needs to correct these by subtracting real intermediate states by hand in order to obtain consistent equations.

The Boltzmann equation, as a central equation of kinetic theory, describes the time evolution of the one-particle distribution function (i.e. the density distribution in the one-particle phase space). The equations, obtained in this bottom-up approach, are then integrated yielding simple differential equations for the abundances. From this derivation of the rate equations it is clear that they describe non-equilibrium physics only in the sense of chemical non-equilibrium and that the quantum effects described by the quantum statistical terms in the Boltzmann equation are not accounted for. But even when the (full) Boltzmann equations are solved directly one is faced with the fundamental problem that these are classical equations from the point of view of non-equilibrium quantum field theory, as their subject are one-particle distribution functions, which are classical objects from this viewpoint. The notion of particles is manifest in the definition of the distribution function and in the explicit (or implicit, in the classical form) kinematics of particle collisions, which was the Boltzmann equation's inventors great achievement. The particle concept, however, is not necessarily applicable in the case of early universe cosmology. Being a phenomenological equation in the beginning, today derivations from basic principles are known, in some cases at least. In other cases, such as the case where quantum statistical factors are included, the derivation is subject to active research [30, 31]. The assumption of low density (long mean free path-length as compared to the intrinsic interaction length) and absence of initial correlations (between the colliding particles) represent integral parts in established approaches, in this form or another. However, the early universe at the energy scales of leptogenesis consists of a dense and hot plasma in which case these assumptions may be wrong. In order to find out how reliable the generalized Boltzmann kinetic equations are in this case, a thorough quantum field theoretic description in a *top-down approach* is desirable.

A suitable first-principle approach can be found in the Schwinger–Keldysh/Kadanoff–Baym formalism. *Kadanoff-Baym equations* [32] may be seen as quantum field theoretical analogues of Boltzmann equations. They can be used, in principle, to overcome the indicated problems as they describe the evolution of spectral functions and statistical propagators which are quantum field theoretical objects. Existing numerical results for simple systems far from thermal equilibrium indicate that Kadanoff–Baym and Boltzmann equations may lead to different results [33–38]. With respect to leptogenesis, implications of this approach have been studied at different levels of approximation and lead to qualitatively new results [39, 40]. However, issues related to the rapid expansion of the universe, which drives the required deviation from thermal equilibrium, have not been addressed there. On the other hand, modifications of the Kadanoff–Baym formalism in curved space-time within simple models have been considered in [41–44] but models with CP-violation have not been studied in this context. Some aspects of leptogenesis have been investigated within this framework at different levels of approximation in *Minkowski* space [23, 24, 39, 40, 45]. As the expansion of the universe is the driving force for the deviation from equilibrium, it is desirable to develop a consistent description of leptogenesis in this top-down approach.

Although Boltzmann equations are meant to describe systems of dilute classical gasses and cannot take into account certain effects for principle reasons, they have been applied successfully to a wide variety of physical problems (in modified or reduced form mainly). In the case of cosmology spatial homogeneity and isotropy in momentum space can be exploited to reduce the number of variables and integrals in order to make it accessible to numerical methods. This seems significantly harder (to the required accuracy) in the case of Kadanoff-Baym equations. The approach of the present work is therefore to use *quantum corrected Boltzmann equations* which include contributions accounting for the finite density of the background plasma. These are derived (in a mathematical non-rigorous way) using the Kadanoff–Baym formalism as starting point. In this approach the structure of the Boltzmann equations itself can be derived by applying a number of systematic approximations. In principle this allows to check the applicability of the particle picture associated with the definition of the distribution functions. Since it is a rather ambitious goal to study a phenomenological theory in the top-down approach, we focus here on a simple scalar Yukawa model which involves only two real and one complex scalar fields. These mimic the heavy right-handed Majorana neutrinos and leptons respectively. While we use it here to describe leptogenesis it can also be matched with other models for baryogenesis, in which the asymmetry is produced in the out-of-equilibrium decay of some heavy species in which the CP-violation enters due to the interference of tree-level amplitudes and vertex and self-energy loop contributions. Despite the simplicity of this toy model its inspection helps to clarify the structure of the quantum corrected Boltzmann equations in presence of the quantum statistical terms and of the medium corrections to the CP-violating parameter. These results have been published recently in the research papers [3, 4]. Here, we focus on the case of hierarchical Majorana neutrino masses. While the usefulness of the particle picture is doubtful in different cases (and hence the usage of Boltzmann-like equations) the top-down approach then leads to quantum corrected Boltzmann equations which give immediately consistent results in equilibrium and include medium contributions.

Previous attempts to obtain such results for leptogenesis where mainly based on the bottom-up approach supplemented by finite-temperature field theory [46, 47]. In this ansatz the Boltzmann equations are employed in their usual form while the (CP-violating) transition amplitudes are computed based on thermal propagators. This means that the fields propagating in the loops, contributing to the amplitudes, feel the presence of the background plasma. Putting both ingredients together one obtains corrected Boltzmann equations which include additional terms involving medium contributions in the transition probabilities but the quantum statistical terms cannot be included consistently. Also other thermal effects, such as thermal masses and renormalized couplings have been taken into account in this approach. It turns out that the corrected Boltzmann equations obtained in this way are in contradiction with the ones derived in the top-down approach. By analogy, this result applies to the equations for the phenomenological scenario as well. We will show that the discrepancy is due to an ambiguity in the real-time-formalism of thermal quantum field theory and that it can be reconciled with the findings based on the top-down approach if one uses so-called causal products for the computation of the CP-violating amplitudes. This is an important result, especially, because the established formulas give a zero contribution (in the ultra-relativistic limit). This is qualitatively different for the new result, which leads to an enhancement of the asymmetry in the decay of the Majorana neutrinos in phenomenological scenarios.

In order to motivate our efforts we have a glimpse on the most simple scenario of thermal leptogenesis in the case of hierarchical neutrino masses in this chapter. To set up the model and to see the

similarity to the scenario of thermal leptogenesis we investigate the toy model in the conventional bottom-up approach in chapter 2. The top-down derivation of the quantum corrected Boltzmann equations within this model is presented in chapter 3. In chapter 4 we reconsider the bottom-up derivation in the framework of thermal quantum field theory in order to settle the apparent conflict. A numerical method for the solution of the Boltzmann equations is then outlined followed by the presentation of the results within the toy model in chapter 5. We conclude in chapter 6.

Throughout this work we use natural units where $\hbar = c = k = 1$ which implies that [energy] = [mass] = [temperature] = [length]$^{-1}$ = [time]$^{-1}$.

In this system we have $1\,\text{GeV} \simeq (2.0 \times 10^{-14}\,\text{cm})^{-1} \simeq (6.6 \times 10^{-25}\,\text{s})^{-1} \simeq 1.2 \times 10^{13}\,\text{K}$, and $G = m_{pl}^{-2}$, where G is Newtons constant and $m_{pl} \simeq 1.2 \times 10^{19}\,\text{GeV}$ denotes the Planck mass.

1.2 General considerations

Evidence for the baryon asymmetry

Experimental evidence for the existence of the baryon asymmetry comes from various experiments. Cosmic rays exhibit an admixture of anti-protons at the level of only $\sim 10^{-4}$ (recent data from the PAMELA experiment are shown in fig. 1.1). But even this small fraction can be explained

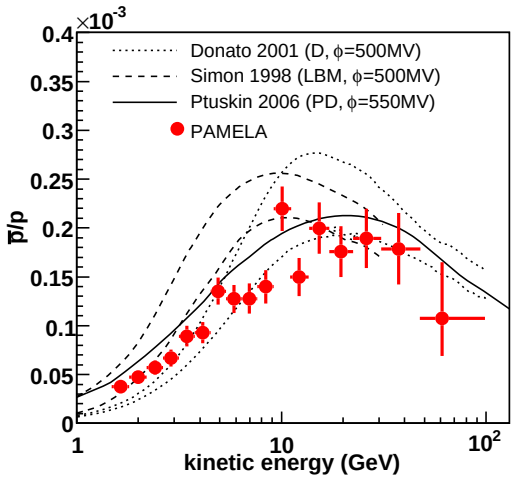

Figure 1.1: PAMELA measurement of the antiproton-to-proton flux ratio [48]. The solid lines represent various theoretical models for purely secondary production. The data is consistent with other contemporary measurements.

by secondary processes such as $p+p \rightarrow 3p+\overline{p}$, induced by high-energetic particles colliding with interstellar matter. Also from the absence of annihilation products (i.e. γ-radiation) it can be concluded that our galaxy contains almost no (baryonic) antimatter and a possible separation on large scales can be excluded on theoretical grounds [49]. A rough value for the baryon to photon ratio can therefore be obtained by comparison of the abundance of (luminous) baryonic matter to the number density of photons in the cosmic microwave background (CMB) $n_B/n_\gamma \sim 10^{-10}$.

Primordial nucleosynthesis or big-bang nucleosynthesis (BBN) [6, 7] which predicts, rather successfully, the abundance of the light elements D, ^{3}He, ^{4}He and ^{7}Li takes place at $T \simeq 0.1\,\mathrm{MeV}$. The predicted relative abundances of the generated elements depend crucially on the baryon to photon ratio and the comparison with experimental measurements can therefore be used to estimate the baryon to photon ratio.

The CMB, which is Planck distributed to a very good approximation, exhibits small deviations from perfect isotropy at a level of $\sim 10^{-5}$. These anisotropies reflect acoustic oscillations in the primordial plasma at the time of photon decoupling at $T \simeq 0.1\,\mathrm{eV}$. They have been measured with high accuracy by the WMAP satellite experiment. The predictions for the angular power spectrum of the CMB do also depend on the baryon abundance. The comparison of theory and experiment leads currently to the best values for the baryon to photon ratio [50]:

$$\eta_B = \frac{n_B - n_{\bar{B}}}{n_\gamma} \simeq \frac{n_B}{n_\gamma} = 6.116^{+0.197}_{-0.249} \cdot 10^{-10}\,. \tag{1.1}$$

It is compatible with the BBN value. The significance of this number is owed to the fact that,

once the process of its generation is finished, it stays approximately constant during the further evolution of the universe.

At temperatures $T \lesssim 1\,\text{GeV}$ processes of the kind $p + \bar{p} \leftrightarrow \gamma + \gamma$ proceed only in the forward direction, because, on average, the photons lack the energy to produce the massive nucleons. At this temperature the baryon to photon ratio would have dropped to a value of $\eta_B \sim 10^{-18}$, if the baryons would still have been in thermal equilibrium at this time. Therefore, a baryon asymmetry must be present at temperatures well above 1 GeV so that the annihilation remains incomplete. The goal of all baryogenesis and leptogenesis theories is to explain the observed value of the baryon asymmetry of the universe eqn. (1.1) in a dynamic way.

The Sakharov conditions

Sakharov realized that a baryon asymmetry could be produced dynamically in the evolution of the universe if three conditions are satisfied:[1]

- *Baryon number violation*
- *C and CP-violation*
- *Departure from thermal equilibrium* [of the relevant B, C and CP-violating processes]

It is well known that the standard model, in principle, includes all ingredients to satisfy the first two conditions. Firstly, there are ('t Hooft 1976) non-perturbative properties that can give rise to so called *sphaleron processes* which violate $B+L$ (but conserve $B-L$) [13, 52]. These processes are suppressed today by the Boltzmann factor

$$\Gamma_{\text{sphaleron}}(T) \propto T^{-3} \exp\left(-\frac{E_{\text{sphaleron}}(T)}{T}\right) , \tag{1.2}$$

but at sufficiently high temperatures (above the electroweak phase transition $100\,\text{GeV} \lesssim T \lesssim 10^{12}\,\text{GeV}$) the sphalerons can be in thermal equilibrium.

Secondly, in the standard model C is maximally broken by the weak interaction. CP-violation has first been observed in 1964 in the $K^0 - \bar{K}^0$ system. It also shows up in the more recent $B^0 - \bar{B}^0$ experiments at BaBaR and BELLE.

This thesis is concerned mainly with the third Sakharov condition. It is easy to see that it is a direct consequence of CPT invariance [53]. Writing θ for the CPT conjugation operator and ρ for the density matrix $\rho(t) = e^{-\beta(t)H(t)}$ with Hamiltonian H, then

$$\begin{aligned} \langle B \rangle_T &= \text{Tr}(e^{-\beta H} B) = \text{Tr}(\theta^{-1}\theta e^{-\beta H} B) \\ &= \text{Tr}(\theta e^{-\beta H} B \theta^{-1}) = \text{Tr}(\theta e^{-\beta H}\theta^{-1}\theta B \theta^{-1}) = \text{Tr}(e^{-\beta H}(-B)) \\ &= -\langle B \rangle_T \ . \end{aligned} \tag{1.3}$$

Here we exploited the fact that θ and H commute, when CPT is preserved and that CP transfers baryons into anti-baryons.

In the standard model the asymmetry (leading to the effects observed in the K and B systems) is generated by the non-zero Jarlskog invariant which depends on the CP-violating complex phase in the CKM-matrix. This CP asymmetry is unfortunately much too small in order to account for

[1] See [51]; Independently Wadim Kuzmin (1970).

the observed baryon asymmetry. Many successful scenarios for baryogenesis share the property that the asymmetry is generated by the CP-violating out-of-equilibrium decay of some speculative heavy state. Thereby the CP-violation is typically generated by the one-loop diagrams contributing to this process.

Moreover, typical reaction rates for annihilation or decay are at least of order $\alpha^2 M$ (α is the coupling constant). Particles with a mass $M \gtrsim 1\,\text{TeV}$ which are charged under the standard model gauge group have rates which are much larger than the expansion rate at temperatures of order of their mass. Any model which intends to generate η_B at this temperature should therefore involve particles without standard model gauge interactions (there may be exceptions to this rule where the deviation from equilibrium is realized in a different way). In order to satisfy this constraint one usually reverts to extended theories. However, it is not difficult to find viable models which can successfully describe baryogenesis. This statement is supported by the existence of a large number of different phenomenological scenarios. Many of these models are very involved. As we are interested mainly in the proper description of the out-of-equilibrium scenario we seek a model which is as simple as possible but sufficiently complex to describe the the phenomenon of baryogenesis properly. The toy model which we employ for this purpose is a scalar Yukawa theory which works for the description of the generation of the asymmetry if one formally assigns baryon or lepton number to the fields. As the model does not include any physical particles which could be matched directly with observations in laboratories, the motivation for its use will be mainly by analogy to existing scenarios. Therefore, before we focus on this toy model, we will now briefly discuss the scenario of *thermal leptogenesis* which can serve as a prototype for the kind of scenario described above. In this case only a minimal extension of the standard model is required, which at the same time addresses the issue of neutrino masses in an elegant way. The crucial properties of this model will be found again in the toy model later.

1.3 Thermal leptogenesis

In this section we discuss the basic scenario of thermal leptogenesis [11, 15, 54] with hierarchical heavy Majorana neutrino masses and its prerequisites in some more detail. Because of its simplicity it can serve as a prototype for a model which can be matched with the toy model to be discussed later. The basic idea of leptogenesis is that first a lepton asymmetry is created which is subsequently converted (partially) into a baryon asymmetry. This conversion between lepton and baryon number is accomplished by sphaleron processes which are assumed to be in equilibrium above the electroweak phase transition. It is important that effectively leptogenesis creates a $B-L$ asymmetry which cannot be washed out by sphalerons.

Majorana neutrinos and the see-saw mechanism

In order to explain the phenomenon of neutrino oscillations one needs to add neutrino mass terms to the standard model (SM). Within this model the masses of the charged quarks and leptons arise from Yukawa couplings of the form

$$\mathscr{L}_Y = -h\phi\overline{\ell_L}\ell_R + h.c.\,, \tag{1.4}$$

where ℓ_L, ℓ_R and ϕ denote the left-handed lepton, right-handed lepton and Higgs fields respectively. All charged fermion masses, generated in this way, are within a range of roughly two orders of magnitude, but the masses of the neutrinos are smaller by several orders of magnitude. Stated differently, the coupling constant for such a Yukawa term would be $h \simeq m_f/\langle\phi\rangle_0 \backsim 10^{-14}$ for

a neutrino of mass $m_\nu \simeq 0.01\,\text{eV}$, whereas the Yukawa coupling for the electron is $h_e \backsim 10^{-6}$. Of course, it would seem natural to assume that these are of approximately the same order. In principle one could account for neutrino masses by simply adding such Dirac mass terms for the neutrinos (including adequate right-handed singlet fields) to the standard model lagrangian [55]. However this would leave the puzzle of the existence of different mass hierarchies within the standard model unresolved.

A popular way to circumvent this unattractive scenario is the so called *see-saw mechanism*.[2] In contrast to Dirac mass terms a Majorana mass term is constructed out of right-handed fields alone (such terms are possible for standard model singlet fields only):

$$\mathscr{L}_{M_R} = -\frac{M_R}{2}\overline{(N_R)^c}N_R + h.c. \tag{1.5}$$

A general neutrino mass term can be written in the form:

$$\mathscr{L}_{m_\nu} = -\frac{1}{2}\left(\overline{\nu_L}, \overline{(N_R)^c}\right)\begin{pmatrix} 0 & m_D \\ m_D & M_R \end{pmatrix}\begin{pmatrix} (\nu_L)^c \\ N_R \end{pmatrix} + h.c. \tag{1.6}$$

One then assumes that $m_R \gg m_D$. Upon diagonalization of the mass matrix one finds two mass eigenvalues

$$m \simeq \frac{m_D^2}{M_R}, \quad M \simeq M_R\,. \tag{1.7}$$

Hence the see-saw mechanism explains the smallness of light neutrino masses by means of the large mass of the heavy Majorana neutrinos.[3] Here we assumed, for the moment, that there is only one generation of neutrinos. Usually m_D and M_R are matrices and the see-saw mechanism results in three light and three heavy Majorana neutrinos. The latter are ideal candidates for the heavy states required for the out-of-equilibrium decay scenario in baryogenesis.

While the elegance of the see-saw mechanism as a theoretical concept is usually taken as a strong hint for its existence, it is unclear today whether neutrinos are Majorana particles or not. A direct proof for the Majorana character would be the observation of neutrinoless double beta decay $\text{Nuc} \rightarrow \text{Nuc}' + 2e^-$. However, current experimental results are not considered to give concluding evidence for this process.

To describe thermal leptogenesis we begin with the SM extended by 3 right-handed neutrino fields:[4]

$$\mathscr{L} = \mathscr{L}_{SM} + i\overline{N_{Ri}}\gamma_\mu\partial^\mu N_{Ri} - h_i\overline{\ell_L}N_{Ri}\tilde{\Phi} - \frac{1}{2}\overline{(N_{Ri})^c}M_{Ri}N_{Ri} + h.c.\,, \tag{1.8}$$

where $i = 1,2,3$ and flavor indices have been suppressed. Spontaneous symmetry breaking generates the Dirac masses

$$m_D = hv\,, \tag{1.9}$$

with vev $v \simeq 246\,\text{GeV}$. The model predicts three heavy Majorana neutrinos with masses M_i which explain the small masses of the light neutrinos by virtue of the see-saw mechanism. Via the

[2] Here, in the context of thermal leptogenesis, we use this term for the so called type-I see-saw mechanism. There exist similar mechanisms (type-II and type-III) which can also be used to explain the mass-hierarchy and leptogenesis is possible in these cases as well.

[3] The Majorana neutrinos, in turn, can be naturally considered as parts of unified theories at high energies.

[4] Φ, ℓ_L, and N_R denote the SM $SU(2)_L$ Higgs-doublet, the $SU(2)_L$ lepton doublet and the right-handed $SU(2)_L \times U(1)_Y$ singlet neutrino fields respectively. h denotes the corresponding Yukawa couplings.

Yukawa interactions the heavy Majorana neutrinos can decay into lepton-Higgs pairs:

$$N_i \to \ell\phi\,, \quad N_i \to \bar{\ell}\bar{\phi}\,. \tag{1.10}$$

These decays obviously violate lepton number and we shall shortly see that they violate CP as well. The relevant temperature scale for this process is $T \sim M_i$. For simplicity we assume here hierarchical Majorana neutrino masses $M_1 \ll M_2,\, M_3$ which means that any lepton asymmetry possibly produced by N_2 and N_3 decays is washed out by processes involving N_1 (which can also proceed in the opposite direction if $T \gtrsim M_1$) and that the final asymmetry eventually is created by the out-of-equilibrium decay of N_1 (N_1 dominated scenario).

CP-violating parameter

The CP asymmetry in the decay of N_i is caused by interference between the tree level and the one-loop diagrams [11, 20, 56] in figure 1.2 which contribute to the CP-violating parameter ϵ_i which is defined as

$$\epsilon_i = \frac{\Gamma_{N_i\to\ell\phi} - \Gamma_{N_i\to\bar{\ell}\bar{\phi}}}{\Gamma_{N_i\to\ell\phi} + \Gamma_{N_i\to\bar{\ell}\bar{\phi}}}\,, \tag{1.11}$$

where $\Gamma_{N_i\to\ell\phi}$ includes a sum over flavour indices: $\Gamma_{N_i\to\ell\phi} = \sum_\alpha \Gamma_{N_i\to\ell_\alpha\phi}$. If we write the

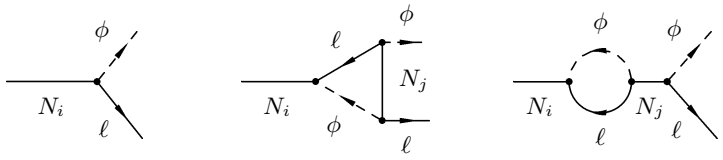

Figure 1.2: Tree level and one-loop contributions to the heavy Majorana neutrino decay $N_i \to \ell\phi$. The asymmetry, at lowest order, is due to the interference of these contributions.

amplitudes (up to one-loop level) as $\mathcal{M}_{N_i\to\ell\phi} = g_0\mathcal{A}_0 + g_1\mathcal{A}_1$ and $\mathcal{M}_{N_i\to\bar{\ell}\bar{\phi}} = g_0^*\mathcal{A}_0 + g_1^*\mathcal{A}_1$, where $g_0\mathcal{A}_0$ and $g_1\mathcal{A}_1$ are the tree-level and one-loop level contributions, respectively, and g_0, g_1 represent the products of all coupling constants in these diagrams, we find that we can write the CP-violating parameter as (neglecting higher orders in the couplings)

$$\epsilon_1 = \frac{|g_0\mathcal{A}_0 + g_1\mathcal{A}_1|^2 - |g_0^*\mathcal{A}_0 + g_1^*\mathcal{A}_1|^2}{|g_0\mathcal{A}_0 + g_1\mathcal{A}_1|^2 + |g_0^*\mathcal{A}_0 + g_1^*\mathcal{A}_1|^2} \simeq -2\frac{\Im\{g_0^* g_1\}\Im\{\mathcal{A}_0^*\mathcal{A}_1\}}{|g_0|^2\,|\mathcal{A}_0|^2}\,. \tag{1.12}$$

We see that, in order to have a non-vanishing CP-violation both $g_0^* g_1$ and $\mathcal{A}_0^*\mathcal{A}_1$, need to have non-vanishing imaginary parts. In particular, this implies that CP-violation can only appear if we include at least the loop level contributions ($\mathcal{A}_1 \neq 0$) and that graphs such as the one-loop graphs in fig. 1.2 with $j = i$ do not contribute to ϵ_i. For the latter the product $g_0^* g_1$ is real. This means that at least two heavy Majorana neutrinos are needed.

In the present case one finds from the diagrams in fig. 1.2:

$$\epsilon_1 = \frac{3}{16\pi}\sum_{j=2,3}\frac{\Im\left\{(h^\dagger h)^2_{1j}\right\}}{(h^\dagger h)_{11}} f\Big(\frac{M_j^2}{M_1^2}\Big)\,, \tag{1.13}$$

where

$$f(x) = \frac{2}{3}\sqrt{x}\left[(1+x)\ln\left(\frac{1+x}{x}\right) - \frac{2-x}{1-x}\right] \underset{x\to\infty}{\longrightarrow} \frac{1}{\sqrt{x}}\,. \tag{1.14}$$

Therefore, using $M_1 \ll M_2,\ M_3$, we have:

$$\epsilon_1 \simeq \frac{3}{16\pi} \sum_{j=2,3} \frac{\Im\left\{(h^\dagger h)^2_{1j}\right\}}{(h^\dagger h)_{11}} \frac{M_1}{M_j} \,. \tag{1.15}$$

This means that the order of magnitude of ϵ_1 is given by the mass hierarchy of the heavy Majorana neutrinos. A rough estimate for ϵ_1 is given by $\epsilon_1 \sim 0.1\, M_1/M_{2,3} \sim 10^{-5}$. In addition to the Majorana neutrino decays there are many different L-violating scattering processes which we do not consider here explicitly but which can give significant contributions which might even exceed the ones by the decays. At least the process $\ell\phi \leftrightarrow \bar{\ell}\bar{\phi}$ needs to be taken into account to overcome the so-called "double counting problem", as we will see later in the framework of the toy model.

Rate equations

The simple scenario of thermal leptogenesis with hierarchical neutrino masses is usually treated by solving a set of two phenomenological rate equations for the heavy neutrino abundance $N_{N_1} = n_{N_1}/s$ and the $B-L$ asymmetry $N_{B-L} = n_{B-L}/s$ [57, 58]:

$$\frac{dN_{N_1}}{dx} = -(D+S)(N_{N_1} - N^{eq}_{N_1})\,, \tag{1.16a}$$

$$\frac{dN_{B-L}}{dx} = \epsilon_1 (D+S)(N_{N_1} - N^{eq}_{N_1}) - W\, N_{B-L}\,, \tag{1.16b}$$

where $x = M_1/T$. The implications of these equations can be understood rather intuitively. Decay and inverse decay processes ($N_1 \leftrightarrow l\phi$ and $N_1 \leftrightarrow \bar{l}\bar{\phi}$), represented by their relative rate $D = \Gamma_D/(Hx)$, and $\Delta L = 1$ scattering processes, represented by $S = \Gamma_S/(Hx)$, lead to the creation of an asymmetry via the first term of the second equation if there is an excess of N_1 relative to its (x dependent) equilibrium value. The second "washout" term (inverse decays, $\Delta L = 1$ and $\Delta L = 2$ scattering processes) in this equation competes with the first one and diminishes the asymmetry (including any preexisting asymmetry at high temperatures $T \gg M_1$). Decay and scattering processes, on the other hand, try to keep the Majorana neutrinos close to their equilibrium abundance via their contributions to the first equation. By doing so they can remove the basis for the generation of an asymmetry via the second equation if their relative rate is large enough. These competing processes set the condition $\Gamma \sim H$ for the onset of leptogenesis. Approximately this condition is fulfilled when the temperature drops below the mass of the lightest neutrino $T \sim M_1$ and the inverse decay to N_1 becomes suppressed. Equation (1.16) does not include spectator processes, such as the sphalerons, which can influence the generated asymmetry indirectly. In the strong washout regime the scattering terms S can be neglected relative to D. Equations (1.16) can approximately be solved analytically in limiting cases. In general this has to be done numerically. The result for typical parameters is depicted in fig. 1.3.

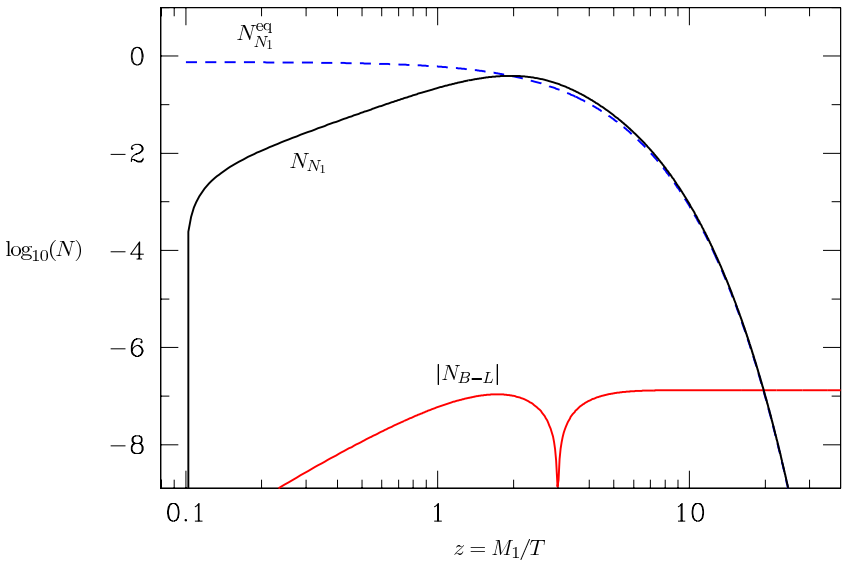

Figure 1.3: Starting from zero initial abundance, N_{N_1} approaches its equilibrium value $N_{N_1}^{eq}$. At the same time a significant $B - L$ asymmetry is produced, because the zero initial abundance represents an extreme non-equilibrium situation. As soon as N_{N_1} reaches its equilibrium value the $B - L$ asymmetry is washed out again. Finally, due to the rapid expansion, the Majorana neutrinos undergo out-of-equilibrium decays and the final asymmetry comes into existence. The parameters are: $M_1 = 10^{10}\,\mathrm{GeV}$, $\epsilon_1 = 10^{-6}$, effective neutrino mass $\tilde{m}_1 = 10^{-3}\,\mathrm{eV}$ and absolute neutrino mass scale $\bar{m} = 0.05\,\mathrm{eV}$. This figure has been taken from [57].

Very roughly the generated final asymmetry can be parametrized as $N_{B-L} = \kappa_f \epsilon_1 / g_*$, where $g_* \sim 106.75$ is the effective number of relativistic degrees of freedom and the efficiency factor $\kappa_f < 1$ takes into account washout factors and needs to be determined by the solution of the rate equations.

In order to find out, how large the final B asymmetry produced by sphaleron processes out of the $B - L$ asymmetry will be, one assumes that the involved leptons, quarks and Higgs particles interact rapidly enough via Yukawa, gauge and sphaleron processes to maintain thermal equilibrium. This yields relations between the chemical potentials of the various species which results in relations for the conversion factors between $B - L$ and B or L asymmetry respectively. For $N_f\,(= 3)$ generations and $T \gg v$ one finds $N_B = c_s N_{B-L}$ and $N_L = (c_s - 1) N_{B-L}$ with $c_s = (8N_f + 4)/(22N_f + 13) = 28/79$. The precise conversion factor may depend on e.g. the precise conditions of the electroweak phase transition, but it can be assumed to be of this order.

Despite its simplicity, the thermal leptogenesis scenario has a very rich phenomenology already. In some cases the efficiency can be related to low energy neutrino parameters, especially when the CP-violation is assumed to be solely to the Dirac phase of the PMNS matrix. In the hierarchical case (via the dependence of the efficiency on the neutrino mass parameters) a bound on the absolute neutrino mass scale of $m_1 \lesssim 0.1\,\mathrm{eV}$ and a relatively large lightest heavy neutrino mass bound $M_1 \gtrsim 10^9\,\mathrm{GeV}$ can be derived. To avoid overproduction of gravitinos in supersymmetric models an upper bound on the reheating temperature of the same order may need to be imposed. Since this is then considered as an upper bound for leptogenesis these requirements are obviously in conflict. For the present scenario the parameter space could be constrained by new bounds on the absolute neutrino mass scale (e.g. by the KATRIN experiment). Such problems can be circumvented in the

quasi-degenerate case, where the CP-violating parameter can be resonantly enhanced and the energy scale lowered to $T \sim 1\,\text{TeV}$. Flavour effects can become important for $M_1 \lesssim 10^{12}\,\text{GeV}$ and can lead to a modification of the CP-violating parameter and to a suppression of washout effects . The general scenario of leptogenesis is hard to disprove, even if the Dirac CP-violating phase or the small neutrino mixing angle θ_{13} is not large enough, because the CP-violation could be due to the high energy CP-violating phases. Instead, an experimental confirmation of the Majorana nature, via neutrinoless double beta decay (e.g. by future experiments such as GERDA), or the measurement of a sufficiently large Dirac phase (e.g. in long-baseline neutrino experiments such as NOνA or T2K) could support the leptogenesis hypothesis. In special cases signals from heavy Majorana neutrinos could also be observed at colliders such as the LHC. See e.g. [14–24, 59] for the discussion of various phenomenological implications of leptogenesis.

As indicated, eqns. (1.16), as their analogues for the toy model, are derived from a set of Boltzmann equations. While eqns. (1.16) are often called Boltzmann equations themselves we do not adopt this nomenclature in order to avoid confusion.[5] To this end one applies a number of approximations with respect to the species' momentum distributions. These include that all species are assumed to be in kinetic equilibrium and to obey Maxwell–Boltzmann statistics. To take non-equilibrium effects into account one needs to solve the full Boltzmann equations or to find more sophisticated methods which allow to obtain some kind of higher order corrections.

The generation of an asymmetry by the decay of some heavy state, the CP-violation being due to the interference of tree- and one-loop level contributions to this decay, is a rather generic feature of many scenarios of leptogenesis and baryogenesis. We have focused here on the simple case of thermal leptogenesis which can be seen as a prototype for many extended scenarios. However, this is not the only example which can be identified with the toy model which will be explored in the next chapter.

[5] We use the term Boltzmann equation here for relativistic kinetic equations describing the evolution of the one-particle distribution function with the generalizations that we include equations for multi-particle processes including decays and inverse decays and the appropriate quantum statistical factors as customary in cosmology.

Chapter 2

Bottom-up approach

2.1 Toy model

The purpose of this section is to set up a toy model which is as simple as possible, but sufficiently intricate as to mimic the phenomenon of leptogenesis or baryogenesis. Our motivation for this approach comes mainly from the observation that the kinetic equations obtained for the different species are very similar, if not the same, to those of established scenarios such as thermal leptogenesis, as described in section 1.3, or GUT-baryogenesis. The advantage is that we can systematically compare the results obtained in the framework of the bottom-up and top-down approach. Despite its simplicity, the model incorporates all important features needed to describe such scenarios. Of course the model does not describe the conversion of the generated asymmetry by means of sphalerons (as these are specific for the standard model), in the case of leptogenesis. As usual, we therefore assume that the processes of generation and conversion of the asymmetry are well separated and can be considered independently. The model is defined by the lagrangian

$$\begin{aligned}\mathscr{L} &= \frac{1}{2}\partial_\mu\psi_i\partial^\mu\psi_i - \frac{1}{2}m_{\psi_i}^2{\psi_i}^2 + \partial_\mu\bar{b}\partial^\mu b - m_b^2\bar{b}b \\ &\quad -\frac{\lambda}{2!2!}(\bar{b}b)^2 - \frac{g_i}{2!}\psi_i bb - \frac{g_i^*}{2!}\psi_i\bar{b}\bar{b} + \mathscr{L}_{rest}\,, \quad i=1,2\,. \end{aligned} \tag{2.1}$$

The complex scalar field b imitates the baryons ($\bar{b}$ denotes the complex conjugate of b) and the real scalar fields ψ_i represent the lightest heavy right-handed neutrinos. For simplicity we include only two ψ_i fields. The model has a $U(1)$ symmetry which can be used to define "baryon" number B (For definiteness we assign $B=1$ to b and $B=0$ to ψ_i). It is explicitly broken by the trilinear interaction terms just as the Majorana mass terms explicitly break the $B-L$ symmetry of the standard model. The couplings g_i correspond the complex Yukawa couplings of the right-handed neutrinos to leptons and the Higgs. We assume that the phases of g_i differ so that only one of them can be made real by rephasing the b field and the other one remains complex. In this way the model violates B and CP and thereby satisfies the first two Sakharov conditions. The purpose of the quartic self-interaction term is to mimic the Yukawa and gauge interactions in established models. It induces additional interactions for the toy-baryons and will keep them close to equilibrium. We assume here that λ is of the same order as $|g_i|/m_{\psi_i}$.

Further terms which are required for renormalizability are accounted for by $\mathscr{L}_{rest}$. By appropriately choosing the corresponding coupling constants we can always make the contributions of these terms negligibly small. It is reasonable to assume that the couplings stay small during the

relevant period despite of the renormalization group running, because the generation of the asymmetry approximately takes place in the relatively short interval $0.1\, m_{\psi_i} \lesssim T \lesssim 10\, m_{\psi_i}$. The Feynman rules for the toy model are given in fig. 2.1.

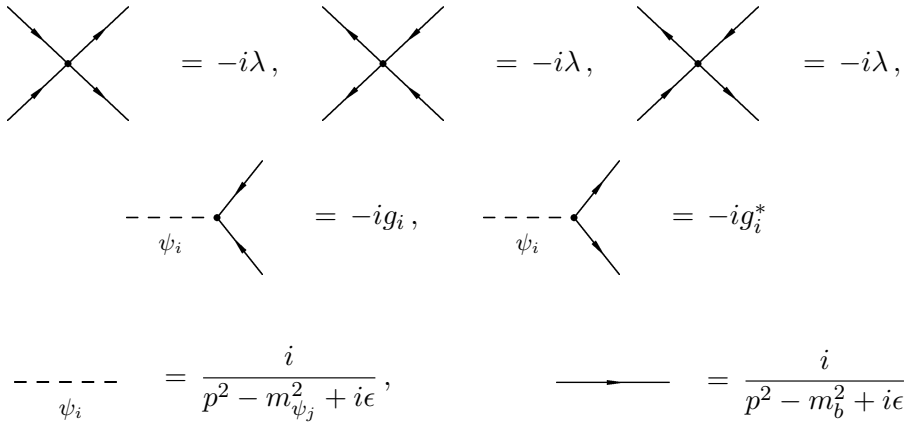

Figure 2.1: Feynman rules for the toy model.

2.2 S-matrix elements

Here we compute the relevant S-matrix element in perturbation theory in the usual in-out formalism. Apart from the tree level graphs it is necessary to take loop corrections into account, because the amplitudes $|\mathcal{M}|^2_{\psi_i \to bb}$ and $|\mathcal{M}|^2_{\psi_i \to \overline{b}\overline{b}}$ are just equal at tree level. As in phenomenological scenarios the CP violation in the decay of ψ_i is due to the interference of tree- and one-loop contributions. The corresponding diagrams for $\psi_i \to bb$ are shown in figure 2.2. The amplitude

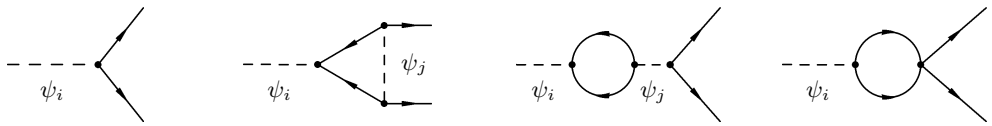

Figure 2.2: One loop contributions to the $\psi_i \to bb$ decay channel. The diagrams for $\psi_i \to \overline{b}\overline{b}$ are analogous. Note the similarity to the relevant contributions in thermal leptogenesis, fig. 1.2. The graphs (b), corresponding to $iS^{(3)}_{\psi_i bb1}$, and (c), corresponding to $iS^{(3)}_{\psi_i bb2}$, contribute to the CP-violating parameter only when $j \neq i$. Depending on λ and g_i graphs like (d), corresponding to $iS^{(3)}_{\psi_i bb3}$ can be of the same order as (b) and (c), but they do not contribute to the CP-violating parameter, because the product of the couplings of (a) and (d) is real, see eqn. (1.12).

$|\mathcal{M}|^2_{\psi_i \to bb}$ can be computed by summing the diagrams in fig. 2.2:

$$|\mathcal{M}|^2_{\psi_i \to bb} = \left| S^{(1)}_{\psi_i bb} + S^{(3)}_{\psi_i bb\,1} + S^{(3)}_{\psi_i bb\,2} + S^{(3)}_{\psi_i bb\,3} \right|^2 , \tag{2.2}$$

and the amplitude $|\mathcal{M}|^2_{\psi_i\to\bar{b}\bar{b}}$ can be found interchanging g_i and g_i^*:

$$|\mathcal{M}|^2_{\psi_i\to\bar{b}\bar{b}} = \left|S^{(1)}_{\psi_i\bar{b}\bar{b}} + S^{(3)}_{\psi_i\bar{b}\bar{b}\,1} + S^{(3)}_{\psi_i\bar{b}\bar{b}\,2} + S^{(3)}_{\psi_i\bar{b}\bar{b}\,3}\right|^2 . \tag{2.3}$$

Without computing these expressions explicitly we can parametrize the matrix elements by defining the CP-violating parameter similar to eqn. (1.11):

$$\epsilon_i^{vac} = \frac{\Gamma_{\psi_i\to bb} - \Gamma_{\psi_i\to\bar{b}\bar{b}}}{\Gamma_{\psi_i\to bb} + \Gamma_{\psi_i\to\bar{b}\bar{b}}} = \frac{|\mathcal{M}|^2_{\psi_i\to bb} - |\mathcal{M}|^2_{\psi_i\to\bar{b}\bar{b}}}{|\mathcal{M}|^2_{\psi_i\to bb} + |\mathcal{M}|^2_{\psi_i\to\bar{b}\bar{b}}} , \tag{2.4}$$

where we used that the decay widths are given by

$$\Gamma_{i\to f} = \frac{|\mathcal{M}|^2_{i\to f}}{16\pi m_{\psi_i}} . \tag{2.5}$$

Then the amplitudes for the ψ_i decay are conveniently parametrised as

$$|\mathcal{M}|^2_{\psi_i\to bb} = \frac{1}{2}(1+\epsilon_i^{vac})\,|\mathcal{M}_{\psi_i}|^2 , \tag{2.6a}$$

$$|\mathcal{M}|^2_{\psi_i\to\bar{b}\bar{b}} = \frac{1}{2}(1-\epsilon_i^{vac})\,|\mathcal{M}_{\psi_i}|^2 . \tag{2.6b}$$

and the amplitudes for the inverse decays can be deduced from CPT invariance:

$$|\mathcal{M}|^2_{bb\to\psi_i} = \frac{1}{2}(1-\epsilon_i^{vac})\,|\mathcal{M}_{\psi_i}|^2 , \tag{2.7a}$$

$$|\mathcal{M}|^2_{\bar{b}\bar{b}\to\psi_i} = \frac{1}{2}(1+\epsilon_i^{vac})\,|\mathcal{M}_{\psi_i}|^2 . \tag{2.7b}$$

In addition we need the matrix elements for the $2-2$ scattering processes of b and $\bar{b}$. Including only the tree level diagrams depicted in fig. 2.3 we obtain for the $bb\to\bar{b}\bar{b}$ scattering amplitude:[1]

$$\begin{aligned}|\mathcal{M}|^2_{bb\to\bar{b}\bar{b}} \simeq \left|(g_i)^2\left(\frac{1}{s-m^2_{\psi_i}+im_{\psi_i}\Gamma_i}+\frac{1}{t-m^2_{\psi_i}}+\frac{1}{u-m^2_{\psi_i}}\right)\right|^2 = \\ |g_i|^4\left(\frac{1}{(s-m^2_{\psi_i})^2+(m_{\psi_i}\Gamma_i)^2}+\left(\frac{1}{t-m^2_{\psi_i}}+\frac{1}{u-m^2_{\psi_i}}\right)^2\right. \\ \left.+\frac{2(s-m^2_{\psi_i})}{(s-m^2_{\psi_i})^2+m^2_{\psi_i}\Gamma_i^2}\left(\frac{1}{t-m^2_{\psi_i}}+\frac{1}{u-m^2_{\psi_i}}\right)\right)+\dots .\end{aligned} \tag{2.8}$$

At this order, loop graphs do not contribute to $|\mathcal{M}|^2_{bb\to\bar{b}\bar{b}}$ and it equals $|\mathcal{M}|^2_{\bar{b}\bar{b}\to bb}$. The remaining $2-2$ scattering amplitudes are dominated by the coupling λ so that, at lowest order, we get $|\mathcal{M}|^2_{bb\to bb} = |\mathcal{M}|^2_{\bar{b}\bar{b}\to\bar{b}\bar{b}} = |\mathcal{M}|^2_{b\bar{b}\to b\bar{b}} = \lambda^2$.[2]

[1] Here we use the Breit–Wigner form of the ψ_i-propagator in the s-channel with $\Gamma_i(s^2)\simeq\Gamma_i = |\mathcal{M}_{\psi_i}|/(16\pi m_{\psi_i})$.

[2] This approximation has the advantage that it will simplify the numerical computations significantly since the angular integration of amplitudes such as eqn. (2.8) is considerably more involved.

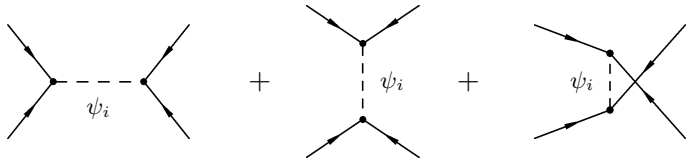

Figure 2.3: s-,t- and u-channel contributions to the tree-level amplitude $\mathcal{M}_{bb\to\bar{b}\bar{b}}$.

2.3 Kinetic theory

Just as in phenomenological scenarios, the toy model requires a deviation from thermal equilibrium (caused by the rapid expansion of the universe) to satisfy the third Sakharov condition. Conventional equilibrium thermodynamics deals with macroscopic quantities such as particle number, energy or pressure which are obtained as average values of a large ensemble of identical systems. In order to understand non-equilibrium phenomena one needs a microscopic description of many particle systems such as the one given by kinetic theory.

A basic object in this theory is the *one-particle distribution function* $f^a(x,k)$. It is defined such that $f^a(x,k)\Delta^3\mathbf{x}\Delta^3\mathbf{k} = \Delta N$ is the average number of particles[3] of species a with momenta in the range $(\mathbf{k},\ \mathbf{k}+\Delta\mathbf{k})$ located in the volume $(\mathbf{x},\ \mathbf{x}+\Delta\mathbf{x})$ at a time t.[4] Once the distribution functions of the different species are known the macroscopic quantities can be computed from it. In the context of relativistic kinetic theory it is important to note that f is a Lorenz scalar. The time evolution of the distribution functions of the different species in a reactive mixture of relativistic gases is determined by a network of *generalized Boltzmann equations*[5] for the one-particle distribution functions of the different particle species [5, 25–27, 60] which we can write in abstract notation as

$$L[f^a](x,k) = \sum_{\text{interactions of } a} C_k^{a+\cdot\leftrightarrow i+\cdot}[.f^a.]\,, \tag{2.9}$$

where the *Liouville operator* $L[]$ is given by

$$L[f^a](x,k) = k^\alpha \mathcal{D}_\alpha f^a(k,x)\,, \tag{2.10}$$

with covariant derivative $\mathcal{D}_\alpha$. In the framework of general relativity the matter content of the universe, given here in terms of distribution functions, contributes to the stress-energy tensor and thereby affects the curvature of the universe via the Einstein equations. In general, these and the Boltzmann equations form therefore a coupled system of equations (Einstein-Boltzmann system). Since individual ultra-relativistic species always make only a small contribution to the total energy density, we can work here in a "test-particle" approximation within which the effect of the considered species (represented by their distribution functions) on the curvature is neglected.[6] We

[3] We omit a normalization factor of $1/(2\pi)^3$ and the factor g_a here.

[4] We use relativistic coordinates $x = x^\mu = (t,\mathbf{x})$. Note that k^0 is not an independent variable as the particle's 4-momentum is confined to a hyperboloid in momentum space $k^0 = \sqrt{\mathbf{k}^2 + m^2} = E_k$. (i.e. f depends on seven independent variables only.)

[5] These equations are generalized Boltzmann equations in a multiple sense: the equations are general relativistic with a Liouville operator which accounts for the expansion; the collision terms are generalized to multiple particle scattering processes including decays and inverse decays; quantum statistical terms for blocking or stimulated emission are included.

[6] In the phenomenological model of thermal leptogenesis the contribution of the heavy right-handed neutrinos to the energy density of the universe is at the level of a few percent .

are interested here in (spatially flat and radiation dominated) Friedman–Robertson–Walker (FRW) space-time. In this context the cosmological principle helps to simplify the Boltzmann equation because it allows us to assume that the distribution functions depend only on the magnitude of the momenta. The Liouville operator can then be simplified to (the time dependence of f^a is suppressed in this notation)

$$L[f^a](x,k) = k^0 \left(\frac{\partial}{\partial t} - |\mathbf{k}|\, H \frac{\partial}{\partial\, |\mathbf{k}|} \right) f^a(|\mathbf{k}|)\,, \tag{2.11}$$

where $H \equiv \dot{a}/a$ is the Hubble parameter. The individual *collision terms* $C^{a+\cdot\leftrightarrow i+\cdot}_{p_a}[.f^a.]$ for multi-particle processes $a+b+c\ldots\leftrightarrow i+j+\ldots$ are

$$\begin{aligned} C^{a+\cdot\leftrightarrow i+\cdot}_{p_a}[.f^a.] = \frac{1}{2}\int d\Pi^b_{p_b}\, d\Pi^c_{p_c} \ldots\, d\Pi^i_{p_i}\, d\Pi^j_{p_j} \ldots (2\pi)^4 \delta^{(4)}(p_a + p_b + p_c \ldots - p_i - p_j) \\ \times \big[\, |M|^2_{i+j+\ldots\to a+b+c\ldots} (1-\xi^a f^a_{p_a})(1-\xi^b f^b_{p_b})(1-\xi^c f^c_{p_c}) \ldots f^i_{p_i} f^j_{p_j} \ldots - \\ |M|^2_{a+b+c\ldots\to i+j+\ldots} f^a_{p_a} f^b_{p_b} f^c_{p_c} \ldots (1-\xi^i f^i_{p_i})(1-\xi^j f^j_{p_j}) \ldots \big]\,. \end{aligned} \tag{2.12}$$

The amplitudes $|M|^2_{i+j+\ldots\to a+b+c\ldots}$ and $|M|^2_{a+b+c\ldots\to i+j+\ldots}$ are spin-averaged S-matrix elements squared computed in usual perturbation theory, furnished with a symmetrization factor $1/n!$ if there are integrals over n identical species in the initial/final state. If CP is violated, as in the present case, the amplitudes for the different directions can differ. ξ^a denote the quantum statistical factors ($\xi^a = +1$ for fermions, $\xi^a = -1$ for bosons, $\xi^a = 0$ for Maxwell–Boltzmann statistics) and the Lorentz invariant phase-space factor $d\Pi^a_p$ is given by[7]

$$d\Pi^a_p = \frac{g_a d^3p}{(2\pi)^3 2E^a_p}\,. \tag{2.13}$$

To understand the physical content of these assignments let us now have a look at the heuristic probability interpretation of the Boltzmann equation [26] for the special case of only one species. Neglecting, for simplicity, the covariant derivative (which acts as a force term), the collisionless Boltzmann equation (Liouville-equation) reads

$$k^\alpha \partial_\alpha f(x,k) = 0\,. \tag{2.14}$$

In order to account for loss and gain of particles, we need to compute the change of the number of particles in the phase space element $\Delta^4 x$ and $\Delta^3 p$ due to collisions. We first consider elastic collisions of two particles with initial four-momenta k^μ and p^μ and final momenta q^μ and r^μ. Under the assumption of *molecular chaos* (absence of initial correlations of the colliding particles) and long free path-length compared to the range of the interaction, the average number of such collisions in the volume element $\Delta^3 x$ around $\mathbf{x}$ and the time interval Δt around t is proportional to

- the average number of particles per unit volume with three-momenta in $(\mathbf{k}, \mathbf{k}+\Delta\mathbf{k})$, i.e. $\Delta^3 k f(x,k)$
- the average number of particles per unit volume with three-momenta in $(\mathbf{p}, \mathbf{p}+\Delta\mathbf{p})$, i.e. $\Delta^3 p f(x,p)$

[7] $E^a_p = \sqrt{p^2 + m_a^2}$ denotes the on-shell energy and g_a the number of internal degrees of freedom ($g_a = 1$ for scalars) of a particle of species a.

- the intervals $\Delta^4 x$ and $\Delta^3 q$, $\Delta^3 r$.

The proportionality factor can be written as $W(k,p|q,r)/(k^0 2p^0(2\pi)^3 2q^0(2\pi)^3 2r^0(2\pi)^3)$. This, in fact, defines the transition rate W which depends only on the four-momenta before and after the collision. It must be a Lorentz scalar. In this argument we have assumed, that the four-volume-element $\Delta^4 x$ is so small that the variation of the distribution functions in this interval may be neglected. Hence the proportionality to $f(x,k)$ and $f(x,p)$ at the same place and at the same instant of time and the independence of W of the space and time coordinates. This ansatz, which requires one to assume molecular chaos as well, is known as Botzmann's *Stoßzahlansatz*.

In this way, we find for the loss of particles:

$$\Delta_{loss} = \Delta^4 x \Delta^3 q \Delta^3 r \frac{W(k,p|q,r)}{k^0 2p^0(2\pi)^3 2q^0(2\pi)^3 2r^0(2\pi)^3} \Delta^3 k f(x,k) \Delta^3 p f(x,p)\,. \tag{2.15}$$

In the same way one obtains the gain of particles:

$$\Delta_{gain} = \Delta^4 x \Delta^3 k \Delta^3 p \frac{W(q,r|k,p)}{k^0 2p^0(2\pi)^3 2q^0(2\pi)^3 2r^0(2\pi)^3} \Delta^3 q f(x,q) \Delta^3 r f(x,r)\,. \tag{2.16}$$

Subtracting the loss from the gain and integrating over the momenta we find

$$\frac{1}{2}\int_{p,q,r} \Delta_{gain} - \frac{1}{2}\int_{p,q,r} \Delta_{loss} = \Delta^4 x \frac{\Delta^3 k}{k^0} C(x,k)\,,$$

with *collision integral*

$$C(x,k) = \frac{1}{2}\int d\Pi_p\, d\Pi_q\, d\Pi_r \Big[W(q,r|k,p) f(x,q) f(x,r) - W(k,p|q,r) f(x,k) f(x,p)\Big]\,. \tag{2.17}$$

Since the differential change of particle number is given by $\Delta^4 x \Delta^3 k/k^0\, k^\alpha \partial_\alpha f$ one finds the Boltzmann kinetic equation

$$k^\alpha \partial_\alpha f(x,k) = C(x,k)\,. \tag{2.18}$$

Now we can identify W with the invariant quantity

$$W(k,p|q,r) = (2\pi)^4 \delta^{(4)}(k+p-q-r)|M|^2_{k,p\to q,r}\,. \tag{2.19}$$

If we introduce the additional quantum statistical terms for blocking or stimulated emission $(1-\xi^a f^a)$ for the final state particles in the interactions we can see that eqn. (2.17) is a special case of eqn. (2.12) for elastic $2-2$ scattering. Setting $f_q \equiv f_r \equiv 1$ in eqn. (2.17) the loss and gain terms corresponds to the usual formulas for the transition probability $\mathcal{P}(k,p \to q,r)$ for the $2-2$ scattering process computed from the $S-$matrix [61]. The Dirac-delta enforces energy-momentum conservation in each individual scattering process.

Kinetic equations for inelastic reactions according to eqn. (2.9) (in particular, as we encounter it here, for decays and inverse decays) are not Boltzmann equations in the original sense, but they can be seen as a generalization of this heuristic probability concept.

As announced in section 1.3, we are interested here in the hierarchical case, i.e. we choose m_{ψ_2} sufficiently large so that it decays already at much higher temperatures[8] and cannot be created

[8] This requires also that the coupling g_2 is not too small.

kinematically anymore. Later we will also assume that the asymmetry generated by the decay of ψ_2 is washed out before ψ_1 starts to decay. This corresponds to the N_1 dominated scenario in thermal leptogenesis. For the toy model the application of eqn. (2.9) then leads to the following system of only three Boltzmann equations:

$$L_k[f^{\psi_1}] = C_k^{\psi_1 \leftrightarrow bb}[f^{\psi_1}, f^b] + C_k^{\psi_1 \leftrightarrow \bar{b}\bar{b}}[f^{\psi_1}, f^{\bar{b}}], \tag{2.20a}$$

$$L_k[f^b] = C_k^{bb \leftrightarrow \psi_1}[f^b, f^{\psi_1}] + C_k^{b\bar{b} \leftrightarrow b\bar{b}}[f^b, f^{\bar{b}}] + C_k^{bb \leftrightarrow bb}[f^b] + C_k^{bb \leftrightarrow \bar{b}\bar{b}}[f^b, f^{\bar{b}}], \tag{2.20b}$$

$$L_k[f^{\bar{b}}] = C_k^{\bar{b}\bar{b} \leftrightarrow \psi_1}[f^{\bar{b}}, f^{\psi_1}] + C_k^{\bar{b}b \leftrightarrow \bar{b}b}[f^{\bar{b}}, f^b] + C_k^{\bar{b}\bar{b} \leftrightarrow \bar{b}\bar{b}}[f^{\bar{b}}] + C_k^{\bar{b}\bar{b} \leftrightarrow bb}[f^{\bar{b}}, f^b], \tag{2.20c}$$

where the different collision terms for ψ_1 are given by

$$\begin{aligned} C_k^{\psi_1 \leftrightarrow bb}[f^b, f^{\psi_i}] &= \frac{1}{2} \int d\Pi_p^b \, d\Pi_q^b (2\pi)^4 \delta^{(4)}(k - p - q) \\ &\quad \times \Big[\frac{1}{2} |\mathcal{M}|^2_{bb \to \psi_1} (1 + f_k^{\psi_1}) f_p^b f_q^b - \frac{1}{2} |\mathcal{M}|^2_{\psi_1 \to bb} f_k^{\psi_1} (1 + f_p^b)(1 + f_q^b) \Big], \\ C_k^{\psi_1 \leftrightarrow \bar{b}\bar{b}}[f^{\bar{b}}, f^{\psi_i}] &= \frac{1}{2} \int d\Pi_p^{\bar{b}} \, d\Pi_q^{\bar{b}} (2\pi)^4 \delta^{(4)}(k - p - q) \\ &\quad \times \Big[\frac{1}{2} |\mathcal{M}|^2_{\bar{b}\bar{b} \to \psi_1} (1 + f_k^{\psi_1}) f_p^{\bar{b}} f_q^{\bar{b}} - \frac{1}{2} |\mathcal{M}|^2_{\psi_1 \to \bar{b}\bar{b}} f_k^{\psi_1} (1 + f_p^{\bar{b}})(1 + f_q^{\bar{b}}) \Big]. \end{aligned} \tag{2.21a}$$

The inverse processes contribute to the equations for b and $\bar{b}$:

$$\begin{aligned} C_k^{bb \leftrightarrow \psi_1}[f^b, f^{\psi_1}] &= \frac{1}{2} \int d\Pi_p^b \, d\Pi_q^{\psi_1} (2\pi)^4 \delta^{(4)}(k + p - q) \\ &\quad \times \Big[|\mathcal{M}|^2_{\psi_1 \to bb} (1 + f_k^b)(1 + f_p^b) f_q^{\psi_1} - |\mathcal{M}|^2_{bb \to \psi_1} f_k^b f_p^b (1 + f_q^{\psi_1}) \Big], \\ C_k^{\bar{b}\bar{b} \leftrightarrow \psi_1}[f^{\bar{b}}, f_q^{\psi_1}] &= \frac{1}{2} \int d\Pi_p^{\bar{b}} \, d\Pi_q^{\psi_1} (2\pi)^4 \delta^{(4)}(k + p - q) \\ &\quad \times \Big[|\mathcal{M}|^2_{\psi_1 \to \bar{b}\bar{b}} (1 + f_k^{\bar{b}})(1 + f_p^{\bar{b}}) f_q^{\psi_1} - |\mathcal{M}|^2_{\bar{b}\bar{b} \to \psi_1} f_k^{\bar{b}} f_p^{\bar{b}} (1 + f_q^{\psi_1}) \Big]. \end{aligned} \tag{2.21b}$$

These species are also subject to B-violating $2 - 2$ scattering processes:

$$\begin{aligned} C_k^{bb \leftrightarrow \bar{b}\bar{b}}[f^b, f^{\bar{b}}] &= \frac{1}{2} \int d\Pi_p^b \, d\Pi_q^{\bar{b}} \, d\Pi_r^{\bar{b}} (2\pi)^4 \delta^{(4)}(k + p - q - r) \\ &\quad \times \Big[\frac{1}{2} |\mathcal{M}|^2_{\bar{b}\bar{b} \to bb} (1 + f_k^b)(1 + f_p^b) f_q^{\bar{b}} f_r^{\bar{b}} - \frac{1}{2} |\mathcal{M}|^2_{bb \to \bar{b}\bar{b}} f_k^b f_p^b (1 + f_q^{\bar{b}})(1 + f_r^{\bar{b}}) \Big], \end{aligned} \tag{2.21c}$$

and B-conserving ones:

$$\begin{aligned} C_k^{bb \leftrightarrow bb}[f^{\bar{b}}] &= \frac{1}{2} \int d\Pi_p^b \, d\Pi_q^b \, d\Pi_r^b (2\pi)^4 \delta^{(4)}(k + p - q - r) \\ &\quad \times \Big[\frac{1}{2} |\mathcal{M}|^2_{bb \to bb} (1 + f_k^b)(1 + f_p^b) f_q^b f_r^b - \frac{1}{2} |\mathcal{M}|^2_{bb \to bb} f_k^b f_p^b (1 + f_q^b)(1 + f_r^b) \Big], \\ C_k^{b\bar{b} \leftrightarrow b\bar{b}}[f^b, f^{\bar{b}}] &= \frac{1}{2} \int d\Pi_p^{\bar{b}} \, d\Pi_q^b \, d\Pi_r^{\bar{b}} (2\pi)^4 \delta^{(4)}(k + p - q - r) \\ &\quad \times \Big[|\mathcal{M}|^2_{bb \to bb} (1 + f_k^b)(1 + f_p^{\bar{b}}) f_q^b f_r^{\bar{b}} - |\mathcal{M}|^2_{bb \to bb} f_k^b f_p^{\bar{b}} (1 + f_q^b)(1 + f_r^{\bar{b}}) \Big]. \end{aligned} \tag{2.21d}$$

The collision terms $C_k^{\bar{b}b\leftrightarrow\bar{b}b}[f^{\bar{b}}, f^b]$, $C_k^{\bar{b}\bar{b}\leftrightarrow\bar{b}\bar{b}}[f^{\bar{b}}]$ and $C_k^{\bar{b}\bar{b}\leftrightarrow bb}[f^{\bar{b}}, f^b]$ follow from these by interchange of b and $\bar{b}$. We shall shortly see that the rate equations corresponding to eqns. (2.20), constructed in the bottom-up approach, are plagued with the problem that they lead to the creation of an asymmetry even in thermal equilibrium. The solution to this problem is known from baryogenesis and leptogenesis as *real intermediate state subtraction* (RIS subtraction). We will see that this procedure does not work in the usual way if one wants to keep the quantum statistical terms. Therefore, strictly speaking, eqn. (2.20) together with eqn. (2.21), i.e. the quoted literature result eqn. (2.12) is inconsistent in this case.

2.4 Rate equations

We use the "pseudo chemical potential" method [25] to obtain *rate equations*[9] by integrating the Boltzmann equations over the remaining phase space volume. This means that we assume a specific equilibrium form for the distribution functions of all species with small chemical potentials. In detail, we make the following simplifying assumptions:

1. All species are in kinetic equilibrium (and have the same temperature T).[10]
2. Maxwell–Boltzmann distribution functions can be used instead of Bose–Einstein (or Fermi–Dirac for fermions) distributions. This implies that we neglect the quantum statistical terms.[11]
3. The chemical potentials are small (i.e. the system is close to chemical equilibrium) $\mu_a/T \ll 1$ and the chemical potentials of b and $\bar{b}$ are equal but opposite in sign. [12]
4. The comoving entropy is conserved, i.e. $d(sa^3) = 0$.[13]

The distribution functions can then be approximated in the following way:[14]

$$f_p^a = \frac{1}{e^{-(E_p^a-\mu_a)/T}-1} \simeq e^{-(E_p^a-\mu_a)/T} \simeq e^{-\frac{E_p^a}{T}}(1+\frac{\mu_a}{T}) = f_p^{a,\,eq}(1+\frac{\mu_a}{T})\,. \tag{2.22}$$

The first of these approximations implies that $n_a = e^{\mu_a/T} n_a^{eq}$.

First of all, we multiply the equations by $g_a/[(2\pi)^3 E_k^a]$ (we keep the internal degrees of freedom although $g_a = 1$ in the present case) and integrate over the remaining three-momenta [5, 25].

[9] We do not use the popular term "Boltzmann equations" for the rate equations, since it would be misleading in the present context.

[10] This is usually a good approximation, if the reaction rate is greater than the expansion rate $\Gamma \gg H$. In the early universe the particles would undergo other thermalizing reactions such as $\gamma + \ell \to \gamma + \ell$ and so on (typically at higher rates) which maintain thermal equilibrium. Within our toy model the interactions $b\bar{b} \leftrightarrow b\bar{b}$, $bb \leftrightarrow bb$ and $\bar{b}\bar{b} \leftrightarrow \bar{b}\bar{b}$ have a similar effect.

[11] Thus the particles are treated as classical particles..

[12] This would follow from the existence of reactions like $\ell + \bar{\ell} \leftrightarrow \gamma + \gamma$ which would lead to $\mu_b + \mu_{\bar{b}} = 2\mu_\gamma = 0$ in equilibrium. For the scalars in the toy model (with Bose–Einstein distribution) the assumption $\mu_b = -\mu_{\bar{b}}$ is an obvious contradiction which is circumvented here by using Maxwell–Boltzmann distribution functions.

[13] This should be a good one if there are no strong non-equilibrium processes.

[14] By writing it this way, we mean that the values of the integrals involving the distributions will take similar values. Since we cannot estimate the error of this approximations analytically, the proof is left to numerical calculations. For small masses and chemical potentials the second of these equations is obviously wrong for small momenta.

Using approximation 4, the left hand side is then given by

$$\frac{g_a}{(2\pi)^3}\int L[f^a]\frac{d^3k}{E_k^a} = \frac{dn_a}{dt} + 3Hn_a = s\frac{dY_a}{dt} = s\frac{H(m)}{x}\frac{dY_a}{dx} = sH(x)x\frac{dY_a}{dx}\,, \tag{2.23}$$

with $Y_a = n_a/s$ and $H(m) = 1.66\sqrt{g_*}m^2/m_{\rm Pl}$.
We first integrate eqn. (2.20a). The left-hand side is given by eqn. (2.23) and applying approximation 1, we find for the first term on the right-hand side:

$$\begin{aligned}\frac{g_{\psi_1}}{(2\pi)^3}\int \frac{d^3k}{E_k^{\psi_1}} C_k^{\psi_1\leftrightarrow bb}[f^{\psi_1}, f^b] \simeq \\ \simeq \int d\Pi_k^{\psi_1}\, d\Pi_p^b\, d\Pi_q^b (2\pi)^4\delta^{(4)}(k-p-q) \\ \times f_k^{\psi_1}(1-\xi^b f_p^b)(1-\xi^b f_q^b)\left[\frac{1}{2}\left|\mathcal{M}\right|^2_{bb\to\psi_1} e^{\frac{2\mu_b}{T}-\frac{\mu_{\psi_1}}{T}} - \frac{1}{2}\left|\mathcal{M}\right|^2_{\psi_1\to bb}\right].\end{aligned} \tag{2.24}$$

Applying approximations 2 and 3 gives

$$\begin{aligned}\frac{g_{\psi_1}}{(2\pi)^3}\int \frac{d^3k}{E_k^{\psi_1}} C_k^{\psi_1\leftrightarrow bb}[f^{\psi_1}, f^b] \simeq \int d\Pi_k^{\psi_1}\, d\Pi_p^b\, d\Pi_q^b (2\pi)^4\delta^{(4)}(k-p-q) \\ \times\left[f_k^{\psi_1,\,eq}\frac{1}{2}\left(1+\frac{2\mu_b}{T}\right)\left|\mathcal{M}\right|^2_{bb\to\psi_1} - f_k^{\psi_1}\frac{1}{2}\left|\mathcal{M}\right|^2_{\psi_1\to bb}\right],\end{aligned} \tag{2.25}$$

where we exploited the fact that, due to energy conservation,

$$f_p^b f_q^b = f_p^{b,\,eq} f_q^{b,\,eq} e^{+2\mu/T} \simeq f_p^{b,\,eq} f_q^{b,\,eq}(1+2\mu_b/T) = f_k^{\psi_1,\,eq}(1+2\mu_b/T)\,. \tag{2.26}$$

The term for $\psi_1 \leftrightarrow \bar{b}\bar{b}$ follows from eqn. (2.25), substituting $b \to \bar{b}$ (this implies $\mu_b \to \mu_{\bar{b}} = -\mu_b$). Summing the two contributions, using $d\Pi^{\bar{b}} = d\Pi^b$ and the parametrization of the matrix elements (2.6a), (2.7a) yields

$$\begin{aligned}&\frac{g_{\psi_1}}{(2\pi)^3}\int \frac{d^3k}{E_k^{\psi_1}} C_k^{\psi_1\leftrightarrow bb}[f^{\psi_1}, f^b] + \frac{g_{\psi_1}}{(2\pi)^3}\int \frac{d^3k}{E_k^{\psi_1}} C_k^{\psi_1\leftrightarrow \bar{b}\bar{b}}[f^{\psi_1}, f^{\bar{b}}] \simeq \\ &\simeq \int d\Pi_k^{\psi_1}\, d\Pi_p^b\, d\Pi_q^b (2\pi)^4\delta^{(4)}(k-p-q)\frac{1}{2}\left|\mathcal{M}_{\psi_1}\right|^2\left[f_k^{\psi_1,\,eq}\left(1-\epsilon\frac{2\mu_b}{T}\right) - f_k^{\psi_1}\right].\end{aligned}$$

Since μ_b/T and ϵ are small we can neglect the $\epsilon 2\mu_b/T$ term compared to 1. The phase space integral over $f_{\psi_1}(k)\left|\mathcal{M}_{\psi_1}\right|^2$ gives the thermally averaged ψ_1-decay width times the number density of ψ_1, so that we can write it as

$$\frac{g_{\psi_1}}{(2\pi)^3}\int \frac{d^3k}{E_k^{\psi_1}} C_k^{\psi_1\leftrightarrow bb}[f^{\psi_1}, f^b] + \frac{g_{\psi_1}}{(2\pi)^3}\int \frac{d^3k}{E_k^{\psi_1}} C_k^{\psi_1\leftrightarrow \bar{b}\bar{b}}[f^{\psi_1}, f^{\bar{b}}] \simeq -\frac{1}{2}\left\langle\Gamma_{\psi_1}\right\rangle\left[n_{\psi_1} - n_{\psi_1}^{eq}\right], \tag{2.27}$$

with averaged decay rate

$$\left\langle\Gamma_{\psi_1}\right\rangle = \frac{1}{n_{\psi_1}^{eq}}\int d\Pi_k^{\psi_1}\, d\Pi_p^b\, d\Pi_q^b (2\pi)^4\delta^{(4)}(k-p-q)\left|\mathcal{M}_{\psi_1}\right|^2 f_k^{\psi_1,\,eq}\,. \tag{2.28}$$

The collision term for $bb \leftrightarrow \psi_1$ on the right-hand side of eqn. (2.20b) can be rewritten in the same way as

$$\begin{aligned}\frac{g_b}{(2\pi)^3}\int \frac{d^3k}{E_k^b} C_k^{bb\leftrightarrow\psi_1}[f^b, f^{\psi_1}] \simeq \\ \simeq \int d\Pi_k^b\, d\Pi_p^b\, d\Pi_q^{\psi_1} (2\pi)^4 \delta^{(4)}(k+p-q) \\ \times(1-\xi^b f_k^b)(1-\xi^b f_p^b) f_q^{\psi_1} \left[|\mathcal{M}|^2_{\psi_1\to bb} - |\mathcal{M}|^2_{bb\to\psi_1}\, e^{\frac{2\mu_b}{T}-\frac{\mu_{\psi_1}}{T}}\right] . \end{aligned} \tag{2.29}$$

The term for $\bar{b}\bar{b} \leftrightarrow \psi_1$ follows from eqn. (2.29) by substituting $b \to \bar{b}$ (this implies $\mu_b \to \mu_{\bar{b}} = -\mu_b$). As in section 1.3 it is convenient to derive a single equation for the toy-baryon asymmetry which is given by $n_B = (n_b - n_{\bar{b}})$. Subtracting the two terms for $bb \leftrightarrow \psi_1$ and $\bar{b}\bar{b} \leftrightarrow \psi_1$ we find

$$\begin{aligned}&\frac{g_b}{(2\pi)^3}\int \frac{d^3k}{E_k^b} C_k^{bb\leftrightarrow\psi_1}[f^b, f^{\psi_1}] - \frac{g_{\bar{b}}}{(2\pi)^3}\int \frac{d^3k}{E_k^{\bar{b}}} C_k^{\bar{b}\bar{b}\leftrightarrow\psi_1}[f^{\bar{b}}, f^{\psi_1}] \simeq \\ &\simeq \int d\Pi_k^b\, d\Pi_p^b\, d\Pi_q^{\psi_1} (2\pi)^4 \delta^{(4)}(k+p-q) \\ &\times f_q^{\psi_1}\left\{ \left[|\mathcal{M}|^2_{\psi_1\to bb} - |\mathcal{M}|^2_{\psi_1\to\bar{b}\bar{b}}\right] - \left[|\mathcal{M}|^2_{bb\to\psi_1}\, e^{\frac{2\mu_b}{T}} - |\mathcal{M}|^2_{\bar{b}\bar{b}\to\psi_1}\, e^{\frac{-2\mu_b}{T}}\right] e^{-\frac{\mu_{\psi_1}}{T}} \right\} . \end{aligned} \tag{2.30}$$

With eqn. (2.28) this leads to

$$\begin{aligned}\frac{g_b}{(2\pi)^3}\int \frac{d^3k}{E_k^b} C_k^{bb\leftrightarrow\psi_1}[f^b, f^{\psi_1}] - \frac{g_{\bar{b}}}{(2\pi)^3}\int \frac{d^3k}{E_k^{\bar{b}}} C_k^{\bar{b}\bar{b}\leftrightarrow\psi_1}[f^{\bar{b}}, f^{\psi_1}] \simeq \\ \simeq \langle\Gamma_{\psi_1}\rangle\, \epsilon\left[n_{\psi_1} + n_{\psi_1}^{eq}\right] - n_B \langle\Gamma_{\psi_1}\rangle \frac{n_{\psi_1}^{eq}}{n_b^{eq}} , \end{aligned} \tag{2.31}$$

where we have used $2\mu_b/T \simeq (n_b - n_{\bar{b}})/n_b^{eq} = n_B/n_b^{eq}$. In approximation 1 the collision terms for $bb \leftrightarrow \bar{b}\bar{b}$ and $b\bar{b} \leftrightarrow b\bar{b}$ on the right-hand side of eqns. (2.20b) and (2.20c) vanish and we need to compute only the remaining ones:

$$\begin{aligned}\frac{g_b}{(2\pi)^3}\int \frac{d^3k}{E_k^b} C_k^{bb\leftrightarrow\bar{b}\bar{b}}[f^b, f^{\bar{b}}] \simeq \int d\Pi_k^b\, d\Pi_p^b\, d\Pi_q^b\, d\Pi_r^b (2\pi)^4 \delta^{(4)}(k+p-q-r) \\ \times(1-\xi^b f_k^b)(1-\xi^b f_p^b) f_q^{\bar{b}} f_r^{\bar{b}} \frac{1}{2}\left[|\mathcal{M}|^2_{\bar{b}\bar{b}\to bb} - |\mathcal{M}|^2_{bb\to\bar{b}\bar{b}}\, e^{\frac{4\mu_b}{T}}\right] . \end{aligned} \tag{2.32}$$

Subtracting the analogous term for $\bar{b}\bar{b} \leftrightarrow bb$ we obtain

$$\begin{aligned}\frac{g_b}{(2\pi)^3}\int \frac{d^3k}{E_k^b} C_k^{bb\leftrightarrow\bar{b}\bar{b}}[f^b, f^{\bar{b}}] - \frac{g_{\bar{b}}}{(2\pi)^3}\int \frac{d^3k}{E_k^{\bar{b}}} C_k^{\bar{b}\bar{b}\leftrightarrow bb}[f^{\bar{b}}, f^b] \simeq \\ \simeq \int d\Pi_k^b\, d\Pi_p^b\, d\Pi_q^b\, d\Pi_r^b (2\pi)^4 \delta^{(4)}(k+p-q-r) \\ \times f_q^{b,\,eq} f_r^{b,\,eq}\left[|\mathcal{M}|^2_{\bar{b}\bar{b}\to bb}\, e^{\frac{-2\mu_b}{T}} - |\mathcal{M}|^2_{bb\to\bar{b}\bar{b}}\, e^{\frac{2\mu_b}{T}}\right] . \end{aligned}$$

In the limit $\mu_b/T \ll 1$ this becomes

$$\begin{aligned}
&\frac{g_b}{(2\pi)^3}\int \frac{d^3k}{E_k^b} C_k^{bb\leftrightarrow\bar{b}\bar{b}}[f^b, f^{\bar{b}}] - \frac{g_{\bar{b}}}{(2\pi)^3}\int \frac{d^3k}{E_k^{\bar{b}}} C_k^{\bar{b}\bar{b}\leftrightarrow bb}[f^{\bar{b}}, f^b] \simeq \\
&\simeq \int d\Pi_k^b\, d\Pi_p^b\, d\Pi_q^b\, d\Pi_r^b (2\pi)^4\delta^{(4)}(k+p-q-r) \\
&\quad \times f_q^{b,\,eq} f_r^{b,\,eq} \left\{ \left[|\mathcal{M}|^2_{\bar{b}\bar{b}\to bb} - |\mathcal{M}|^2_{bb\to\bar{b}\bar{b}} \right] - \frac{2\mu_b}{T}\left[|\mathcal{M}|^2_{\bar{b}\bar{b}\to bb} + |\mathcal{M}|^2_{bb\to\bar{b}\bar{b}} \right] \right\} .
\end{aligned} \tag{2.33}$$

We can write the second term as

$$-\frac{4\mu_b}{T}\langle\sigma\,|v|\rangle\,(n_b^{eq})^2\,, \tag{2.34}$$

with cross section times velocity averaged

$$\langle\sigma\,|v|\rangle = \frac{1}{(n_b^{eq})^2}\int d\Pi_k^b\, d\Pi_p^b\, d\Pi_q^b\, d\Pi_r^b (2\pi)^4\delta^{(4)}(k+p-q-r)\,|\mathcal{M}|^2_{bb\to\bar{b}\bar{b}}\, e^{-(E_k^b+E_p^b)/T} . \tag{2.35}$$

With $|\mathcal{M}|^2_{\bar{b}\bar{b}\to bb} = |\mathcal{M}|^2_{bb\to\bar{b}\bar{b}}$ the first term in eqn. (2.33) vanishes. Summing the remaining contributions eqn. (2.31) and (2.34) we see that an asymmetry is created even in thermal equilibrium. Because the decay $\psi_1 \to bb$ is preferred over the decay $\psi_1 \to \bar{b}\bar{b}$ according to eqn. (2.21a) and the inverse decay $bb \to \psi_1$ is suppressed compared to the decay, according to eqn. (2.21b), this is clear even without integrating the Boltzmann equations. The (well-known) reason for this problem [62] is that the current approximation of the amplitudes found in section 2.2 is inconsistent. The matrix elements for the processes $bb \to \bar{b}\bar{b}$ ($\bar{b}\bar{b} \to bb$) include s-channel processes in which ψ_1 can be in real intermediate (on-shell) states. This process is already taken into account by successive inverse decay and decay $bb \to \psi_1 \to \bar{b}\bar{b}$ ($\bar{b}\bar{b} \to \psi_1 \to bb$). This issue is usually called the *double counting problem*. Consequently *the real intermediate state* (RIS) contributions need to be subtracted from the complete amplitude $|\mathcal{M}|^2_{bb\to\bar{b}\bar{b}}$ ($|\mathcal{M}|^2_{\bar{b}\bar{b}\to bb}$). In the narrow width approximation these contributions are given by

$$\begin{aligned}
|\mathcal{M}|^2_{bb\to\bar{b}\bar{b},\,\mathrm{RIS}} &= \left| \mathcal{M}_{bb\to\psi_1} \frac{i}{s - m^2_{\psi_1} + i m_{\psi_1}\Gamma_{\psi_1}} \mathcal{M}_{\psi_1\to\bar{b}\bar{b}} \right|^2 \\
&= |\mathcal{M}|^2_{bb\to\psi_1}\,|\mathcal{M}|^2_{\psi_1\to\bar{b}\bar{b}}\,\frac{1}{(s-m_{\psi_1})^2 + (m_{\psi_1}\Gamma_{\psi_1})^2} \\
&\to |\mathcal{M}|^4_{\psi_1\to\bar{b}\bar{b}}\,\frac{\pi}{m_{\psi_1}\Gamma_{\psi_1}}\delta(s-m^2_{\psi_1})\,,
\end{aligned} \tag{2.36a}$$

and, analogously,

$$|\mathcal{M}|^2_{\bar{b}\bar{b}\to bb,\,\mathrm{RIS}} = |\mathcal{M}|^4_{\psi_1\to bb}\,\frac{\pi}{m_{\psi_1}\Gamma_{\psi_1}}\delta(s-m^2_{\psi_1})\,. \tag{2.36b}$$

The RIS-subtracted amplitudes for 2-2 scattering are then given by[15]

$$|\mathcal{M}|'^2_{\bar{b}\bar{b}\to bb} = |\mathcal{M}|^2_{\bar{b}\bar{b}\to bb} - 2\,|\mathcal{M}|^2_{\bar{b}\bar{b}\to bb,\,\mathrm{RIS}}\,, \tag{2.37a}$$

[15] We need to include here an additional factor of 2 which is absent in the case of leptogenesis. This is due to the fact that the collision term for the RIS term has an extra symmetrization factor $1/2$ in the toy model which is absent in the case of leptogenesis where the initial and final state of the RIS contribution each include two different species.

$$|\mathcal{M}|^{\prime 2}_{bb\to\bar{b}\bar{b}} = |\mathcal{M}|^2_{bb\to\bar{b}\bar{b}} - 2\,|\mathcal{M}|^2_{bb\to\bar{b}\bar{b},\,\mathrm{RIS}}\ . \tag{2.37b}$$

In contrast to the full matrix element for $2-2$ scattering eqn. (2.8) these amplitudes do violate CP. To obtain the rate equations corresponding to the RIS subtracted Boltzmann equations we need to substitute $|\mathcal{M}|^2_{\bar{b}\bar{b}\to bb} \to |\mathcal{M}|^{\prime 2}_{\bar{b}\bar{b}\to bb}$ and $|\mathcal{M}|^2_{bb\to\bar{b}\bar{b}} \to |\mathcal{M}|^{\prime 2}_{bb\to\bar{b}\bar{b}}$ in eqn. (2.33). Then the first term includes

$$|\mathcal{M}|^{\prime 2}_{\bar{b}\bar{b}\to bb} - |\mathcal{M}|^{\prime 2}_{bb\to\bar{b}\bar{b}} = -32\pi^2\epsilon\,|\mathcal{M}_{\psi_1}|^2\,\delta(s-m^2_{\psi_1})\,.$$

and can therefore be written as

$$-\,32\pi^2\epsilon\,|\mathcal{M}_{\psi_1}|^2\,n^{eq}_{\psi_1} I$$

with

$$I = \frac{1}{n^{eq}_{\psi_1}}\int d\Pi^b_k\,d\Pi^b_p\,d\Pi^b_q\,d\Pi^b_r(2\pi)^4\delta^{(4)}(k+p-q-r)\delta(s-m^2_{\psi_1})e^{-(E^b_k+E^b_p)/T}\,. \tag{2.38}$$

It can be shown that

$$I = \frac{1}{16\pi^2\,|\mathcal{M}_{\psi_1}|^2}\,\langle\Gamma_{\psi_1}\rangle\ .$$

Therefore, the contribution from the first term of eqn. (2.33) is $-2\epsilon\,\langle\Gamma_{\psi_1}\rangle\,n^{eq}_{\psi_1}$. After substituting $|\mathcal{M}|^2 \to |\mathcal{M}|^{\prime 2}$ the second term becomes

$$-\,\frac{4\mu_b}{T}\,\langle\sigma'\,|v|\rangle\,(n^{eq}_b)^2\,, \tag{2.39}$$

where we defined the averaged cross section times velocity (with real intermediate state contributions subtracted) analogous to eqn. (2.34) by

$$\begin{aligned}\langle\sigma'\,|v|\rangle = \frac{1}{(n^{eq}_b)^2}\int d\Pi^b_k\,d\Pi^b_p\,d\Pi^b_q\,d\Pi^b_r(2\pi)^4\delta^{(4)}(k+p-q-r)e^{-(E^b_k+E^b_p)/T}\\ \times\left[|\mathcal{M}|^2_{bb\to\bar{b}\bar{b}} - \frac{\pi}{2m_{\psi_1}\Gamma_{\psi_1}}\,|\mathcal{M}_{\psi_1}|^4\,\delta(s-m^2_{\psi_1})\right]\,.\end{aligned} \tag{2.40}$$

Using $2\mu_b/T \simeq n_B/n^{eq}_b$ we find

$$\frac{dn_B}{dt} + 3Hn_B = \langle\Gamma_{\psi_1}\rangle\,\epsilon\big[n_{\psi_1} - n^{eq}_{\psi_1}\big] - n_B\Big(\,\langle\Gamma_{\psi_1}\rangle\,\frac{n^{eq}_{\psi_1}}{n^{eq}_b} + 2n^{eq}_b\,\langle\sigma'\,|v|\rangle\,\Big)\,. \tag{2.41}$$

With help of eqn. (2.23) we obtain from eqn. (2.27) and (2.41)

$$\frac{dY_{\psi_1}}{dx} = -\,\frac{\langle\Gamma_{\psi_1}\rangle}{2H(x)x}\left[Y_{\psi_1} - Y^{eq}_{\psi_1}\right]\,, \tag{2.42a}$$

$$\frac{dY_B}{dx} = \frac{\langle\Gamma_{\psi_1}\rangle}{H(x)x}\epsilon\left[Y_{\psi_1} - Y^{eq}_{\psi_1}\right] - \frac{\langle\Gamma_{\psi_1}\rangle\,\frac{n^{eq}_{\psi_1}}{n^{eq}_b} + 2\,\langle\sigma'\,|v|\rangle\,n^{eq}_b}{H(x)x}Y_B\,. \tag{2.42b}$$

These equations are very similar to the phenomenological rate eqns. (1.16) for thermal leptogenesis, especially when the lepton number violating scattering terms S are neglected (which is approximately possible in the strong washout regime). Its interpretation is essentially the same. Here only decays and inverse decays contribute to the generation of the asymmetry. The second term on the right-hand side of eqn. (2.42b) acts as washout term.

To see explicitly when and why the RIS subtraction in eqn. (2.37) works one can exploit the unitarity of the S-matrix. We want to check whether the difference of eqn. (2.29), eqn. (2.32) and the corresponding terms for $\bar{b}$ in equilibrium:

$$\begin{aligned}
-2\int d\Pi_k^b\, d\Pi_p^b\, d\Pi_q^{\psi_1}(2\pi)^4\delta^{(4)}(k+p-q)& \\
\times(1-\xi^b f_k^b)(1-\xi^b f_p^b) f_q^{\psi_1}&\left[|\mathcal{M}|^2_{bb\to\psi_1}-|\mathcal{M}|^2_{\bar{b}\bar{b}\to\psi_1}\right] \\
-2\int d\Pi_k^b\, d\Pi_p^b\, d\Pi_q^b\, d\Pi_r^b(2\pi)^4\delta^{(4)}(k+p-q-r)& \\
\times(1-\xi^b f_k^b)(1-\xi^b f_p^b) f_q^{\bar{b}} f_r^{\bar{b}}\frac{1}{2}&\left[|\mathcal{M}|^2_{bb\to\bar{b}\bar{b}}-|\mathcal{M}|^2_{\bar{b}\bar{b}\to bb}\right], \qquad (2.43)
\end{aligned}$$

which is the right-hand side of the rate equation for n_B in equilibrium (here CPT-invariance was used), vanishes as required by the argument given in eqn. (1.3). To this end, we apply the generalized optical theorem eqn. (C.1) above the energy thresholds $s > m^2_{\psi_i}$ and $s > 4m_b^2 = 4m_{\bar{b}}^2$ to the amplitudes for $bb \to bb$ and $\bar{b}\bar{b} \to \bar{b}\bar{b}$ at order $\mathcal{O}(g^4)$. Summing the corresponding graphs in fig. 2.4 and fig. 2.5 we find for $bb \to bb$:

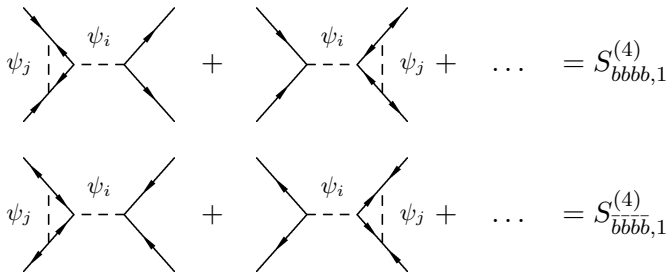

Figure 2.4: Vertex corrected graphs contributing to $\mathcal{M}_{bb\to bb}$ and $\mathcal{M}_{\bar{b}\bar{b}\to\bar{b}\bar{b}}$ at order $\mathcal{O}(g^4)$. The sums include all possible combinations of i and j.

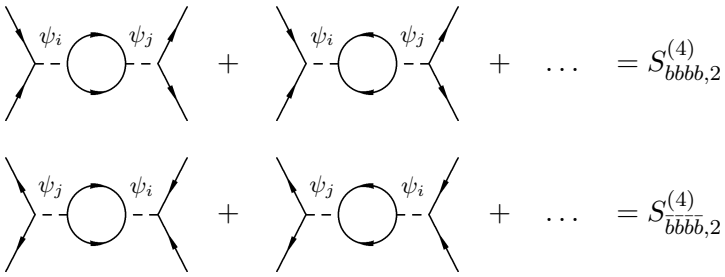

Figure 2.5: self-energy loop corrected graphs contributing to $\mathcal{M}_{bb\to bb}$ and $\mathcal{M}_{\bar{b}\bar{b}\to\bar{b}\bar{b}}$ at $\mathcal{O}(g^4)$. The diagrams in $S^{(4)}_{\bar{b}\bar{b}\bar{b}\bar{b},2}$ cancel the contributions in $S^{(4)}_{bbbb,2}$. The sums include all possible combinations of i and j.

$$\begin{aligned}
-i\left[\mathcal{M}^{(4)}_{bb\to bb}(k,p;k,p)-\mathcal{M}^{(4)*}_{bb\to bb}(k,p;k,p)\right] &= \\
= \int d\Pi_q^{\psi_1}(2\pi)^4\delta^{(4)}(k+p-q)\,|\mathcal{M}|^2_{bb\to\psi_1}(k,p;q)& \\
+\int d\Pi_q^b\, d\Pi_r^b(2\pi)^4\delta^{(4)}(k+p-q-r)\frac{1}{2}\,|\mathcal{M}|^2_{bb\to\bar{b}\bar{b}}(k,p;q,r)& \quad (2.44)
\end{aligned}$$

In the same way one finds for $\bar{b}\bar{b} \leftrightarrow \bar{b}\bar{b}$

$$\begin{aligned} -i\Big[\mathcal{M}^{(4)}_{\bar{b}\bar{b}\to\bar{b}\bar{b}}(k,p;q,r) - \mathcal{M}^{(4)*}_{\bar{b}\bar{b}\to\bar{b}\bar{b}}(k,p;q,r)\Big] = \\ = \int d\Pi^{\psi_1}_q (2\pi)^4 \delta^{(4)}(k+p-q)\, |\mathcal{M}|^2_{\bar{b}\bar{b}\to\psi_1}(k,p;q) \\ + \int d\Pi^b_q\, d\Pi^b_r (2\pi)^4 \delta^{(4)}(k+p-q-r) \frac{1}{2} |\mathcal{M}|^2_{\bar{b}\bar{b}\to bb}(k,p;q,r)\,. \end{aligned} \tag{2.45}$$

Subtracting eqn. (2.45) from eqn. (2.45) we obtain

$$\begin{aligned} -2i\Big[\Im\big\{\mathcal{M}^{(4)}_{bb\to bb}(k,p;k,p)\big\} - \Im\big\{\mathcal{M}^{(4)}_{\bar{b}\bar{b}\to\bar{b}\bar{b}}(k,p;k,p)\big\}\Big] = \\ = \int d\Pi^{\psi_1}_q (2\pi)^4 \delta^{(4)}(k+p-q)\big[\,|\mathcal{M}|^2_{bb\to\psi_1}(k,p;q) - |\mathcal{M}|^2_{\bar{b}\bar{b}\to\psi_1}(k,p;q)\big] \\ + \int d\Pi^b_q\, d\Pi^b_r (2\pi)^4 \delta^{(4)}(k+p-q-r) \frac{1}{2}\big[\,|\mathcal{M}|^2_{bb\to\bar{b}\bar{b}}(k,p;q,r) - |\mathcal{M}|^2_{\bar{b}\bar{b}\to bb}(k,p;q,r)\big]\,. \end{aligned} \tag{2.46}$$

Being a direct consequence of the unitarity of the S-matrix (necessary for the preservation of probability) this equation must hold for a consistent approximation of the amplitudes. Now the left-hand side of eqn. (2.46) equals zero, because the diagrams cancel pairwise $S^{(4)}_{bbbb,l}(k,p;k,p) = S^{(4)}_{\bar{b}\bar{b}\bar{b}\bar{b},l}(k,p;k,p)$ and $\big(S^{(4)}_{bbbb,l}(k,p;k,p)\big)^* = \big(S^{(4)}_{\bar{b}\bar{b}\bar{b}\bar{b},l}(k,p;k,p)\big)^*$, see fig. 2.4 and fig. 2.5. Multiplying eqn. (2.46) by $f^{b,eq}_k f^{b,eq}_p$ (Maxwell–Boltzmann equilibrium distributions) and integrating over $d\Pi^b_k$ and $d\Pi^b_p$ we find

$$\begin{aligned} 0 = \int d\Pi^b_k\, d\Pi^b_p\, d\Pi^{\psi_1}_q (2\pi)^4 \delta^{(4)}(k+p-q) f^{\psi_1,eq}_q \big[\,|\mathcal{M}|^2_{bb\to\psi_1}(k,p;q) - |\mathcal{M}|^2_{\bar{b}\bar{b}\to\psi_1}\,\big] \\ + \int d\Pi^b_k\, d\Pi^b_p\, d\Pi^b_q\, d\Pi^b_r (2\pi)^4 \delta^{(4)}(k+p-q-r) f^{b,eq}_q f^{b,eq}_r \frac{1}{2}\big[\,|\mathcal{M}|^2_{bb\to\bar{b}\bar{b}} - |\mathcal{M}|^2_{\bar{b}\bar{b}\to bb}\,\big]\,, \end{aligned} \tag{2.47}$$

where we have used that the species are in thermal equilibrium. Comparing eqn. (2.47) with eqn. (2.43), we see that the equilibrium contributions from scattering and decays cancel exactly if the species are assumed to obey Maxwell–Boltzmann statistics. In this case, no asymmetry is generated in thermal equilibrium. On the other hand, it is clear from this comparison that the cancellation cannot be exact if the quantum statistical terms are included. Therefore, the question arises how consistent Boltzmann equations can be obtained in this case. We will see that it can be answered in the top-down approach.

2.5 CP-violating parameter

To complete the discussion of the bottom-up approach we need to compute the CP-violating parameter in vacuum defined in eqn. (2.4). As in the phenomenological scenario, it is generated by the interference of the tree-level and one-loop amplitudes, see fig. 3.8. The result of this computation is well-known but we repeat it here for the vertex contribution, since we will need to perform similar calculations later. According to eqn. (1.12) the contributions of the interference

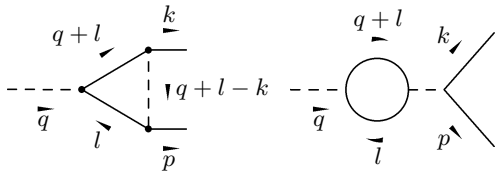

Figure 2.6: Momentum flow in the vertex and the self-energy loop.

terms (between tree-level and vertex or self-energy loop corrections) to the CP-violating parameter are given by

$$\epsilon_i^{vac} = -2\,|g_j|^2\,\Im\Big\{\frac{g_i g_j^*}{g_i^* g_j}\Big\}\Im\Big\{\frac{S^{(3)}_{\psi_i bb}}{g_i (g_j^*)^2}\Big\}\,.$$

The contribution of the vertex loop diagram to the amplitude can be written as

$$iS^{(3)}_{\psi_i bb1} = \frac{-ig_i(g_j^*)^2}{16\pi^2} C_0(q^2, k^2, 0, 0, m^2_{\psi_j})\,, \tag{2.48}$$

where the scalar 1-loop vertex three-point function C_0 is given by [63, 64]:

$$\begin{aligned} &C_0(q^2, k^2, m_b^2, m_b^2, m^2_{\psi_j}) = \\ &\qquad = -\frac{i}{\pi^2}\int d^4l \frac{1}{(q+l)^2 - m_b^2 + i\epsilon}\frac{1}{l^2 - m_b^2 + i\epsilon}\frac{1}{(q+l-k)^2 - m^2_{\psi_j} + i\epsilon}\,. \end{aligned} \tag{2.49}$$

The assignment of the momenta is depicted in fig. 2.6. The tree-level and one-loop amplitudes of the decay process $\psi \to \bar{b}\bar{b}$ differ from eqn. (2.48) only by conjugation of the couplings. Therefore, at leading order, we obtain for the CP-violating parameter:

$$\epsilon_i^{V,vac} = \frac{|g_j|^2}{8\pi^2}\Im\left(\frac{g_i g_j^*}{g_i^* g_j}\right)\Im\Big\{C_0(q^2, k^2, 0, 0, m^2_{\psi_j})\Big\}\,. \tag{2.50}$$

The imaginary part of the loop integral $C_0(q^2, k^2, m_b^2, m_b^2, m^2_{\psi_j})$ is caused by a branch cut discontinuity above the threshold $q_0 > 2m_b$ when the two b propagators in the loop go on-shell. We can in principle compute ϵ_i^{vac} by first computing the vertex loop integral C_0 and then taking the imaginary part. C_0 can be calculated by introducing Feynman parameters [63, 64] in eqn. (2.49). The result in the massless limit, $m_b = 0$, reads

$$C_0(m^2_{\psi_i}, 0, 0, 0, m^2_{\psi_j}) = \frac{1}{m^2_{\psi_i}}\left[\mathrm{Li}_2\left(1 + \frac{m^2_{\psi_i}}{m^2_{\psi_j}}\right) - \frac{\pi^2}{6}\right]\,. \tag{2.51}$$

With dilogarithm Li_2 as defined in [64] the imaginary part of this coincides with eqn. (2.61). For $\epsilon_i^{V,vac}$ we obtain

$$\epsilon_i^{V,vac} = -\frac{1}{8\pi}\frac{|g_j|^2}{m^2_{\psi_i}}\Im\left(\frac{g_i g_j^*}{g_i^* g_j}\right)\ln\left(1 + \frac{m^2_{\psi_i}}{m^2_{\psi_j}}\right)\,. \tag{2.52}$$

Identifying the imaginary part of C_0 as branch cut discontinuity, $\mathrm{Disc}C_0 = 2i\Im\{C_0\}$, we can alternatively evaluate it with help of the Cutkosky cutting rules (see appendix C) as

$$\mathrm{Disc}C_0 = C_0'(q^2, k^2, m_b^2, m_b^2, m^2_{\psi_j})\,, \tag{2.53}$$

with

$$C_0'(q^2,k^2,m_b^2,m_b^2,m_{\psi_j}^2) = -\frac{i}{\pi^2}\int d^4l\left[-2\pi i\Theta(q_0+l_0)\delta((q+l)^2-m_b^2)\right] \times\left[-2\pi i\Theta(-l_0)\delta(l^2-m_b^2)\right]\frac{1}{(q+l-k)^2-m_{\psi_j}^2+i\epsilon}\,. \tag{2.54}$$

Using $\delta(x^2-a^2)=(2\,|a|)^{-1}(\delta(x-a)+\delta(x+a))$ we find

$$C_0' = \int d^4l\frac{1}{E_{q+l}^b}\left[\delta(q_0+l_0-E_{q+l}^b)+\delta(q_0+l_0+E_{q+l}^b)\right] \times\frac{1}{E_q^b}\left[\delta(l_0-E_l^b)+\delta(l_0+E_l^b)\right]G_{q+l-k}^{\psi_j}\,. \tag{2.55}$$

with $G_p^{\psi_j}=i/[p^2-m_{\psi_j}^2+i\epsilon]$, where we can drop the $i\epsilon$ prescription in the propagator because ψ_j cannot go on-shell. Since the expression is Lorentz invariant we can evaluate it in the CMS frame ($\mathbf{q}=0$, $E_{q+l}^b=E_l^b$). In this frame it is easy to see that

$$C_0' = \int\frac{d^4l}{(E_l^b)^2}\delta(q_0+l_0-E_l^b)\delta(l_0+E_l^b)G_{q+l-k}^{\psi_j}\,. \tag{2.56}$$

Upon integration over l_0 this becomes

$$C_0' = \int\frac{d^3l}{(E_l^b)^2}\delta(q_0-2E_l^b)G_{q+l-k}^{\psi_j}\Big|_{l_0=-E_l^b} = \int\frac{d\Omega_l\,dE_l^b\,|\mathbf{l}|}{2E_l^b}\delta\big(\frac{q_0}{2}-E_l^b\big)G_{q+l-k}^{\psi_j}\Big|_{l_0=-E_l^b}\,, \tag{2.57}$$

which evaluates to

$$C_0' = \int\frac{d\Omega_l\,|\mathbf{l}|}{2E_l^b}G_{q+l-k}^{\psi_j}\Big|_{l_0=-\frac{q_0}{2},\,|\mathbf{l}|=\sqrt{l_0^2-m_b^2}}\,. \tag{2.58}$$

In the CMS frame we have $(q+l-k)^2\big|_{l_0=-k_0=-\frac{q_0}{2}} = -2\,|\mathbf{l}|^2\,(1-\cos\theta_{kl})$ and

$$G_{q+l-k}^{\psi_j} = \frac{i}{-2\,|\mathbf{l}|^2\,(1+\frac{m_{\psi_j}^2}{2|\mathbf{l}|^2}-\cos\theta_{kl})}\,,$$

where, here and in the following, we always imply $|\mathbf{l}|=\sqrt{\big(\frac{q_0}{2}\big)^2-m_b^2}$. With this we find

$$C_0' = \frac{-i}{4\,|\mathbf{l}|\,E_l^b}\int\frac{d\phi_l\,d\cos\theta_l}{1+\frac{m_{\psi_j}^2}{2|\mathbf{l}|^2}-\cos\theta_{kl}} = \frac{-i\pi}{2\,|\mathbf{l}|\,E_l^b}\int_{-1}^{1}\frac{d\cos\theta_l}{1+\frac{m_{\psi_j}^2}{2|\mathbf{l}|^2}-\cos\theta_l}\,. \tag{2.59}$$

Performing the remaining integral we get

$$C_0' = -\frac{i\pi}{2\,|\mathbf{l}|\,E_l^b}\ln\left(1+\frac{4\,|\mathbf{l}|^2}{m_{\psi_j}^2}\right)\,. \tag{2.60}$$

Inserting the expression for $|\mathbf{l}|$ and $q_0 = m_{\psi_i}$ we obtain

$$C_0'(m_{\psi_i}^2, m_b^2, m_b^2, m_b^2, m_{\psi_j}^2) = -\frac{2\pi i}{m_{\psi_i}\sqrt{m_{\psi_i}^2 - 4m_b^2}} \ln\left(1 + \frac{m_{\psi_i}^2 - 4m_b^2}{m_{\psi_j}^2}\right), \tag{2.61}$$

which leads directly to eqn. (2.52) if we set $m_b = 0$. This result is, of course, well known. We have repeated the computation here in order to illustrate the connection with the cutting rules at finite temperature given in chapter 4. In the same place we will also obtain the result for the self-energy loop contribution to the CP-violating parameter as zero temperature limit of the general case. It reads

$$\epsilon_i^{S,vac} = -\frac{|g_j|^2}{16\pi} \Im\left(\frac{g_i g_j^*}{g_i^* g_j}\right) \frac{1}{m_{\psi_i}^2 - m_{\psi_j}^2}\,. \tag{2.62}$$

It is well known that this expression can be used only in the hierarchical case. The case $m_{\psi_i} \simeq m_{\psi_j}$ corresponds to the scenario of resonant leptogenesis. Note that in the strongly hierarchical case $m_{\psi_j} \gg m_{\psi_i}$ the contributions eqn. (2.52) and eqn. (2.62) differ by just a factor of 2 and the sum of both contributions gives

$$\epsilon_i^{vac} = \epsilon_i^{V,vac} + \epsilon_i^{S,vac} \simeq \frac{3}{16\pi} \frac{\Im\{(g_i^* g_j)^2\}}{|g_i|^2} \frac{1}{m_{\psi_j}^2}\,. \tag{2.63}$$

Note the similarity to CP-violating parameter in the phenomenological scenario eqn. (1.15).

In this chapter we have established the similarity between the toy model and and the scenario of thermal leptogenesis with respect to the source of the CP-violation and the kinetic equations. At the same time we have seen that the usual rate equations are based on kinetic equations which have been developed for dilute gases and that the inclusion of the quantum statistical terms in the straight-forward way would lead to the creation of an asymmetry even in equilibrium. This and the observation that the creation of the asymmetry via leptogenesis depends crucially on the loop contributions to the amplitudes, which are inherently quantum effects encourage us to study the toy model of the present section in the framework of non-equilibrium quantum field theory.

Chapter 3

Top-down approach

The goal of this chapter is to derive kinetic equations for the one-particle distribution functions for the toy model eqn. (2.1) in the Kadanoff–Baym formalism by applying a number of well-known approximations [65–68]. Since this systematic derivation starts from complete evolution equations for the two-point functions (based on the in-in or Schwinger–Keldysh description of non-equilibrium quantum fields [69, 70]) we refer to this ansatz as top-down approach. We will denote the resulting "Boltzmann-like" equations as quantum corrected Boltzmann equations due to their similarity to the equations obtained in chapter 2. The qualitative difference with respect to the classic approach which was presented there is that the overall structure of the kinetic equations as well as the transition amplitudes are derived self-consistently from a common starting point. We will see that the top-down approach is free of the double-counting problem and that the transition amplitudes include terms which account for finite-density effects. Since, in the context of leptogenesis, the driving force for the deviation from thermal equilibrium is the rapid expansion of the universe we work in a covariant formulation [43, 71, 72].

3.1 Schwinger–Keldysh formalism in curved space-time

In this section we present the Schwinger–Keldysh formalism and the derivation of Boltzmann equations from Kadanoff-Baym equations [65–68, 73–75] in a manifestly covariant fashion [2]. To illustrate the important points, we use a model containing a single real scalar field with quartic self-interactions, minimally coupled to gravity. The results can later be applied to the toy model. Here we use the lagrangian

$$\mathscr{L} = \frac{1}{2}\partial^\mu\varphi\partial_\mu\varphi - \frac{1}{2}m^2\varphi^2 - \frac{\lambda}{4!}\varphi^4\,. \tag{3.1}$$

Since the procedure for the $\lambda\varphi^4$ theory is well known in Minkowski space-time it will be easy to compare it with the results obtained in [35, 41–44] and elsewhere.[1]

Beginning with the generating functional for connected Green's functions in covariant form, the individual steps are roughly:

- a Legendre transformation to obtain the effective action

[1] We note that a self-consistently dressed description of the vertex in $\lambda\varphi^4$ theory requires the use of the 4PI effective action, which is beyond the scope of this work.

- derivation of the Schwinger–Dyson equation
- derivation of the Kadanoff–Baym equations for the spectral function and the statistical propagator
- a first-order gradient expansion and a Wigner transformation to obtain a system of quantum kinetic equations for the correlation functions
- neglecting the Poisson brackets and employing a quasi-particle approximation to get the Boltzmann-like equation for the one-particle distribution function

If the respective requirements are met the different steps can be generalized to more sophisticated models, such as the toy model.

3.1.1 Schwinger–Dyson equations

We begin with the generating functional for Green's functions with local and bi-local external scalar sources $J(x)$ and $K(x,y)$,

$$\mathcal{Z}[J,K] = \int \mathscr{D}\varphi \, \exp\left[i(S + J\varphi + \frac{1}{2}\varphi K\varphi)\right], \tag{3.2}$$

where the action S is given by the space-time integral of the Lagrange density:

$$S = \int \sqrt{-g}d^4x \, \mathscr{L},$$

with invariant space-time volume element

$$\sqrt{-g}d^4x, \quad g \equiv \det g_{\mu\nu}. \tag{3.3}$$

The scalar products of the sources and the fields in eqn. (3.2) are defined as

$$J\varphi \equiv \int \sqrt{-g}d^4x J(x)\varphi(x), \tag{3.4a}$$

$$\varphi K\varphi \equiv \iint \sqrt{-g}d^4x\sqrt{-g}d^4y \, \varphi(x)K(x,y)\varphi(y). \tag{3.4b}$$

The path integral measure in curved space-time is given by [71]

$$\mathscr{D}\varphi = \prod_x d\left[(-g)^{\frac{1}{4}}\varphi(x)\right],$$

and the fields and external sources are defined independently on the positive and negative branches of a closed real-time contour, see fig. 3.1. In particular, there are two local (J_+ and J_-) and four bi-local (K_{++}, K_{+-}, K_{-+} and K_{--}) sources. Analogously, the field expectation values on the two branches are denoted by φ_+ and φ_- and the components of the two-point function by G_{++}, G_{+-}, G_{-+} and G_{--} [76]. This applies also to the metric tensor, i.e. $g^+_{\mu\nu} \neq g^-_{\mu\nu}$ in general. In our notation the branch indices are suppressed.

As explained in chapter 2.3, the effect of the individual fields on the curvature of space-time was neglected in the bottom-up approach and we make the same test-field approximation here.

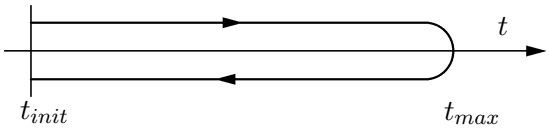

Figure 3.1: Closed real-time path $\mathcal{C}$.

Analyses of this back-reaction effect have been carried out in [41, 44]. This means in particular that the metric tensor on the positive and negative branches is determined by external processes only so that it is the same on both branches.

We define a generalized Dirac-delta δ^g such that $\delta^g(x,y)$ is always zero if its arguments lie on different branches of the time-path [65] and otherwise satisfies the relation

$$\int d^4y\sqrt{-g}\, f(y)\, \delta^g(x,y) = f(x)\,, \tag{3.5}$$

where the integration is performed over the closed contour. The solution to this equation is given by [71]

$$\delta^g(x,y) = (-g_x)^{-\frac{1}{4}}\delta(x,y)(-g_y)^{-\frac{1}{4}}\,. \tag{3.6}$$

The generalized Dirac-delta is then used to define functional differentiation in curved space-time:

$$\frac{\delta\mathcal{F}[\phi]}{\delta\phi(y)} \equiv \lim_{\varepsilon\to 0}\frac{\mathcal{F}[\phi(x)+\varepsilon\,\delta^g(x,y)]-\mathcal{F}[\phi(x)]}{\varepsilon}\,. \tag{3.7}$$

Consequently, we obtain:

$$\frac{\delta J(x)}{\delta J(y)} = \delta^g(x,y)\,, \quad \frac{\delta K(x,y)}{\delta K(u,v)} = \delta^g(x,u)\delta^g(y,v)\,. \tag{3.8}$$

As usual, the generating functional for connected Green's functions is given in terms of $\mathcal{Z}[J,K]$ by

$$\mathcal{W}[J,K] = -i\ln\mathcal{Z}[J,K]\,. \tag{3.9}$$

Its functional derivatives with respect to the external sources read

$$\frac{\partial\mathcal{W}[J,K]}{\partial J(x)} = \Phi(x)\,, \quad \frac{\partial\mathcal{W}[J,K]}{\partial K(x,y)} = \frac{1}{2}[G(y,x)+\Phi(x)\Phi(y)]\,, \tag{3.10a}$$

where Φ denotes expectation value of the field and G is the propagator. The *two-particle-irreducible (2PI) effective action* is defined as the (functional) Legendre transform of $\mathcal{W}[J,K]$:

$$\Gamma[\Phi,G] \equiv \mathcal{W}[J,K] - J\Phi - \frac{1}{2}\mathrm{Tr}[KG] - \frac{1}{2}\Phi K\Phi\,. \tag{3.11}$$

Analogously to the conventional Legendre transform the external sources can be reproduced as its functional derivatives with respect to the expectation value and the propagator:

$$\frac{\delta\Gamma[G,\Phi]}{\delta\Phi(x)} = -J(x) - \int\sqrt{-g}d^4z\; K(x,z)\Phi(z)\,, \tag{3.12a}$$

$$\frac{\delta\Gamma[G,\Phi]}{\delta G(x,y)} = -\frac{1}{2}K(y,x)\,. \tag{3.12b}$$

When we shift the field by its expectation value $\varphi \to \varphi + \Phi$ we can write the action as a sum of two terms:

$$S[\varphi] \to S_{cl}[\Phi] + S[\varphi, \Phi]\,, \tag{3.13}$$

where S_{cl} denotes the classical action, which depends only on Φ and $S[\varphi, \Phi] = S_0[\varphi] + S_{int}[\varphi, \Phi]$ contains terms quadratic, cubic and quartic in φ. The free field action can be written in the form

$$S_0 = \frac{1}{2}\iint \sqrt{-g_x} d^4x \sqrt{-g_y} d^4y\, \varphi \left(i\mathscr{G}^{-1}\right) \varphi\,, \tag{3.14}$$

where $\mathscr{G}^{-1}$ is the zero-order inverse propagator

$$\mathscr{G}^{-1}(x, y) = i(\Box_x + m^2)\, \delta^g(x, y)\,, \tag{3.15}$$

with $\Box_x \equiv g_{\mu\nu}\nabla_x^\mu \nabla_x^\nu$. Now we can exploit the translational invariance of the path integral measure to rewrite the effective action as

$$\Gamma[\Phi, G] = -\,i \ln \int \mathscr{D}\varphi \exp\left[i(S + J\varphi + \frac{1}{2}\varphi K \varphi)\right] + S_{cl}[\Phi] - \frac{1}{2}\mathrm{Tr}[KG]\,. \tag{3.16}$$

We define the *2PI functional* Γ_2 by writing Γ in the form

$$\Gamma[\Phi, G] \equiv S_{cl}[\Phi] + \frac{i}{2}\ln\det\left[G^{-1}\right] + \frac{i}{2}\mathrm{Tr}\left[\mathscr{G}^{-1}G\right] + \Gamma_2[\Phi, G]\,. \tag{3.17}$$

The second and third term are given by

$$\det\left[\frac{G^{-1}}{2\pi}\right] \equiv \int \mathscr{D}\varphi \exp\left(\varphi\, G^{-1} \varphi\right)$$

and

$$\mathrm{Tr}\left[\mathscr{G}^{-1}G\right] \equiv \iint \sqrt{-g_x} d^4x \sqrt{-g_y} d^4y\, \mathscr{G}^{-1}(x, y) G(y, x)\,,$$

respectively. We are interested in finding the functional derivative of Γ_2 with respect to G. It can be obtained by using eqn. (3.12) and computing the derivatives of the second and third term. The functional derivative of the second term can be found upon use of

$$\int \sqrt{-g}\, d^4z\, G^{-1}(u, z) G(z, v) = \delta^g(u, v)\,. \tag{3.18}$$

The result of this calculation is

$$\frac{\delta}{\delta G(x, y)} \ln\det\left[G^{-1}\right] = -G^{-1}(y, x)\,. \tag{3.19}$$

Differentiating the third term of eqn. (3.17) we find

$$\frac{\delta}{\delta G(x, y)}\mathrm{Tr}\left[\mathscr{G}^{-1}G\right] = \mathscr{G}^{-1}(y, x)\,. \tag{3.20}$$

The functional derivative of the complete eqn. (3.17) with respect to G then reads

$$\frac{\delta\Gamma[G,\Phi]}{\delta G(x,y)} = -\frac{i}{2}G^{-1}(y,x) + \frac{i}{2}\mathscr{G}^{-1}(y,x) + \frac{\delta\Gamma_2[G,\Phi]}{\delta G(x,y)} = -\frac{1}{2}K(y,x)\,. \tag{3.21}$$

Substituting this expression for K into eqn. (3.17) we can rewrite the 2PI effective action in the form

$$\begin{aligned}\Gamma_2[G,\Phi] = &-i\ln\int\mathscr{D}\varphi\exp\left[i\left(S + J\varphi - \varphi\frac{\delta\Gamma_2}{\delta G}\varphi\right)\right]\\ &+\mathrm{Tr}\left[\frac{\delta\Gamma_2}{\delta G}G\right] - \frac{i}{2}\ln\det\left[G^{-1}\right] + \mathrm{const}\,.\end{aligned} \tag{3.22}$$

Here $S = S_0 + S_{int}$, but S_0 is now given by

$$S_0 = \frac{1}{2}\iint\sqrt{-g}_x d^4x\sqrt{-g}_y d^4y\,\varphi\left(iG^{-1}\right)\varphi\,. \tag{3.23}$$

The functional $i\Gamma_2$ is represented by the sum of all vacuum diagrams, which cannot be disconnected by cutting any two internal lines [77]. The vertices as given by $\mathscr{L}_{int}$ and the internal lines represent the complete connected propagator G. Hence the name two-particle-irreducible.

We are interested in physical situations corresponding to vanishing sources. In this case eqn. (3.21) can be written in the form

$$G^{-1}(x,y) = \mathscr{G}^{-1}(x,y) - \Pi(x,y)\,, \tag{3.24}$$

where we defined the *self-energy* Π as

$$\Pi(x,y) \equiv 2i\frac{\delta\Gamma_2[G,\Phi]}{\delta G(y,x)}\,. \tag{3.25}$$

Equation (3.24) is the *Schwinger–Dyson equation*. The structure of this equations is completely determined by the particle content of the theory.

3.1.2 2PI effective action

The 2PI effective action is given by the (infinite) sum of all 2PI diagrams which can be drawn given the set of vertices defined by the interaction lagrangian and the set of internal lines representing the complete connected two-point functions. We write the 2PI effective action as

$$i\Gamma_2[G] = \sum_n i\Gamma_2^{(n)}[G]\,,$$

and consider the lowest order contributions $\Gamma_2^{(2)}$, $\Gamma_2^{(3)}$ and $\Gamma_2^{(4)}$ given by the diagrams in fig. 3.2. The expressions for these contributions differ from those given in [34, 35, 43, 78] by the presence of $\sqrt{-g}$ factors which ensure invariance of the effective action under coordinate transformations:

$$\begin{aligned}i\Gamma_2^{(2)}[G] &= -\frac{i\lambda}{8}\int\sqrt{-g}_x d^4x\,G^2(x,x),\\ i\Gamma_2^{(3)}[G] &= -\frac{\lambda^2}{48}\int\sqrt{-g}_x d^4x\sqrt{-g}_y d^4y\,G^2(x,y)G^2(y,x),\\ i\Gamma_2^{(4)}[G] &= \frac{i\lambda^3}{48}\int\sqrt{-g}_x d^4x\sqrt{-g}_y d^4y\sqrt{-g}_z d^4z G^2(y,x)G^2(x,z)G^2(z,y).\end{aligned} \tag{3.26}$$

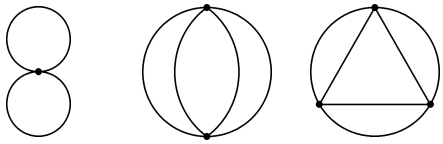

(a) (b) (c)

Figure 3.2: Two–, three–, and four-loop contributions, $i\Gamma_2^{(2)}$ (a), $i\Gamma_2^{(3)}$ (b) and $i\Gamma_2^{(4)}$ (c) to the 2PI effective action in the scalar φ^4 theory.

We use the definition of the self-energy eqn. (3.25) and the functional differentiation rule and split the self-energy also into the contributions from the different loop orders:

$$\Pi(x,y) = \sum_n \Pi^{(n)}(x,y)\,. \tag{3.27}$$

For each vertex in the loop diagrams there is a corresponding integral in the effective action. The functional differentiation leads to the appearance of two Dirac-delta's due to which two of the integrals can be carried out trivially. Four- and higher-loop contributions to Γ_2 contain more than two integrations over space-time. This means that the corresponding contributions to Π contain such integrals as well. The different contributions corresponding to the terms in eqn. (3.26) are:

$$\begin{aligned}
\Pi^{(2)}(x,y) =& -i\delta^g(x,y)\frac{\lambda}{2}G(x,x)\,,\\
\Pi^{(3)}(x,y) =& -\frac{\lambda^2}{6}G(y,x)G(x,y)G(x,y)\,,\\
\Pi^{(4)}(x,y) =& \frac{i\lambda^3}{4}G(y,x)\int\sqrt{-g_z}d^4z G^2(x,z)G^2(z,y)\,.
\end{aligned} \tag{3.28}$$

We see that, for the reason given above, the lowest order contribution $\Pi^{(2)}$, which corresponds to the two-loop diagram in fig. 3.2(a), is local and cannot describe thermalization. It will later be absorbed in the effective mass. Therefore, one usually considers also the three-loop diagram fig. 3.2(b) which describes $2-2$ scattering. The four-loop contribution fig. 3.2(c) describes one-loop corrections to $2-2$ scattering processes and was also taken into account in [2] where it led to a Boltzmann equation which includes medium corrections for the φ^4-theory. For brevity we ignore this contribution here.

3.1.3 Kadanoff–Baym equations

In order to derive evolution equations for the propagator one can convolve the Schwinger–Dyson eqns. (3.24) with G from the right and use eqn. (3.18) to obtain

$$i\big[\Box_x + m^2\big]G(x,y) = \delta^g(x,y) + \int\sqrt{-g}d^4z\,\Pi(x,z)G(z,y)\,. \tag{3.29}$$

Next, we define the *spectral function*:

$$G_\rho(x,y) \equiv i\langle[\varphi(x),\varphi(y)]_-\rangle\,, \tag{3.30}$$

and the *statistical propagator*:

$$G_F(x,y) \equiv \frac{1}{2}\langle[\varphi(x),\varphi(y)]_+\rangle\,, \tag{3.31}$$

where $[.,.]_-$ denotes the commutator and $[.,.]_+$ the anti-commutator. As is clear from the terminology G_ρ contains information about spectral properties of the system, whereas G_F contains information about its statistical state. From the definitions (3.30) and (3.31) it is also clear that the spectral function is antisymmetric with respect to permutation of its arguments, while the statistical propagator is symmetric under this transformation. Note that $G_F(x,y)$ and $G_\rho(x,y)$ are real-valued functions for a real scalar field [33]. With help of this definitions, the full Schwinger-Keldysh propagator can be decomposed into statistical and spectral part:

$$G(x,y) = G_F(x,y) - \frac{i}{2}\mathrm{sgn}_\mathcal{C}(x^0-y^0)G_\rho(x,y)\,. \tag{3.32}$$

We now insert this expression into eqn. (3.29) to obtain equations for $G_F(x,y)$ and $G_\rho(x,y)$. The action of the $\Box_x$ operator on the second term on the right-hand side of eqn. (3.32) yields the product $g^{00}\delta(x^0,y^0)\nabla_0^x G_\rho(x,y)$. Using the definition of G_ρ and the canonical commutation relations in curved space-time [79],

$$\lim_{y^0\to x^0}[\varphi(x^0,\mathbf{x}),\pi(x^0,\mathbf{y})]_- = i\delta(\mathbf{x},\mathbf{y})\,, \tag{3.33}$$

where[2] $\pi = g^{00}\sqrt{-g}\,\nabla_0\varphi$, we find for the derivative of the spectral function:

$$\nabla_0^x G_\rho(x,y) = \frac{\delta(\mathbf{x},\mathbf{y})}{g^{00}\sqrt{-g}}\,. \tag{3.34}$$

The product which appears on the right-hand side of eqn. (3.32) upon differentiation then gives the generalized Dirac-delta $\delta^g(x,y)$ which cancels the Dirac-delta on the right-hand side of eqn. (3.29). As announced, the local term from the lowest order contribution $\Pi^{(2)}$ to the self-energy (3.28), can be absorbed in an *effective mass*:

$$m^2(x) \equiv m^2 + \Pi_{loc}(x)\,. \tag{3.35}$$

In the present case we have:

$$m^2(x) = m^2 + \frac{\lambda}{2}G(x,x)\,.$$

The effective mass, which contains the local self-energy, describes mean-field effects. In analogy to eqn. (3.32), the remaining non-local part of the self-energy can also be split into a spectral part Π_ρ and a statistical part Π_F:

$$\Pi(x,y) = \Pi_F(x,y) - \frac{i}{2}\mathrm{sgn}_\mathcal{C}(x^0-y^0)\Pi_\rho(x,y)\,. \tag{3.36}$$

Now the integral in eqn. (3.29) which is along the closed time path in fig. 3.1 can be broken into different parts. Thereby we take into account that any point of the negative branch is considered as

[2] In the FRW universe we have $g_{0i}=0$. In general, the off-diagonal components of the metric tensor can always be set to zero by an appropriate choice of the coordinate system [80].

a later instant of time than any point on the positive branch. In this way we obtain the *Kadanoff–Baym equations* for the φ^4-theory:

$$\begin{aligned}\big[\Box_x + m^2(x)\big] G_F(x,y) &= \int_0^{y^0} \sqrt{-g} d^4z\, \Pi_F(x,z) G_\rho(z,y) - \int_0^{x^0} \sqrt{-g} d^4z\, \Pi_\rho(x,z) G_F(z,y)\,, \\ \big[\Box_x + m^2(x)\big] G_\rho(x,y) &= -\int_{y^0}^{x^0} \sqrt{-g} d^4z\, \Pi_\rho(x,z) G_\rho(z,y)\,. \end{aligned} \tag{3.37}$$

Comparing with the literature results [33, 35], we find that eqns. (3.37) are the covariant generalization of the corresponding Kadanoff–Baym equations in Minkowski space-time. Equations (3.37) are exact equations for the quantum dynamical evolution of the statistical propagator and the spectral function. Since these are quantum field theoretic objects, there are no inherent problems related to the definition quasi-particles. In other words, eqns. (3.37) are free of any possible uncertainties associated with definition of quasi-particle excitations in the hot plasma of the rapidly expanding universe. Furthermore, eqns. (3.37) are written in terms of *resummed* propagators, i.e. they take into account the full series of daisy and ladder diagrams. Because of the presence of the characteristic *memory integrals* on the right-hand sides the dynamics of the system depends on the complete history of its evolution [81]. The different quantities which enter the Kadanoff–Baym equations must be renormalized, which is, however, beyond the scope of this thesis. The renormalization at finite temperature has been developed in [82–85]. It has been generalized to out-of-equilibrium systems with non-Gaussian initial conditions in [86, 87]. A renormalization procedure at tadpole order in the Gaussian scheme in the expanding universe has been applied to the analysis of Kadanoff–Baym equations in [44]. The number and the precise form of the equations depends on the particle content of the theory and will be different for the toy model or for a phenomenological theory. As stated above, the spectral and statistical self-energies encode the information about the interactions of the model. Despite all advantages, the full Kadanoff–Baym equations are relatively rarely used for the analysis of out-of-equilibrium processes, partially because of the complexity of the numerical solution, see e.g. [33, 35, 36, 85, 88–92].

To complete this section we derive explicit expressions for the different components of the self-energies. Using the symmetry (anti-symmetry) of the statistical propagator (spectral function), we obtain for the three-loop contribution:

$$\Pi_F^{(3)}(x,y) = -\frac{\lambda^2}{6}\Big[G_F(x,y)G_F(x,y)G_F(x,y) - \frac{3}{4}G_F(x,y)G_\rho(x,y)G_\rho(x,y)\Big]\,, \tag{3.38a}$$

$$\Pi_\rho^{(3)}(x,y) = -\frac{\lambda^2}{6}\Big[3G_F(x,y)G_F(x,y)G_\rho(x,y) - \frac{1}{4}G_\rho(x,y)G_\rho(x,y)G_\rho(x,y)\Big]\,. \tag{3.38b}$$

Four- and higher-loop contributions to the self-energy components contain space-time integrals. The explicit results for the four-loop contributions can be found in [2].

3.1.4 Quantum kinetic equations

We proceed now with the next step towards the Boltzmann kinetic equations which consists in the derivation of quantum kinetic equations. To this end, we introduce *retarded* and *advanced*

propagators in order to decompose the spectral component of the propagator in eqns. (3.37) as follows:

$$G_R(x,y) \equiv \theta(x^0-y^0)G_\rho(x,y)\,, \quad G_A(x,y) \equiv -\theta(y^0-x^0)G_\rho(x,y)\,, \tag{3.39}$$

and, analogously, *retarded* and *advanced self-energies* for the decomposition of the spectral component of the self-energy:

$$\Pi_R(x,y) \equiv \theta(x^0-y^0)\Pi_\rho(x,y)\,, \quad \Pi_A(x,y) \equiv -\theta(y^0-x^0)\Pi_\rho(x,y)\,. \tag{3.40}$$

The retarded and advanced components of propagator and self-energy satisfy the relations

$$G_A(y,x) = G_R(x,y)\,, \quad \Pi_A(y,x) = \Pi_R(x,y)\,. \tag{3.41}$$

The Kadanoff–Baym eqns. (3.37) can then be written in the form:

$$\begin{aligned}\big[\Box_x + m^2(x)\big]G_F(x,y) = &-\int\sqrt{-g}d^4z\theta(z^0)\\ &\times\big[\Pi_F(x,z)G_A(z,y)+\Pi_R(x,z)G_F(z,y)\big]\,, \qquad (3.42a)\\ \big[\Box_x + m^2(x)\big]G_\rho(x,y) = &-\int\sqrt{-g}d^4z\theta(z^0)\\ &\times\big[\Pi_\rho(x,z)G_A(z,y)+\Pi_R(x,z)G_\rho(z,y)\big]\,. \qquad (3.42b)\end{aligned}$$

The system (3.42) must be supplemented by equations for the retarded and advanced propagators which can be derived from the second of eqns. (3.37) upon use of eqn. (3.34):

$$\big[\Box_x + m^2(x)\big]G_A(x,y) = \delta^g(x,y) - \int\sqrt{-g}d^4z\,\Pi_A(x,z)G_A(z,y)\,, \tag{3.43a}$$

$$\big[\Box_x + m^2(x)\big]G_R(x,y) = \delta^g(x,y) - \int\sqrt{-g}d^4z\,\Pi_R(x,z)G_R(z,y)\,. \tag{3.43b}$$

We are free to interchange x and y on both sides of the Kadanoff–Baym equations. The difference and the sum of the original eqns. (3.42) and the equations resulting after this substitution are referred to as the *quantum kinetic equations* and *constraint equations* (for the statistical propagator and the spectral function), respectively. Using eqn. (3.41) and the symmetry properties of the statistical propagator and the spectral function we obtain:

$$\begin{aligned}\big[\Box_x \mp \Box_y + m^2(x) \mp m^2(y)\big]G_F(x,y) = &\\ = -\int\sqrt{-g}d^4z\theta(z^0)\big[&\Pi_F(x,z)G_A(z,y) \mp G_R(x,z)\Pi_F(z,y)\\ &+\Pi_R(x,z)G_F(z,y) \mp G_F(x,z)\Pi_A(z,y)\big]\,, \qquad (3.44a)\\ \big[\Box_x \mp \Box_y + m^2(x) \mp m^2(y)\big]G_\rho(x,y) = &\\ = -\int\sqrt{-g}d^4z\theta(z^0)\big[&\Pi_\rho(x,z)G_A(z,y) \mp G_R(x,z)\Pi_\rho(z,y)\\ &+\Pi_R(x,z)G_\rho(z,y) \mp G_\rho(x,z)\Pi_A(z,y)\big]\,. \qquad (3.44b)\end{aligned}$$

In the same way we can interchange x and y on both sides of eqn. (3.43a) and add it to eqn. (3.43b) to obtain the constraint equation for the retarded propagator:

$$\begin{aligned}\big[\Box_x + \Box_y + m^2(x) + m^2(y)\big]G_R(x,y) = &\\ = 2\delta^g(x,y) - \int\sqrt{-g}d^4z\big[&\Pi_R(x,z)G_R(z,y)+G_R(x,z)\Pi_R(z,y)\big]\,. \qquad (3.45)\end{aligned}$$

Next, following the usual procedure in Minkowski space-time, we introducing center and relative coordinates. In Minkowski space-time geodesics are straight lines and center and relative coordinate are given by $X = (x + y)/2$ and $s = (x - y)$, respectively [35]. This means that the center coordinate corresponds to the middle of the geodesic connecting x and y, while the relative coordinate gives the length of this line-segment. To proceed, this concept must be generalized, in a covariant way, to curved space-time [93].[3] Let $\varsigma \in [\varsigma', \varsigma'']$ be an affine parameter on the geodesic

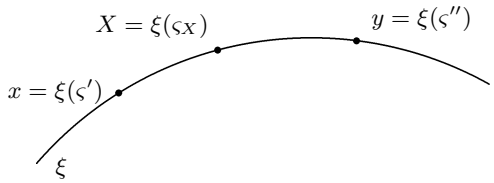

Figure 3.3: A short line-segment of the geodesic.

connecting x and y and ξ a mapping of $[\varsigma', \varsigma'']$ onto this segment of the geodesic, with

$$x^\alpha = \xi^\alpha(\varsigma'), \quad y^\alpha = \xi^\alpha(\varsigma'') \,. \tag{3.46}$$

The center coordinate X can then be defined in terms of the affine parameter $\varsigma_X = (\varsigma' + \varsigma'')/2$ as $X^\alpha = \xi^\alpha(\varsigma_X)$. This is illustrated in fig. 3.3. The relative coordinate s is now defined as the sum of the infinitesimal distance vectors $d\xi^\alpha$ at $\xi^\alpha = \xi^\alpha(\varsigma)$ along the geodesic which are submitted to parallel transfer from the point $\xi^\alpha(\varsigma)$ to the center coordinate $\xi^\alpha(\varsigma_X)$. According to [93] this implies

$$X^\alpha \equiv X^\alpha_{xy} = \xi^\alpha\left(\varsigma_X\right) \,, \quad s^\alpha \equiv s^\alpha_{xy} = (\varsigma' - \varsigma'')u^\alpha\left(\varsigma_X\right) \,, \tag{3.47}$$

where the four-velocity $u^\alpha(\varsigma) = d\xi^\alpha(\varsigma)/\, d\varsigma$ has been introduced. On the geodesic it satisfies the equation

$$\frac{du^\alpha}{d\varsigma} = -\Gamma^\alpha_{\beta\gamma} u^\beta u^\gamma \,. \tag{3.48}$$

As announced above, we want to recast eqns. (3.44) in terms of X and s. On the left-hand side we need to express the Laplace–Beltrami operator in these coordinates:[4]

$$\Box_{x,y} \simeq \frac{1}{4} D^\alpha D_\alpha + \frac{\partial^2}{\partial s^\alpha \partial s_\alpha} \pm D^\alpha \frac{\partial}{\partial s_\alpha} \,, \tag{3.49}$$

where D_α is the covariant derivative in center and relative coordinates:

$$D_\alpha \equiv \frac{\partial}{\partial X^\alpha} - \Gamma^\beta_{\alpha\gamma} s^\gamma \frac{\partial}{\partial s^\beta} \,. \tag{3.50}$$

Next, we perform a first order Taylor expansion of the effective mass around the center coordinate X:

$$\begin{aligned} m^2(x) &\simeq m^2(X) + \frac{1}{2} s^\alpha D_\alpha m^2(X) \,, \\ m^2(y) &\simeq m^2(X) - \frac{1}{2} s^\alpha D_\alpha m^2(X) \,, \end{aligned} \tag{3.51}$$

[3] In [42, 94] a different method based on the use of Riemann normal coordinates and the momentum representation of the propagators has been employed. This approach has some advantages for the study of the quantum kinetic equations.

[4] We neglect here higher order terms proportional to the Riemann and Ricci tensors, see [93].

The spectral function and the statistical propagator on the left-hand side of eqn. (3.44) can also be rewritten in terms of the center and relative coordinates:[5] $G_F(x,y) \to G_F(X,s)$ and $G_\rho(x,y) \to G_\rho(X,s)$.

On the right-hand sides of eqns. (3.44) we have convolutions of functions depending on x and z and functions of z and y. We use the identity

$$(\varsigma' + \varsigma) = (\varsigma' + \varsigma'') + (\varsigma - \varsigma'') = 2\,\varsigma_X + (\varsigma - \varsigma'')$$

and Taylor expand around ς_X to obtain at first order (the dots represent the various indices of the different components)

$$\begin{aligned}\Pi_\cdot(x,z) \to \Pi_\cdot(X_{xz}, s_{xz}) \simeq & \Pi_\cdot(X, s_{xz}) \\ & + \left(\frac{\partial \Pi_\cdot}{\partial \xi^\alpha}\frac{d\xi^\alpha}{d\varsigma} + \frac{\partial \Pi_\cdot}{\partial u^\alpha}\frac{du^\alpha}{d\varsigma}\right)\frac{\varsigma - \varsigma''}{2}\,. \end{aligned} \tag{3.52}$$

Defining $s^\alpha_{zy} \equiv (\varsigma - \varsigma'')u^\alpha(\varsigma_X)$ this may be written in the form

$$\Pi_\cdot(x,z) \to \Pi_\cdot(X, s_{xz}) + \frac{1}{2} s^\alpha_{zy} D_\alpha \Pi_\cdot(X, s_{xz})\,. \tag{3.53}$$

Using the identity

$$(\varsigma'' + \varsigma) = (\varsigma' + \varsigma'') - (\varsigma' - \varsigma) = 2\,\varsigma_X - (\varsigma' - \varsigma)$$

we get a similar expression for functions of z and y:

$$G_{\cdot\cdot}(z,y) \to G_{\cdot\cdot}(X, s_{zy}) - \frac{1}{2} s^\alpha_{xz} D_\alpha G_{\cdot\cdot}(X, s_{zy})\,. \tag{3.54}$$

To perform the integrations over products of the form eqn. (3.53) times (3.54), we shift the coordinate origin to $X^\alpha = \xi^\alpha(\varsigma_X)$ and replace the integrals with respect to z by integrals with respect to the distance s_{Xz} from X to z along the geodesic. Moreover, we approximate $\sqrt{-g}_z$ by its value at the origin $\sqrt{-g}_z \simeq \sqrt{-g}_X$.[6]

The spectral function and the statistical propagator have been defined as functions of two coordinates in four-dimensional space-time. By introducing center and relative coordinates we have traded one space-time coordinate system for another one. On our road towards Boltzmann kinetic equations we clearly need to derive equations for functions which depend on space-time and momentum space arguments (such as the one-particle distribution function does). Performing the so-called *Wigner transformation*, one can trade one of the space-time variables for a momentum space variable. In curved space-time the Wigner transformation and the corresponding inverse transform are defined by [93]

$$G_F(X,p) = \sqrt{-g}_X \int d^4s\, e^{ips} G_F(X,s)\,, \tag{3.55a}$$

$$G_F(X,s) = \int d\Pi_p^4\, e^{-ips} G_F(X,p)\,. \tag{3.55b}$$

[5] We use the same symbol for both functions. Which one is meant should be clear from the context and the symbols used for the arguments.

[6] The next-to-leading term of the Taylor expansion is proportional to the convolution of the Christoffel symbol [80], $\sqrt{-g}_z \approx \sqrt{-g}_X(1 + \Gamma^\nu_{\alpha\nu} s^\alpha)$. This correction can in principle be taken into account and would induce additional terms proportional to $i\partial/\partial p^\alpha$ on the right-hand side of the quantum kinetic equation. Since such term are neglected in the Boltzmann approximation, the collision terms do not receive any corrections.

The definition of the Wigner transform of $G_\rho(X,s)$ differs from (3.55a) by a factor of $-i$ so that $G_\rho(X,p)$ is again real valued. Note that we use contravariant space-time coordinates and covariant momentum space coordinates and that $d\Pi_p^4$ denotes the invariant volume element in momentum space:

$$d\Pi_p^4 \equiv \frac{1}{\sqrt{-g}_X}\frac{d^4p}{(2\pi)^4}\,. \tag{3.56}$$

We shall later need a property of the Wigner transform which is similar to the convolution theorem for the Fourier transformation:

$$\begin{aligned} &f_1(x,y)\ldots f_n(x,y) \to f_1\ldots f_n(X,p) \\ &\quad\equiv \int d\Pi_{p_1}^4\ldots d\Pi_{p_n}^4 (2\pi)^4\sqrt{-g}_X\delta^4(p_1+\ldots+p_n-p)f(X,p_1)\ldots f(X,p_n)\,. \end{aligned} \tag{3.57}$$

Again, similar to the conventional Fourier transform, it follows from eqn. (3.55b) that differentiation of the Wigner transformed quantities with respect to s^α brings down a factor of $-ip^\alpha$,

$$\frac{\partial}{\partial s^\alpha} \to -ip^\alpha\,, \tag{3.58}$$

and upon integration by parts s^α is replaced by differentiation with respect to p^α:

$$s^\alpha \to -i\frac{\partial}{\partial p^\alpha}\,. \tag{3.59}$$

Consequently, after the Wigner transform, the covariant derivative reads

$$D_\alpha \to \mathcal{D}_\alpha = \frac{\partial}{\partial X^\alpha} + \Gamma^\beta_{\alpha\gamma}p_\beta\frac{\partial}{\partial p_\gamma}\,. \tag{3.60}$$

Combining eqns. (3.49) and (3.51), the Wigner transform of the left-hand side of eqn. (3.44) becomes[7]

$$\Box_x - \Box_y + m^2(x) - m^2(y) \to -i\left(2p^\alpha\mathcal{D}_\alpha + D_\alpha m^2\frac{\partial}{\partial p_\alpha}\right)\,. \tag{3.61}$$

We assume now that there is a gradual loss of the dependence on the initial conditions due to the exponential suppression of correlations between earlier and later times [35, 81]. One can then drop the θ function from the integrals in the difference eqns. (3.44). Furthermore, we let the relative-time coordinate s^0_{Xz} range from $-\infty$ to ∞ in order to perform the Wigner transformation. See [81, 95] for a discussion of these approximations. Using eqn. (3.59) and (3.60), we then obtain for the Wigner transform of the product terms on the right-hand side of eqn. (3.44a):

$$\begin{aligned} &\int\sqrt{-g}_z d^4z\;\Pi_\cdot(x,z)G_{\cdot\cdot}(z,y) \to \\ &\qquad\qquad \Pi_\cdot(X,p)G_{\cdot\cdot}(X,p) + \frac{i}{2}\{\Pi_\cdot(X,p),G_{\cdot\cdot}(X,p)\}_{PB}\,, \end{aligned} \tag{3.62}$$

[7] Additional contributions arising from the decomposition of the Laplace–Beltrami operator may be relevant in strong gravitational fields [93]. Since these terms contain at least one $i\partial/\partial p_\alpha$ derivative, they do not contribute in the Boltzmann approximation.

where the following covariant generalization (derivatives with respect to X are replaced by the covariant derivative) of the definition of the Poisson brackets has been used:

$$\{A(X,p),B(X,p)\}_{PB} \equiv \frac{\partial}{\partial p_\alpha}A(X,p)\mathcal{D}_\alpha B(X,p) - \mathcal{D}_\alpha A(X,p)\frac{\partial}{\partial p_\alpha}B(X,p)\,. \tag{3.63}$$

This leads to a rather lengthy expression which can be simplified with the help of a set of relations between $G_R(X,p)$, $G_A(X,p)$, and $G_\rho(X,p)$ (and for the analogous components of the self-energy) which are related to the symmetry properties of the propagators in space-space time coordinates. Using the well-known expression for the Fourier transform of the θ function,

$$\int ds^0 \exp(iws^0)\theta(\pm s^0) = \lim_{\epsilon\to 0}\frac{\pm i}{\omega \pm i\epsilon},$$

and also the familiar representation of the Dirac-delta,

$$\delta(\omega) = \lim_{\epsilon\to+0}\frac{\epsilon}{\pi(\omega^2+\epsilon^2)}\,, \tag{3.64}$$

one finds the following relations for the retarded and advanced propagators

$$G_R(X,p) = -\int\frac{d\omega}{2\pi}\frac{G_\rho(X,\mathbf{p},\omega)}{p_0-\omega+i\epsilon}\,, \tag{3.65a}$$

$$G_A(X,p) = -\int\frac{d\omega}{2\pi}\frac{G_\rho(X,\mathbf{p},\omega)}{p_0-\omega-i\epsilon}\,. \tag{3.65b}$$

From comparison of these two expressions, it follows that (analogous relations hold between the retarded and advanced self-energies)

$$G_A(X,p) = G_R^*(X,p)\,, \tag{3.66}$$

and

$$G_R(X,p) - G_A(X,p) = iG_\rho(X,p)\,. \tag{3.67}$$

Equation (3.66) and (3.67) imply that

$$G_\rho(X,p) = 2\,\Im\{G_R(X,p)\}\,. \tag{3.68}$$

To shorten the notation, we also introduce the quantity

$$\Omega(X,p) \equiv p^\mu p_\mu - m^2(X) - \Pi_h(X,p)\,, \tag{3.69}$$

where $\Pi_h(X,p) \equiv \Re\{\Pi_R(X,p)\}$, and collect the terms on the right-hand side of eqn. (3.44). The kinetic equations for the Wigner transform of the statistical propagator and the Wigner transform of the spectral function may then be written in the compact form:

$$\begin{aligned}\{\Omega(X,p),G_F(X,p)\}_{PB} =& G_F(X,p)\Pi_\rho(X,p) - \Pi_F(X,p)G_\rho(X,p)\\ &- \{G_h(X,p),\Pi_F(X,p)\}_{PB}\,,\end{aligned} \tag{3.70a}$$

$$\{\Omega(X,p),G_\rho(X,p)\}_{PB} = -\{G_h(X,p),\Pi_\rho(X,p)\}_{PB}\,, \tag{3.70b}$$

where $G_h(X,p) \equiv \Re\{G_R(X,p)\}$.

These equations are local in time although, as stated previously, the exact quantum dynamical evolution of the system (at each instant of time) according to eqns. (3.37) depends on the whole history of its evolution. This is manifest in the presence of the memory integrals. The reason is, that by performing the linear order Taylor expansion in the relative coordinate s around X, we take into account only a very short (infinitesimal) part of the history of the evolution.

Next, we consider the Wigner transform of the constraint equation for the retarded propagator eqn. (3.45). On the left-hand side we have $\Box_x + \Box_y \simeq 2\partial_{s^\alpha}\partial_{s_\alpha}$, to first order in the covariant derivative, whereas $m^2(x)+m^2(y) \simeq m^2(X)$. On the right-hand side the Poisson brackets cancel and only the product of Π_R and G_R survives. Finally, the Wigner transform of the generalized Dirac-delta equals unity. Therefore, we get an algebraic equation for the Wigner transform of the retarded propagator:

$$\big[p^\mu p_\mu - m^2(X) - \Pi_R(X,p)\big]G_R(X,p) = -1\,. \tag{3.71}$$

This implies that the real part of the retarded propagator is given by

$$G_h(X,p) = \frac{-\Omega(X,p)}{\Omega^2(X,p) + \frac{1}{4}\Pi_\rho^2(X,p)}\,. \tag{3.72}$$

Note that $G_h(X,p)$ vanishes on the mass shell, which is defined by the condition $\Omega(X,p) = 0$. Using eqn. (3.68), we find:

$$G_\rho(X,p) = \frac{-\Pi_\rho(X,p)}{\Omega^2(X,p) + \frac{1}{4}\Pi_\rho^2(X,p)}\,. \tag{3.73}$$

This is also a particular solution of eqn. (3.70b). To first order in the covariant derivative the Wigner-transform of the constraint equation for the statistical propagator reads

$$\begin{aligned}\Omega(X,p)G_F(X,p) =& \frac{1}{4}\{\Pi_F(X,p), G_\rho(X,p)\}_{PB} \\ &+ \frac{1}{4}\{G_F(X,p), \Pi_\rho(X,p)\}_{PB} + \Pi_F(X,p)G_h(X,p).\end{aligned} \tag{3.74}$$

This equation for $G_F(X,p)$ is not algebraic and can not be solved analytically in general. Let us assume, for a moment, that the system is in thermal equilibrium. In this case all quantities are constant in time and space and the Poisson brackets in eqn. (3.74) vanish identically. The solution of the resulting algebraic equation is known as *fluctuation-dissipation relation*:

$$G_F^{eq}(p) = \frac{\Pi_F(p)}{\Pi_\rho(p)}\,G_\rho^{eq}(p)\,. \tag{3.75}$$

The ratio of Π_F and Π_ρ can be computed from relation eqn. (3.32) with help of the Kubo-Martin-Schwinger (KMS) periodicity condition, $G(x,y)|_{x=0} = G(x,y)|_{x=-i\beta}$, where β is the inverse temperature. Wigner-transforming this equation we obtain from eqn. (3.75):

$$G_F^{eq}(p) = \Big[f^{eq}(p) + \frac{1}{2}\Big]G_\rho^{eq}(p)\,, \tag{3.76}$$

where f^{eq} denotes the Bose–Einstein equilibrium distribution function. This equation will serve as a motivation to make a particular ansatz for the statistical propagator out-of-equilibrium.

To complete this section we need to compute explicit expressions for the Wigner transforms of the spectral and statistical self-energies eqn. (3.38) for the φ^4-theory. Using eqn. (3.57) we can write the Wigner transforms of the three-loop contributions as (remembering that the definition of $G_\rho(X,p)$ contains an additional factor of $-i$)

$$\Pi_F^{(3)}(X,p) = -\frac{\lambda^2}{6}[\,G_F^3(X,p) + \frac{3}{4}G_F G_\rho^2(X,p)]\,, \tag{3.77a}$$

$$\Pi_\rho^{(3)}(X,p) = -\frac{\lambda^2}{6}[3G_F^2 G_\rho(X,p) + \frac{1}{4}G_\rho^3(X,p)]\,. \tag{3.77b}$$

The expression for the Wigner transform of the three-loop retarded self-energy can be obtained from eqn. (3.77) by replacing one of the G_ρ's by G_R. The Wigner transforms of the four-loop contributions can be written in a similar way [2].

3.1.5 Boltzmann kinetic equations

We are now about to make the final steps towards the Boltzmann kinetic equations. It is obvious that we need to relate the propagators to the one-particle distribution function to achieve this. The spectral function eqn. (3.73) has approximately Breit–Wigner shape with a width proportional to the spectral self-energy. As a direct consequence of eqn. (3.34) and the anti-symmetry of the spectral function, $G_\rho(X,p)$ satisfies a normalization condition:

$$\int \frac{g^{00}}{2\pi} G_\rho(X,p)\, p_0\, dp_0 = 1\,. \tag{3.78}$$

In the limit of vanishing coupling constant the width of the spectral function approaches zero, since the magnitudes of Π_ρ (and also of Π_h and of the local term of the self-energy, implicit in the definition of $\Omega(X,p)$), are controlled by the coupling. At the same time its on-shell value goes to infinity, see eqn. (3.73). We can infer from eqn. (3.64) that the spectral function takes the form [32],

$$G_\rho(X,p) = 2\pi\,\mathrm{sgn}(p_0)\,\delta\left(g^{\mu\nu}p_\mu p_\nu - m^2\right)\,, \tag{3.79}$$

in this limit. This ansatz for $G_\rho(X,p)$ is referred to as *quasi-particle approximation*. Note that it is consistent with the normalization condition (3.78). The signum-function appears in eqn. (3.79), because $\Pi_\rho(X,p)$ is an odd function of p_0. In the same limit eqn. (3.70b) for the spectral function becomes

$$p^\alpha \mathcal{D}_\alpha G_\rho(X,p) = 0\,, \tag{3.80}$$

and indeed admits a quasi-particle solution of the from of eqn. (3.79). Note that eqns. (3.80) and (3.79) state that the effective mass $m(X)$ of the field quanta is constant along the geodesic just as for particles.

We are free to replace $G_F(X,p)$ by some other function:

$$G_F(X,p) = \left[f(X,p) + \frac{1}{2}\right] G_\rho(X,p)\,. \tag{3.81}$$

This ansatz is motivated by the fluctuation-dissipation relation (3.76). If $G_F(X,p)$ and $G_\rho(X,p)$ are smooth functions then eqn. (3.81) is merely a definition of $f(X,p)$. In the quasi-particle approximation the spectral function is proportional to a Dirac-delta and eqn. (3.81) must be understood in the distributional sense. In the presence of an adequate momentum integral $G_\rho(X,p)$ then

forces the momentum argument of f onto the mass shell. This quasi-particle approximation for the statistical propagator (3.81) is usually referred to as *Kadanoff–Baym ansatz* [32, 78].

The final step in the derivation is to neglect the Poisson brackets in the quantum kinetic equations. It has been noted above that these take into account a short part of the history of the systems evolution. To neglect the Poisson brackets means to ignore the previous evolution of the system, i.e. to neglect the memory effects completely. Physically this corresponds to the Stoßzahlansatz of Boltzmann which we have related, in section 2.3, to the absence of correlations between particles before they collide (assumption of molecular chaos).

Inserting eqn. (3.81) together with (3.79) into eqn. (3.70a) we finally obtain a kinetic equation for the evolution of the one-particle distribution function $f(X,p)$ (which is implicit):

$$\big[p^\alpha \mathcal{D}_\alpha f(X,p)\big] G_\rho(X,p) = \frac{1}{2}\big[\Pi_>(X,p)G_<(X,p) - G_>(X,p)\Pi_<(X,p)\big]\,, \tag{3.82}$$

where we have introduced

$$G_{\gtrless}(X,p) \equiv G_F(X,p) \pm \frac{1}{2} G_\rho(X,p)\,, \tag{3.83}$$

and the analog for the self-energies:

$$\Pi_{\gtrless}(X,p) \equiv \Pi_F(X,p) \pm \frac{1}{2}\Pi_\rho(X,p)\,. \tag{3.84}$$

The symmetry (anti-symmetry) of the statistical (spectral) propagator with respect to permutation of the arguments imply that their Wigner transforms satisfy the relations

$$G_F(X,p) = G_F(X,-p), \quad G_\rho(X,p) = -G_\rho(X,-p)\,. \tag{3.85}$$

Therefore, we find for the single real scalar field:

$$G_{\gtrless}(X,-p) = G_{\lessgtr}(X,p)\,, \tag{3.86}$$

and a similar relation for the corresponding components of the self-energies.

If we insert the Kadanoff-Baym ansatz into eqn. (3.83) we find:

$$G_>(X,p) = \big(1+f(X,p)\big)G_\rho(X,p)\,, \quad G_<(X,p) = f(X,p)G_\rho(X,p)\,. \tag{3.87}$$

This indicates already that the first and second term in eqn. (3.82) correspond to the loss- and gain-term of the Boltzmann equation. In order to simplify further, we need to find explicit expressions for $\Pi_{\gtrless}(X,p)$ for the φ^4-theory. These can be obtained after some algebra from eqn. (3.77). For illustration purposes we first derive $\Pi_{\gtrless}(x,y)$ and perform the Wigner transformation subsequently. Using the decomposition

$$G(x,y) = \theta(x^0-y^0)G_>(x,y) + \theta(y^0-x^0)G_<(x,y) \tag{3.88}$$

we obtain for the three-loop contribution

$$\Pi^{(3)}_{\gtrless}(x,y) = -\frac{\lambda^2}{6} G_{\gtrless}(x,y)G_{\gtrless}(x,y)G_{\gtrless}(x,y)\,. \tag{3.89}$$

Its Wigner transform reads

$$\Pi^{(3)}_{\gtrless}(X,p) = -\frac{\lambda^2}{6}\int d\Pi^4_{p_1} d\Pi^4_{p_2} d\Pi^4_{p_3} (2\pi)^4 \delta^g(p+p_1-p_2-p_3) \\ \times G_{\lessgtr}(X,p_1) G_{\gtrless}(X,p_2) G_{\gtrless}(X,p_3) \tag{3.90}$$

where we have used relation (3.86). As announced in the beginning, it describes $2-2$ scattering processes and corresponds to the tree-level Feynman diagram in fig. 3.4.

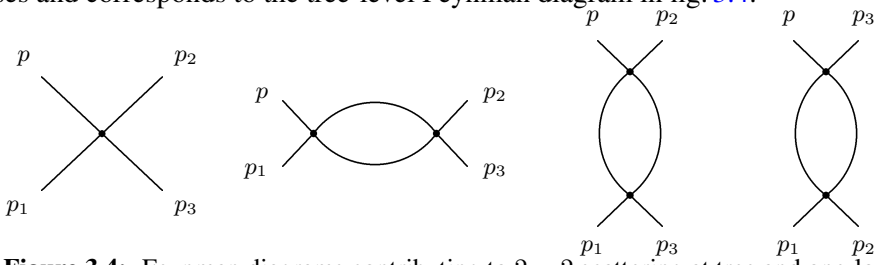

Figure 3.4: Feynman diagrams contributing to $2-2$ scattering at tree and one-loop level.

The corresponding four-loop contributions have been presented in [2].

Next, we insert the explicit expressions for $G_{\gtrless}(X,p)$ eqn. (3.87) and for $\Pi_{\gtrless}(X,p)$ eqn. (3.90) into eqn. (3.82) and obtain:

$$\begin{aligned}\big[p^\alpha \mathcal{D}_\alpha f(X,p)\big] G_\rho(X,p) = \\ +\frac{\lambda^2}{12}\int d\Pi^4_{p_1} d\Pi^4_{p_2} d\Pi^4_{p_3} (2\pi)^4 \delta^g(p+p_1-p_2-p_3)\times \\ \times\Big[\big(1+f(X,p)\big)G_\rho(X,p)\big(1+f(X,p_1)\big)G_\rho(X,p_1) \\ \times f(X,p_2)G_\rho(X,p_2)f(X,p_3)G_\rho(X,p_3) - \\ -f(X,p)G_\rho(X,p)f(X,p_1)G_\rho(X,p_1) \\ \times\big(1+f(X,p_2)\big)G_\rho(X,p_2)\big(1+f(X,p_3)\big)G_\rho(X,p_3)\Big]\,.\end{aligned} \tag{3.91}$$

After the quasi-particle ansatz for $G_\rho(X,p)$ has been inserted we integrate the left– and right-hand side of (3.91) over p_0 and choose the positive energy solution on the left-hand side. On the right-hand side both, the positive and the negative energy, solutions contribute. For positive p_0 energy-momentum conservation allows the following three combinations:

$$\begin{aligned} p_{20}>0, \quad p_{30}>0, \quad p_{10}>0\,, \\ p_{20}>0, \quad p_{30}<0, \quad p_{10}<0\,, \\ p_{20}<0, \quad p_{30}>0, \quad p_{10}<0\,. \end{aligned}$$

As far as the three-loop self-energy eqn. (3.90) is concerned, each combination leads to the same result, i.e. an overall factor of 3 appears. After a renaming of the momentum variables we finally arrive at the Boltzmann equation for the distribution function:

$$\begin{aligned} k^\alpha \mathcal{D}_\alpha f(X,\mathbf{k}) = \frac{1}{2}\int d\Pi^3_p\, d\Pi^3_q\, d\Pi^3_r (2\pi)^4 \delta(E_k+E_p-E_q-E_r)\delta(\mathbf{k}+\mathbf{p}-\mathbf{q}-\mathbf{r}) \\ \times\frac{1}{2}\Lambda^2\Big[\big(1+f(X,\mathbf{k})\big)\big(1+f(X,\mathbf{p})\big)f(X,\mathbf{q})f(X,\mathbf{r}) - \\ -f(X,\mathbf{k})f(X,\mathbf{p})\big(1+f(X,\mathbf{q})\big)\big(1+f(X,\mathbf{r})\big)\Big]\,, \end{aligned} \tag{3.92}$$

where the transition amplitude is given trivially by $\Lambda^2 = \lambda^2$. On the right-hand side, all the $\sqrt{-g_X}$ factors have disappeared due to the introduction of "physical" momenta and energies.

This means that, after a long calculation, we have reproduced the same result as we would have obtained from eqn. (2.9) with the transition amplitude computed from the S-matrix (in lowest order). One may then ask what the advantages of this approach are. Firstly, it shows that in this non-rigorous derivation we were required to make various assumption, the implications of which are hard to quantify in general, to extract the classical Boltzmann kinetic equations out of the quantum dynamical Kadanoff–Baym equations. Secondly, it turns out that the next-to-leading order (four-loop) contribution to the self-energies leads to corrections to the transition amplitude, which include integrals over the distribution function, i.e. medium contributions. In [2] it was shown that it contains a sum of three loop-integrals $L(X,p)$ with arguments corresponding to s-, t- and u-channel scattering:

$$\begin{aligned}\Lambda^2 \to \Lambda^2(X,p_2,p_3,p_1) = \\ \lambda^2(1-\lambda[L(X,p_2+p_3)+L(X,p_2-p_1)+L(X,p_3-p_1)])\,,\end{aligned} \tag{3.93}$$

with

$$L(X,p) = \lim_{\epsilon\to 0}\int \frac{d^3k}{(2\pi)^3}\frac{2f(X,\mathbf{k})+1}{2E_k}\left[\frac{p^2-2pk}{(p^2-2pk)^2+\epsilon^2}+\frac{p^2+2pk}{(p^2+2pk)^2+\epsilon^2}\right], \tag{3.94}$$

where $k = (E_k, \mathbf{k})$ is the on-shell four-momentum expressed in terms of the "physical" components: $E_k \equiv k_0/\sqrt{g_{00}}$, etc. It has also been shown that this expression reduces to the vacuum result at one-loop level in the zero density limit $f \to 0$. The obvious interpretation of eqn. (3.94) is, therefore, that the particles propagating in the loop feel the presence of the non-zero density and that this affects only one of the internal lines. The other one is off-shell and we can not associate the particle number density with it. The expression is therefore only linear in the distribution function.[8] Finally, the structure of eqn. (3.92) has been derived self-consistently. In the present case this does not have any advantage over the canonical approach, but for the toy model of leptogenesis it leads to a qualitative difference as we will see.

Let us note here that the different contributions to the Boltzmann equation corresponding to a particular term of the 2PI effective action have a simple diagrammatic interpretation [75]. They can be deduced by cutting the 2PI diagrams "in one stroke", i.e. by drawing a single connected line which divides the diagrams into two pieces. This needs to be done in all possible ways, see fig. 3.5. For example, the three-loop diagram can be cut in just one way and the result represents a product of two tree-level scattering diagrams. On the other hand, the four-loop contribution could be cut in three equivalent ways and the result represents a product of tree-level and one-loop scattering diagrams.

The properties observed above make the Kadanoff–Baym equations a prime candidate for the analysis of leptogenesis. If the quasi-particle picture is applicable, they account for the time-dependence of the quasi-particle parameters. In particular, an effective time-dependent mass and width induced by the interactions of the system can be extracted from the Wigner transform of the

[8] We should note in this context that the dependence of Λ on the distribution functions represents a further generalization of Boltzmann equations. The symmetry properties of the usual Boltzmann equations (with amplitudes which do not depend on the distribution) lead to a number of collisional invariants, such as the total particle number density (in Minkowski space-time), see section 2.3. This property is considered as very elementary within classical kinetic theory. Because such conservation laws do in general not hold for the "Boltzmann-like" equations presented in this thesis, we do refer to these as quantum corrected Boltzmann equations.

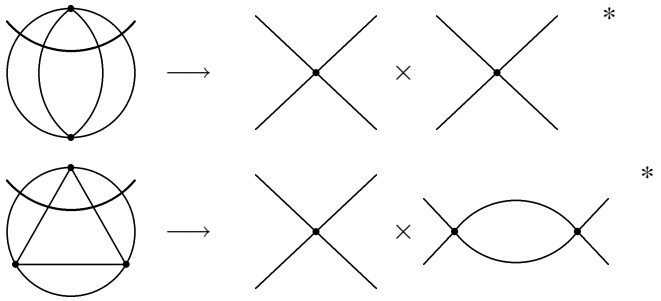

Figure 3.5: The diagrammatic interpretation of the contributions to the Boltzmann equation in terms of 2PI diagrams. These must be separated into two pieces by a single connected line.

spectral function [34]. Finally, in the "classical limit" the Kadanoff–Baym equations reduce to the Boltzmann equation [65–68]. To conclude this section, we summarize the results:

- Kadanoff–Baym equations and the deduced Boltzmann equation in curved space-time are covariant generalizations of their Minkowski-space counterparts
- in the given approximation, the space-time metric enters only the left-hand side of the Boltzmann equation in the form of the covariant derivative
- at tree-level the collision terms coincide with those computed in vacuum, whereas loop contributions contain medium corrections in the form of integrals over the distribution functions
- concerning loop contributions one can clearly distinguish between initial, final states on the one hand and on-shell intermediate states on the other hand

3.2 Quantum corrected Boltzmann equations

As explained in section 1.3 and section 2.2 there is a vertex contribution, which has been considered alone in the early times [11], and a self-energy (or "wave") contribution to the CP-violating parameter. This is true for the phenomenological scenario of thermal leptogenesis as well as for the toy model. Within the Kadanoff–Baym formalism the analysis of the former contribution is rather independent (and technically different) of the latter. It will turn out later that the self-energy contribution is very similar to the vertex contribution in the strongly hierarchical case. We have observed this behaviour already in section 2.5 with respect to the contributions in vacuum which can be expected to result in the zero-density limit. Here, we consider only the vertex contribution in the top-down approach. As soon as we have established the correspondence between the results obtained in this and the bottom-up approach, supplemented by thermal quantum field theory, in chapter 4, we will be able to deduce the form of the self-energy contribution. It is investigated within the top-down approach in [4] in the general (non-hierarchical) case, which leads to very interesting new results. Let us consider now the toy model, defined by the lagrangian eqn. (2.1) in the framework of the Schwinger–Keldysh/Kadanoff–Baym formalism in curved space-time discussed in the previous section. In order to obtain Boltzmann equations we follow the steps which have been outlined there. For brevity we begin here with the system of Kadanoff–Baym equations. The qualitatively different, but technically similar derivation of the Kadanoff–Baym equations for complex scalar fields is presented in appendix A.

3.2.1 Kadanoff–Baym equations

As outlined in section 3.1 the number and precise form of the Kadanoff–Baym equations depends on the particle content of the theory. For the complex scalar field b, which corresponds to the toy-baryons, they read

$$[\Box_x + m_b^2(x)]D_F(x,y) = \int_0^{y^0} \mathscr{D}^4 z\, \Sigma_F(x,z) D_\rho(z,y) - \int_0^{x^0} \mathscr{D}^4 z\, \Sigma_\rho(x,z) D_F(z,y)\,, \tag{3.95a}$$

$$[\Box_x + m_b^2(x)]D_\rho(x,y) = \int_{x^0}^{y^0} \mathscr{D}^4 z\, \Sigma_\rho(x,z) D_\rho(z,y)\,, \tag{3.95b}$$

where we have introduced a short-hand notation $\mathscr{D}^4 z$ for the invariant volume element eqn. (3.3):

$$\mathscr{D}^4 z \equiv \sqrt{-g} d^4 z\,.$$

It ensures that the Kadanoff–Baym equations can be applied not only in Minkowski, but also in curved space-time. The Kadanoff–Baym equations for the two real scalar fields are very similar to the ones for the single real scalar field discussed in section 3.1.3:

$$[\Box_x + m_{\psi_i}^2]G_F^{ij}(x,y) = \int_0^{y^0} \mathscr{D}^4 z\, \Pi_F^{ik}(x,z) G_\rho^{kj}(z,y) - \int_0^{x^0} \mathscr{D}^4 z\, \Pi_\rho^{ik}(x,z) G_F^{kj}(z,y)\,, \tag{3.96a}$$

$$[\Box_x + m_{\psi_i}^2]G_\rho^{ij}(x,y) = \int_{x^0}^{y^0} \mathscr{D}^4 z\, \Pi_\rho^{ik}(x,z) G_\rho^{kj}(z,y)\,. \tag{3.96b}$$

The propagators and self-energies are now 2×2 matrices, the off-diagonal components of which describe the mixing of the fields.[9]

The system of integro-differential equations formed by eqns. (3.95) and (3.96) can be applied to a theory of one complex and two real scalar fields with arbitrary interactions. As discussed in section 3.1, the information about the particular form of the interactions is encoded in the corresponding self-energies $\Sigma(x,y)$ and $\Pi^{ij}(x,y)$. Again, the latter ones can be derived by functional differentiation of the 2PI effective action $\Gamma_2[G,D]$ with respect to the propagators, here $D(y,x)$ and $G^{ji}(y,x)$. To obtain a qualitative similarity between the toy model and phenomenological models, we must take into account processes which generate and washout the asymmetry. Hence the infinite sum of 2PI diagrams must be truncated in a suitable way. The relevant contributions are shown in fig. 3.6. To understand which physical processes these diagrams describe in the Boltz-

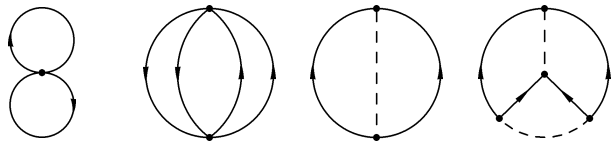

Figure 3.6: Relevant two- and three-loop contributions to the 2PI effective action.

mann approximation one has to distinguish between local and non-local contributions. Since the diagram fig. 3.6(a) includes only one vertex, and hence only one space-time integral, it yields a local (mean-field) contribution to the effective mass $m_b^2(x)$:

$$m_b^2(x) = m_b^2 + \Sigma^{\mathrm{loc}}(x)\,, \quad \Sigma^{\mathrm{loc}}(x) = \lambda D(x,x)\,. \tag{3.97}$$

The remaining diagrams fig. 3.6(b)-(d) give non-local contributions, because they include more

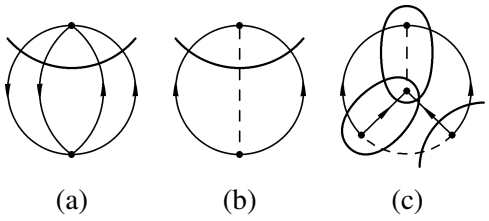

Figure 3.7: Processes described by the 2PI diagrams in fig. 3.6.

than one space-time integral, and describe scattering and decay processes. This becomes clear when the diagrammatic interpretation based on cuts "in one stroke", exemplified at the end of section 3.1, is applied to the different diagrams. The possible cuts are shown in fig. 3.7 for the different contributions. Cutting diagram fig. 3.6(b), we obtain squares of tree-level amplitudes of $bb \to bb$ and $b\bar{b} \to b\bar{b}$, similar to the φ^4-theory. Cutting diagram fig. 3.6(c), we get squares of the tree-level amplitudes of $\psi_i \to bb$ and $\psi_i \to \bar{b}\bar{b}$ decay processes. In the Kadanoff–Baym formalism the leading "vertex" CP-violating contribution is described by diagram fig. 3.6(d). Cutting it in the way shown in fig. 3.8, we obtain a product of the tree-level and one-loop vertex amplitudes.

[9] This can, of course, be generalized to an arbitrary number of real scalars.

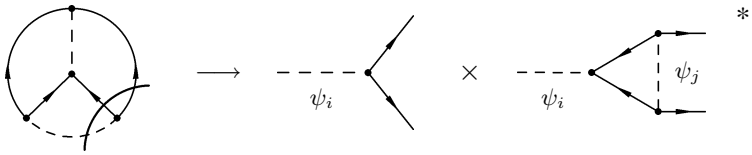

Figure 3.8: Interference of the tree-level and one-loop vertex decay amplitudes.

This corresponds indeed to the interference terms which contributed $\epsilon_i^{V,vac}$ to the CP-violating parameter within the bottom-up approach. In addition, there are two further ways of cutting for this diagram, which are denoted by the ellipses in fig. 3.7. They describe the processes $bb \to \bar{b}\bar{b}$, $b\bar{b} \to \psi_i\psi_j$ and $\psi_i b \to \psi_j b$.[10]

Instead of calculating the spectral and statistical components of the self-energies, it is easier to calculate the Wightman components $\Sigma_{\gtrless}(x,y) \equiv \Sigma_F(x,y) \mp \frac{i}{2}\Sigma_\rho(x,y)$. They are also convenient to work with, because their Wigner transforms can be identified with the gain and loss terms, see eqn. (3.87). After some simple but tedious algebra, see appendix B, one obtains the components of the self-energies corresponding to the diagrams in fig. 3.6:

$$\Sigma^{(b)}_{\gtrless}(x,y) = -\frac{1}{2}\lambda^2 D_{\gtrless}(x,y)D_{\gtrless}(x,y)D_{\lessgtr}(y,x)\,, \tag{3.98a}$$

$$\Sigma^{(c)}_{\gtrless}(x,y) = -\, g_i g_j^* G^{ij}_{\lessgtr}(y,x) D_{\lessgtr}(y,x)\,, \tag{3.98b}$$

$$\begin{aligned}\Sigma^{(d)}_{\gtrless}(x,y) = -\, g_i g_j g_m^* g_n^* \int \mathscr{D}^4 v \mathscr{D}^4 u \\ \times \Big[& D_R(y,v)D_F(u,v)D_{\lessgtr}(u,x)G^{ij}_R(y,u)G^{mn}_{\gtrless}(x,v) \\ & + D_R(y,v)D_A(u,v)D_{\lessgtr}(u,x)G^{ij}_F(y,u)G^{mn}_{\gtrless}(x,v) \\ & + D_F(y,v)D_R(u,v)D_{\lessgtr}(u,x)G^{ij}_R(y,u)G^{mn}_{\gtrless}(x,v) \\ & + D_{\lessgtr}(y,v)D_F(u,v)D_A(u,x)G^{ij}_{\lessgtr}(y,u)G^{mn}_R(x,v) \\ & + D_{\lessgtr}(y,v)D_A(u,v)D_F(u,x)G^{ij}_{\lessgtr}(y,u)G^{mn}_R(x,v) \\ & + D_{\lessgtr}(y,v)D_R(u,v)D_A(u,x)G^{ij}_{\lessgtr}(y,u)G^{mn}_F(x,v) \\ & + D_R(y,v)D_{\gtrless}(u,v)D_A(u,x)G^{ij}_{\lessgtr}(y,u)G^{mn}_{\gtrless}(x,v) \\ & + D_{\lessgtr}(y,v)D_{\lessgtr}(u,v)D_{\lessgtr}(u,x)G^{ij}_R(y,u)G^{mn}_R(x,v)\Big]\,. \end{aligned} \tag{3.98c}$$

The diagrams fig. 3.6(b) and (c) lead to the contributions $\Sigma^{(b)}$ and $\Sigma^{(c)}$ which contain only the Wightman two-point correlation functions $D_{\gtrless}$ and $G^{ij}_{\gtrless}$. As we have seen, these correspond to the on-shell initial and final states in the Boltzmann approximation. To write the last term $\Sigma^{(d)}$ in compact form, we have introduced the retarded and advanced propagators, $D_R(x,y) \equiv \theta(x^0 - y^0)D_\rho(x,y)$ and $D_A(x,y) \equiv -\theta(y^0 - x^0)D_\rho(x,y)$, in complete analogy to eqn. (3.1.4). The first

[10] Note that the three-loop 2PI diagram only describes the interference of the s, t and u-channel scattering amplitudes: $\mathcal{M}_{st}$, $\mathcal{M}_{su}$, $\mathcal{M}_{tu}$. The missing topologies, which generate the $\mathcal{M}_{ss}$, $\mathcal{M}_{tt}$, and $\mathcal{M}_{uu}$ terms, appear only upon use of the *extended quasi-particle approximation*. This analysis is beyond the scope of this thesis.

six contributions describe the one-loop correction to the decay width. The combinations of the statistical, retarded and advanced propagators in eqn. (3.98c) correspond to the three internal lines in the loop, whereas the $\gtrless$ components, again, correspond to the on-shell initial and final states. The seventh term in eqn. (3.98c) describes the scattering process $\psi_i b \to \psi_i b$. This is clear from the fact that it contains one $D_{\gtrless}$ and two $G_{\gtrless}$ components, i.e. one "external" complex scalar and two "external" real scalars. Similarly, the eighth term of eqn. (3.98c) describes the scattering process $bb \to \bar{b}\bar{b}$, because it contains three $D_{\gtrless}$ two-point functions, i.e. three "external" complex scalars.

Since we do not take into account possible quartic interactions of the real scalar fields, in the toy model, there are no local corrections to their masses. It is for this reason that eqns. (3.96) contain only the bare masses $m^2_{\psi_i}$ of the fields. Now let us consider the Wightman components of the non-local self-energies for the real scalar fields $\Pi_{\gtrless}(x,y) \equiv \Pi_F(x,y) \mp \frac{i}{2}\Pi_\rho(x,y)$:

$$\Pi^{(c)ij}_{\gtrless}(x,y) = -\frac{1}{2} g_i g_j^* D^2_{\gtrless}(x,y) - \frac{1}{2} g_i^* g_j D^2_{\lessgtr}(y,x)\,, \tag{3.99a}$$

$$\begin{aligned}
\Pi^{(d)ij}_{\gtrless}(x,y) = -\frac{1}{2} g_i g_j g_m^* g_n^* \int \mathscr{D}^4 v \mathscr{D}^4 u \\
\times \Big[& G_F^{mn}(v,u) D_{\gtrless}(x,v) D_{\gtrless}(x,u) D_R(y,v) D_R(y,u) \\
& + G_R^{mn}(v,u) D_{\gtrless}(x,v) D_{\gtrless}(x,u) D_R(y,v) D_F(y,u) \\
& + G_A^{mn}(v,u) D_{\gtrless}(x,v) D_{\gtrless}(x,u) D_F(y,v) D_R(y,u) \\
& + G_F^{mn}(v,u) D_R(x,v) D_R(x,u) D_{\lessgtr}(y,v) D_{\lessgtr}(y,u) \\
& + G_R^{mn}(v,u) D_R(x,v) D_F(x,u) D_{\lessgtr}(y,v) D_{\lessgtr}(y,u) \\
& + G_A^{mn}(v,u) D_F(x,v) D_R(x,u) D_{\lessgtr}(y,v) D_{\lessgtr}(y,u) \\
& + G_{\lessgtr}^{mn}(v,u) D_{\gtrless}(x,v) D_R(x,u) D_R(y,v) D_{\lessgtr}(y,u) \\
& + G_{\gtrless}^{mn}(v,u) D_R(x,v) D_{\gtrless}(x,u) D_{\lessgtr}(y,v) D_R(y,u) \Big] \\
- \frac{1}{2} g_i^* g_j^* g_m g_n \int \mathscr{D}^4 v \mathscr{D}^4 u \\
\times \Big[& G_F^{mn}(v,u) D_{\lessgtr}(v,x) D_{\lessgtr}(u,x) D_A(v,y) D_A(u,y) \\
& + \quad \dots \qquad\qquad\qquad\qquad\qquad\qquad \Big]\,.
\end{aligned} \tag{3.99b}$$

The first term $\Pi^{(c)}$ describes the decay of the heavy scalar at tree-level. The first six terms in each of the two square brackets of $\Pi^{(d)}$ describe the one-loop corrections to the scattering width.[11] Their structure is very similar to that of the first six terms of eqn. (3.98c) and the combinations of the statistical, retarded and advanced propagators again correspond to the three internal lines in the loop.

The Kadanoff–Baym eqns. (3.95) and (3.96) together with the expression for the self-energies (3.98) and (3.99) form a closed system of integro-differential equations. Its solutions carry the full

[11] The seventh and eighth terms of eqn. (3.99b) describe the scattering processes $\psi_i b \to \psi_j b$ and $b\bar{b} \to \psi_i \psi_j$.

information about the spectral and statistical properties of the system, including the information about the generated asymmetry at each instant of time.

3.2.2 Boltzmann kinetic equations

In thermal equilibrium the two-point correlation functions $D(x,y)$ and $G^{ij}(x,y)$ depend only on the relative coordinate s and are independent of the center coordinate X. With this property in mind, we trade the variables x and y for the new arguments X and s: $D(x,y) \to D(X,s)$. Out of equilibrium the two-point functions depend on both, the relative and center coordinate. Assuming that the deviation from equilibrium is small, one can perform the gradient expansion of the correlation functions and the self-energies in the vicinity of X keeping only the leading terms. The fast dynamics associated with the relative coordinate is responsible for the spectral properties of the system, which are conveniently described in the momentum representation. Performing the Wigner transformation, we trade the relative coordinate s for a coordinate p in momentum space: $D(X,s) \to D(X,p)$. The next steps in the derivation of the Boltzmann equations are the Kadanoff–Baym ansatz eqn. (3.81) for the statistical propagator $D_F(X,p)$ and the quasi-particle approximation, where one replaces the exact smooth spectral function $D_\rho(X,p)$ by a Dirac-delta peaked on the mass-shell of the quasi-particles. These steps have been performed for the φ^4-theory in section 3.1 and are generalized to the toy model in appendix A. They result in two equations for the one-particle distribution functions $f^b(X,p)$ and $f^{\bar{b}}(X,p)$ for toy-baryons and toy-anti-baryons, respectively:

$$\big[p^\alpha \mathcal{D}_\alpha f^b(X,p)\big] D_\rho(X,p) = \frac{1}{2}\big[D_<(X,p)\Sigma_>(X,p) - D_>(X,p)\Sigma_<(X,p)\big]\,, \tag{3.100a}$$

$$\big[p^\alpha \mathcal{D}_\alpha f^{\bar{b}}(X,p)\big] \bar{D}_\rho(X,p) = \frac{1}{2}\big[\bar{D}_<(X,p)\bar{\Sigma}_>(X,p) - \bar{D}_>(X,p)\bar{\Sigma}_<(X,p)\big]\,, \tag{3.100b}$$

where $\bar{D}_{\gtrless}(X,p) \equiv D_{\lessgtr}(X,-p)$, $\bar{\Sigma}_{\gtrless}(X,p) \equiv \Sigma_{\lessgtr}(X,-p)$. To obtain a closed system of quantum corrected Boltzmann equations, we also need to Wigner-transform the self-energies eqn. (3.98), which encode the scattering and decay rates including quantum non-equilibrium effects, see below for more details. By employing the relations (3.87) for the components $D_{\gtrless}(X,p)$, which follow directly from the Kadanoff–Baym ansatz, we will then be able to rewrite eqns. (3.100) in a way resembling the usual form of Boltzmann equations.

Within the 2PI three-loop approximation, we find that there are two physically distinct contributions to the self-energy. The first one, corresponding to $\Sigma^{(b)}$, describes CP-conserving two body scatterings, $bb \to bb$, at tree-level:

$$\begin{aligned}\Sigma^{\times}_{\gtrless}(X,p) = -\frac{1}{2}\lambda^2 \int d\Pi^4_{p_1} d\Pi^4_{p_2} d\Pi^4_{p_3} (2\pi)^4 \delta^g(p + p_1 - p_2 - p_3) \\ \times D_{\lessgtr}(X,p_1) D_{\gtrless}(X,p_2) D_{\gtrless}(X,p_3)\,,\end{aligned} \tag{3.101}$$

where the invariant volume element in momentum space $d\Pi^4_p$ is defined by eqn. (3.56). The second contribution, given by the sum of $\Sigma^{(c)}$ and $\Sigma^{(d)}$, describes decay processes $\psi_i \to bb$ and $\psi_i \to \bar{b}\bar{b}$ at tree- and one-loop level:

$$\begin{aligned}\Sigma^{\lhd}_{\gtrless}(X,p) = -|g_i|^2 \int d\Pi^4_{p_1} d\Pi^4_{p_2} (2\pi)^4 \delta^g(p_1 - p_2 - p) \\ \times \big[1 + \Delta^i_b(X,p_1,p_2)\big] G^{ii}_{\gtrless}(X,p_1) D_{\lessgtr}(X,p_2)\,.\end{aligned} \tag{3.102}$$

The function $\Delta_b^i(X,p_1,p_2)$ takes into account the one-loop corrections to the decay width and is given by

$$\begin{aligned}\Delta_b^i(X,p_1,p_2) = |g_j|^2 \left(\frac{g_i g_j^*}{g_i^* g_j}\right) \int d\Pi_{k_1}^4 d\Pi_{k_2}^4 d\Pi_{k_3}^4 \\ \times (2\pi)^4 \delta^g(p_1+k_1+k_2)(2\pi)^4\delta^g(k_2-k_3+p_2) \\ \times \big[D_A(X,k_1)D_F(X,k_2)G_A^{jj}(X,k_3) \\ + D_A(X,k_1)D_R(X,k_2)G_F^{jj}(X,k_3) \\ + D_F(X,k_1)D_A(X,k_2)G_A^{jj}(X,k_3)\big] + \text{c.c.}\end{aligned} \tag{3.103}$$

Proceeding in the same way, we derive quantum corrected Boltzmann equations for the distribution functions of the real scalar fields, which is a two-by-two differential matrix equation. The off-diagonal components of the correlation functions are generated dynamically, when the system deviates from equilibrium, by the exchange of two complex scalars and are therefore assumed to be of order g^2. The one-loop vertex terms, which generate the CP-violating parameter, are proportional to the fourth power of the coupling constant. Therefore the contribution of the off-diagonal terms to the vertex CP-violating parameter is of the order of g^6. Here, we limit ourselves to terms of at most fourth power in the coupling constant and therefore we can neglect the off-diagonal terms in the corresponding matrix equation. The resulting equations coincide then with those derived in section 3.1:

$$\big[p^\alpha \mathcal{D}_\alpha f^{\psi_i}(X,p)\big] G_\rho^{ii}(X,p) = \frac{1}{2}\big[G_<^{ii}(X,p)\Pi_>^{ii}(X,p) - G_>^{ii}(X,p)\Pi_<^{ii}(X,p)\big]\,. \tag{3.104}$$

Note that we have in fact used this diagonal approximation in eqns. (3.102) and (3.103). The Wigner-transform of the self-energy eqn. (3.99) is given in the same approximation by

$$\begin{aligned}\Pi_{\gtrless}^{\lhd\, ii}(X,p) = -\frac{1}{2}|g_i|^2 \int d\Pi_{p_1}^4 d\Pi_{p_2}^4 (2\pi)^4\delta^g(p_1+p_2-p) \\ \times \Big\{\big[1+\Delta_\psi^i(X,p,p_2)\big]\, D_{\gtrless}(X,p_1)D_{\gtrless}(X,p_2) \\ + \big[1+\bar{\Delta}_\psi^i(X,p,p_2)\big]\, \bar{D}_{\gtrless}(X,p_1)\bar{D}_{\gtrless}(X,p_2)\Big\}\,.\end{aligned} \tag{3.105}$$

The second line of this equation describes the process $\psi_i \to bb$. The one-loop correction to this process is given by

$$\begin{aligned}\Delta_\psi^i(X,p,p_2) = |g_j|^2 \left(\frac{g_i g_j^*}{g_i^* g_j}\right) \int d\Pi_{k_1}^4 d\Pi_{k_2}^4 d\Pi_{k_3}^4 \\ \times (2\pi)^4 \delta^g(p+k_1+k_2)(2\pi)^4\delta^g(k_2-k_3+p_2) \\ \times \big[D_R(X,k_1)D_R(X,k_2)G_F^{jj}(X,k_3) \\ + D_R(X,k_1)D_F(X,k_2)G_A^{jj}(X,k_3) \\ + D_F(X,k_1)D_R(X,k_2)G_R^{jj}(X,k_3)\big] + \text{c.c.}\end{aligned} \tag{3.106}$$

The third line of eqn. (3.105) describes the $\psi_i \to \bar{b}\bar{b}$ process and the corresponding one-loop contribution is related to eqn. (3.106) by $\bar{\Delta}_\psi^i(X,p_1,p_2) \equiv \Delta_\psi^i(X,-p_1,-p_2)$.

Comparing the Boltzmann equations for particles and anti-particles, (3.100a) and (3.100b), we see that the dynamical generation of the asymmetry is only possible if $\Sigma_{\gtrless}(X,p) \neq \bar{\Sigma}_{\gtrless}(X,p)$. Since

$\bar{\Sigma}_{\gtrless}(X,p) \equiv \Sigma_{\lessgtr}(X,-p)$, in the diagonal approximation, this is equivalent to the requirement that $\Delta_b^i(X,p_1,p_2) \neq \Delta_b^i(X,-p_1,-p_2)$. The CP-violating parameter can then be defined as

$$\epsilon_i^V(X,p_1,p_2) \equiv \frac{1}{2}\big[\Delta_b^i(X,p_1,p_2) - \Delta_b^i(X,-p_1,-p_2)\big]\,. \tag{3.107}$$

We will compute it explicitly in the next sub-section. A very important feature of the expressions for the self-energies, eqns. (3.102) and (3.105), is that the loop corrections Δ_b^i and Δ_ψ^i appear as overall factors on the right-hand sides of the corresponding quantum corrected Boltzmann equations. To see what this means, we focus now on the hierarchical limit $m_{\psi_1} \ll m_{\psi_2}$ in which the interactions with on-shell ψ_2's can be neglected due to their large mass and their negligible abundance in the universe when ψ_1 begins to decay, see section 1.3. To obtain the three Boltzmann equations for f^b, $f^{\bar{b}}$ and f^{ψ_1}, we integrate each of eqns. (3.100a), (3.100b) and (3.104) for $i=1$, after inserting the Wigner transforms of the self-energies (3.101), (3.102) and (3.105), over p_0 (left- and right-hand side) and choose the positive energy solution, just as in section 3.1.5. In agreement with the cosmological principle, we assume spatially homogeneous and momentum isotropic distribution functions in (spatially flat and radiation dominated) FRW space-time. With these modifications, the network of quantum corrected Boltzmann equations takes the form:

$$L[f^{\psi_1}](|\mathbf{k}|) = C^{\psi_1\leftrightarrow bb}_{|\mathbf{k}|}[f^{\psi_1},f^b] + C^{\psi_1\leftrightarrow \bar{b}\bar{b}}_{|\mathbf{k}|}[f^{\psi_1},f^{\bar{b}}]\,, \tag{3.108a}$$

$$L[f^b](|\mathbf{k}|) = C^{bb\leftrightarrow bb}_{|\mathbf{k}|}[f^b] + C^{b\bar{b}\leftrightarrow b\bar{b}}_{|\mathbf{k}|}[f^b,f^{\bar{b}}] + C^{bb\leftrightarrow \psi_1}_{|\mathbf{k}|}[f^b,f^{\psi_1}]\,, \tag{3.108b}$$

$$L[f^{\bar{b}}](|\mathbf{k}|) = C^{\bar{b}\bar{b}\leftrightarrow \bar{b}\bar{b}}_{|\mathbf{k}|}[f^{\bar{b}}] + C^{\bar{b}b\leftrightarrow \bar{b}b}_{|\mathbf{k}|}[f^{\bar{b}},f^b] + C^{\bar{b}\bar{b}\leftrightarrow \psi_1}_{|\mathbf{k}|}[f^{\bar{b}},f^{\psi_1}]\,, \tag{3.108c}$$

where the Liouville operator is given by eqn. (2.11) and the notation of section 2.3 is used for the different "collision terms", the distribution functions and the Lorentz invariant phase-space volumes $d\Pi_p^3$. For the $2-2$ scattering processes in (3.108b) we find

$$\begin{aligned} C^{bb\leftrightarrow bb}_{|\mathbf{k}|}[f^b] = \frac{1}{2}\int d\Pi_p^b\, d\Pi_q^b\, d\Pi_r^b (2\pi)^4\delta^{(4)}(p+p-q-r)\frac{1}{2}\lambda^2 \\ \times\Big[\big(1+f^b_{|\mathbf{k}|}\big)\big(1+f^b_{|\mathbf{p}|}\big)f^b_{|\mathbf{q}|}f^b_{|\mathbf{r}|} - f^b_{|\mathbf{k}|}f^b_{|\mathbf{p}|}\big(1+f^b_{|\mathbf{q}|}\big)\big(1+f^b_{|\mathbf{r}|}\big)\Big]\,, \end{aligned} \tag{3.109a}$$

$$\begin{aligned} C^{b\bar{b}\leftrightarrow b\bar{b}}_{|\mathbf{k}|}[f^b,f^{\bar{b}}] = \frac{1}{2}\int d\Pi_p^{\bar{b}}\, d\Pi_q^{\bar{b}}\, d\Pi_r^b (2\pi)^4\delta^{(4)}(p+p-q-r)\lambda^2 \\ \times\Big[\big(1+f^b_{|\mathbf{k}|}\big)\big(1+f^{\bar{b}}_{|\mathbf{p}|}\big)f^{\bar{b}}_{|\mathbf{q}|}f^b_{|\mathbf{r}|} - f^b_{|\mathbf{k}|}f^{\bar{b}}_{|\mathbf{p}|}\big(1+f^{\bar{b}}_{|\mathbf{q}|}\big)\big(1+f^b_{|\mathbf{r}|}\big)\Big]\,. \end{aligned} \tag{3.109b}$$

The corresponding terms in the equation for $\bar{b}$ can be obtained by replacing f^b with $f^{\bar{b}}$ in eqns. (3.109a) and (3.109b). If the generated asymmetry is small, as we assume here, then $f^b \approx f^{\bar{b}}$. In this case the CP-violating contributions to the right-hand side of eqn. (3.108a) cancel out and we obtain

$$\begin{aligned} &C^{\psi_1\leftrightarrow bb}_{|\mathbf{k}|}[f^{\psi_1},f^b] + C^{\psi_1\leftrightarrow \bar{b}\bar{b}}_{|\mathbf{k}|}[f^{\psi_1},f^{\bar{b}}] \\ &\qquad\simeq \frac{1}{2}\int d\Pi_p^b\, d\Pi_q^b (2\pi)^4\delta^{(4)}(p-p-q)\frac{1}{2}|g_1|^2 \\ &\qquad\quad\times\Big\{\Big[\big(1+f^{\psi_1}_{|\mathbf{k}|}\big)f^b_{|\mathbf{p}|}f^b_{|\mathbf{q}|} - f^{\psi_1}_{|\mathbf{k}|}\big(1+f^b_{|\mathbf{p}|}\big)\big(1+f^b_{|\mathbf{q}|}\big)\Big] \\ &\qquad\quad+\Big[\big(1+f^{\psi_1}_{|\mathbf{k}|}\big)f^{\bar{b}}_{|\mathbf{p}|}f^{\bar{b}}_{|\mathbf{q}|} - f^{\psi_1}_{|\mathbf{k}|}\big(1+f^{\bar{b}}_{|\mathbf{p}|}\big)\big(1+f^{\bar{b}}_{|\mathbf{q}|}\big)\Big]\Big\}\,. \end{aligned} \tag{3.110}$$

The collision terms for the (inverse) decay of the heavy particle into a bb or $\bar{b}\bar{b}$ pair explicitly contain the CP-violating parameter ϵ_1^V given in eqn. (3.120):

$$C^{bb\leftrightarrow\psi_1}_{|\mathbf{k}|}[f^b, f^{\psi_1}] = \frac{1}{2}\int d\Pi^b_p\, d\Pi^{\psi_1}_q (2\pi)^4\delta^{(4)}(p-p-q)|g_1|^2[1+\epsilon_1^V(|\mathbf{q}|)] \times\Big[\big(1+f^b_{|\mathbf{k}|}\big)\big(1+f^b_{|\mathbf{p}|}\big)f^{\psi_1}_{|\mathbf{q}|} - f^b_{|\mathbf{k}|}f^b_{|\mathbf{p}|}\big(1+f^{\psi_1}_{|\mathbf{q}|}\big)\Big]\,, \tag{3.111a}$$

$$C^{\bar{b}\bar{b}\leftrightarrow\psi_1}_{|\mathbf{k}|}[f^{\bar{b}}, f^{\psi_1}] = \frac{1}{2}\int d\Pi^{\bar{b}}_p\, d\Pi^{\psi_1}_q (2\pi)^4\delta^{(4)}(p-p-q)|g_1|^2[1-\epsilon_1^V(|\mathbf{q}|)] \times\Big[\big(1+f^{\bar{b}}_{|\mathbf{k}|}\big)\big(1+f^{\bar{b}}_{|\mathbf{p}|}\big)f^{\psi_1}_{|\mathbf{q}|} - f^{\bar{b}}_{|\mathbf{k}|}f^{\bar{b}}_{|\mathbf{p}|}\big(1+f^{\psi_1}_{|\mathbf{q}|}\big)\Big]\,. \tag{3.111b}$$

The network of Boltzmann equations (3.108) should be understood in the generalized sense: the transition amplitudes differ from the usual perturbative matrix elements and do not have their symmetry properties as explained at the end of section 3.1.3.

Equations (3.108) can be compared directly to the network obtained in the bottom-up approach, eqns. (2.20). As announced, the structure of eqns. (3.111) differs from the conventional one. In particular, we did not need to include the processes $bb \leftrightarrow \bar{b}\bar{b}$ explicitly, because our collision terms for the processes $bb \leftrightarrow \psi_1$ and $\bar{b}\bar{b} \leftrightarrow \psi_1$ do not suffer from the generation of an asymmetry in equilibrium. If we would use the conventional approximations and integrate eqns. (3.108) to obtain rate equations, as shown in the bottom-up approach in section 2.4, we would obtain in the vacuum limit the structure[12]

$$\begin{aligned}\frac{d}{dx}(Y_b, Y_{\bar{b}}) &\propto (1\pm\epsilon_i^V)(Y_{\psi_i} - Y^{eq}_{\psi_i}) + \dots\,, \quad \text{i.e.}\\ \frac{d}{dx}(Y_b - Y_{\bar{b}}) &\propto 2\,\epsilon_i^V (Y_{\psi_i} - Y^{eq}_{\psi_i}) + \dots\,.\end{aligned} \tag{3.112}$$

To obtain the equivalent result for $Y_b - Y_{\bar{b}}$ in the canonical approach we needed to subtract the RIS part of the S-matrix element for the processes $bb \leftrightarrow \bar{b}\bar{b}$. This means that, here, the structure of the equations automatically ensures that no asymmetry is generated in thermal equilibrium. Stated differently, the Kadanoff–Baym formalism is free of the "double-counting problem".

In the homogeneous and isotropic early universe the canonical Boltzmann equations conserve the linear combination

$$2\,Y_{\psi_i} + Y_b + Y_{\bar{b}} \tag{3.113}$$

of the different species' abundances. However, the conservation of this quantity is "accidental", i.e. not guaranteed by a symmetry of the underlying lagrangian. It is not conserved by the full Kadanoff–Baym equations (see [35] for another example). This is also true for the quantum corrected Boltzmann equations which we have derived from the Kadanoff–Baym equations here. To see this one can sum eqns. (3.100a) and (3.100b) as well as eqn. (3.104) multiplied by two and use the explicit expressions for the self-energies (3.102) and (3.105). Although the expressions for the loop corrections (3.103) and (3.106) are similar, they are not equal. Close to equilibrium, this results in a small time-dependence of the quantity (3.113) (see also chapter 5).

The factors $1/2$ associated with the couplings in (3.109a) and (3.110) correctly account for the symmetrisation of collision integrals which include integration over the momenta of two identical particles in the initial/final state. They have been consistently obtained in the derivation from the Kadanoff–Baym equations.

[12] For the numerical analysis we will use the full Boltzmann equation, since the approximations required to obtain rate equations are not appropriate if the toy model is considered as closed and no additional interactions are introduced, see section 5.

3.2.3 CP-violating parameter

Using properties of the Wigner transforms of the statistical, retarded and advanced propagators, we find that in an approximately toy-baryon-symmetric medium the CP-violating parameter defined by eqn. (3.107) is given by[13]

$$\begin{aligned}\epsilon_i^V(X,p_1,p_2) = |g_j|^2 \Im\left(\frac{g_i g_j^*}{g_i^* g_j}\right) \int d\Pi_{k_1}^4 d\Pi_{k_2}^4 d\Pi_{k_3}^4 \\ \times (2\pi)^4 \delta^g(p_1+k_1+k_2)(2\pi)^4\delta^g(k_2-k_3+p_2) \\ \times \big[D_\rho(X,k_1)D_F(X,k_2)G_h^{jj}(X,k_3) + \{k_1 \leftrightarrow k_2\} \\ + D_h(X,k_1)D_F(X,k_2)G_\rho^{jj}(X,k_3) + \{k_1 \leftrightarrow k_2\} \\ + D_\rho(X,k_1)D_h(X,k_2)G_F^{jj}(X,k_3) - \{k_1 \leftrightarrow k_2\}\big]\,, \end{aligned} \tag{3.114}$$

where, as before, $D_h(X,p) \equiv \Re\{D_R(X,p)\} = \Re\{D_A(X,p)\}$ and G_h is defined analogously. We can now show that only the first two terms in this expression contribute to the CP-violating parameter in the integrated Boltzmann equations. In the Kadanoff–Baym ansatz together with the quasi-particle approximation the spectral functions and the statistical propagators are forced on the mass shell. At the same time, the real parts of the retarded propagators, D_h and G_h, vanish on-shell. This means that only processes contribute in which two of the internal lines are on-shell

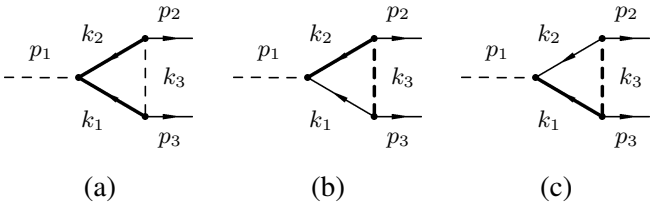

Figure 3.9: Graphical representation of the terms in eqn. (3.114). Thick lines represent on-shell particles. Only the first diagram, with two on-shell internal $\bar{b}$'s, contributes.

and the third one is off-shell, see fig. 3.9. We can also see, that in each term in (3.114) only one of the internal lines includes D_F or G_F^{jj}, i.e. explicitly depends on the one-particle distribution function. In other words the medium corrections are linear in the particle number densities. We will see later, in chapter 4, that this is in conflict with literature results for the medium contributions derived in the framework of thermal quantum field theory by replacing vacuum propagators with thermal ones in the computation of the CP-violating parameter.

We have seen in chapter 3 that the rate equations are obtained by integrating the left- and right-hand sides of the Boltzmann eqns. (3.100a) and (3.100b) over the remaining free momentum. In the integrated gain and loss terms,

$$\begin{aligned}\int d\Pi_p^4 d\Pi_{p_1}^4 d\Pi_{p_2}^2 (2\pi)^4\delta^g(p_1-p_2-p)[1 \pm \epsilon_i^V(X,p_1,p_2)] \\ \times G_{\gtrless}^{ii}(X,p_1)D_{\lessgtr}(X,p_2)D_{\lessgtr}(X,p)\,, \end{aligned} \tag{3.115}$$

[13] The CP-violating parameter, defined in this way, is different for particles and anti-particles if the corresponding distribution functions are different. Since the expected asymmetry is small, this is only a second order effect and can be neglected here.

one can perform the transformation $p \leftrightarrow p_2$ and add half of the result to the half of the original expression without changing it. This is equivalent to the replacement

$$\epsilon_i^V(X, p_1, p_2) \to \frac{1}{2}[\epsilon_i^V(X, p_1, p_2) + \epsilon_i^V(X, p_1, p)] \tag{3.116}$$

in eqn. (3.115). At the same time we can transform the variables $k_1 \leftrightarrow k_2$ and $k_3 \to -k_3$ in $\epsilon_i^V(X, p_1, p)$ given by eqn. (3.114). Using the anti-symmetry of the spectral function of the real scalar fields $G_\rho^{ii}(X, -k_1) = -G_\rho^{ii}(X, k_1)$ we find indeed that only the first two terms in eqn. (3.114) contribute, while the other terms cancel. In other words, only the terms represented by the diagram fig. 3.9(a) contribute to the CP-violating parameter.

Applying the quasi-particle approximation and the Kadanoff–Baym ansatz in eqn. (3.114), one obtains the following expression for the CP-violating parameter:

$$\epsilon_i^V(p_1, p_2) = -\frac{1}{8\pi}\frac{|g_j|^2}{m_{\psi_i}^2}\Im\left(\frac{g_i g_j^*}{g_i^* g_j}\right)\int\frac{d\Omega_l}{4\pi}\frac{1 + f^{\bar{b}}(E_1) + f^{\bar{b}}(E_2)}{m_{\psi_j}^2/m_{\psi_i}^2 + \frac{1}{2}(1 + \cos\theta_l)}\,, \tag{3.117}$$

where $E_{k_{1,2}}$ are the energies of the intermediate toy-baryons as a function of p_1 and p_2 (we have omitted the time-space coordinate X to shorten the notation). The CP-violating parameter is a sum of vacuum and medium contributions. In the zero-density limit we can perform the integration over the solid angle following the steps which led from eqn. (2.57) to eqn. (2.61). We obtain the standard expression for the CP-violating parameter in eqn. (2.52). The medium contributions are proportional to the one-particle distribution function. Hence, within the toy model the CP-violating parameter is always enhanced.

Because of the fact that the intermediate toy-baryons propagate with respect to the rest frame of the thermal bath, a speciality arises in the derivation of eqn. (3.117) which is due to the presence of the distribution functions. As the equilibrium distribution function, these are functions of the Lorentz invariant product $p_\mu U^\mu$ of the particles' four-momentum and the four-velocity U of the plasma in a general frame. In the rest-frame of the plasma $U = (1, 0, 0, 0)$ we obtain the standard form which depends on p_0. One can therefore go to the rest frame of the decaying particle to perform the integration along the same lines which led from eqn. (2.54) to eqn. (2.57). However, one needs to evaluate U in the same frame. It is given by $U = (m_{\psi_1})^{-1}(E_{p_1}^{\psi_1}, -\mathbf{p}_1)$. This leads to the dependence on the energies of the intermediate complex scalars E_1 and E_2 which are given by (see also [3]):

$$E_{1,2} = \frac{1}{2}\left[E_{p_1}^{\psi_1} + |\mathbf{p}_1|(\sin\theta_l\cos\varphi_l\cos\delta' \mp \cos\theta_l\sin\delta')\right], \tag{3.118}$$

where θ_l and φ_l are elements of the solid angle Ω_l and the angle δ' is given by $\sin\delta' = (|\mathbf{p}_3| - |\mathbf{p}_2|)/|\mathbf{p}_1|$.

As noted above, In the limit of almost equal one-particle distribution functions of particles and anti-particles, $f^b \simeq f^{\bar{b}}$, the CP-violating parts of Δ_ψ^i do not contribute to the Boltzmann equations for the real scalars, just as in the canonical approach. For this reason, we do not consider these contributions here.

In order to estimate the size of the medium corrections, we consider again the hierarchical case. By expanding eqn. (3.117) in $m_{\psi_1}^2/m_{\psi_2}^2$, we obtain a simplified expression for the relevant CP-violating parameter ϵ_1^V,

$$\epsilon_1^V(p_1, p_2) \simeq \epsilon_1^{V,vac}\left[1 + \int\frac{d\Omega}{4\pi}\left\{f^{\bar{b}}(E_1) + f^{\bar{b}}(E_2)\right\}\right], \tag{3.119}$$

where $\epsilon_1^{V,vac}$ is the CP-violating parameter in vacuum given in eqn. (2.52). Exploiting the $k_1 \leftrightarrow k_2$ symmetry and integrating over the full solid angle we find that ϵ_1^V depends on the absolute value of $\mathbf{p}_1$ only. That is $\epsilon_1^V(p_1, p_2) = \epsilon_1^V(|\mathbf{p}_1|)$, where

$$\epsilon_1^V(|\mathbf{p}|) \simeq \epsilon_1^{V,vac}\left[1 + \frac{2}{r\,|\mathbf{p}|}\int_{E_{min}/2}^{E_{max}/2} f^{\bar{b}}(E)dE\right], \tag{3.120}$$

with $E_{min} = E_p^{\psi_1} - r|\mathbf{p}|$ and $E_{max} = E_p^{\psi_1} + r|\mathbf{p}|$ are the largest and smallest kinematically allowed energies of the light scalars produced in the decay $\psi_1 \to bb$. Here $E_p^{\psi_1}$ and $|\mathbf{p}|$ denote the energy and momentum of ψ_1 in the rest-frame of the medium and we have defined $r \equiv \sqrt{1 - 4m_b^2/m_{\psi_1}^2}$.

The medium corrections depend on the one-particle distribution function of the light scalars (toy-baryons) and the masses of the particles. We emphasize that eqn. (3.120) is valid even if the light scalars are out-of-equilibrium. Nevertheless, since we assume that, in agreement with the phenomenological scenario, the toy-baryons are close to kinetic equilibrium, we insert a Bose–Einstein distribution function. Then the integrals can be performed analytically and we obtain

$$\frac{\epsilon_1^V(|\mathbf{p}|)}{\epsilon_1^{V,vac}} = 1 + \frac{2T_b}{r|\mathbf{p}|}\ln\left(\frac{1 - e^{-\frac{E_{max}-2\mu_b}{2T_b}}}{1 - e^{-\frac{E_{min}-2\mu_b}{2T_b}}}\right), \quad \text{(BE)}\,. \tag{3.121}$$

For comparison we also consider the case of a Maxwell–Boltzmann distribution:

$$\frac{\epsilon_1^V(|\mathbf{p}|)}{\epsilon_1^{V,vac}} = 1 + \frac{2T_b}{r|\mathbf{p}|}\left(e^{-\frac{E_{min}-2\mu_b}{2T_b}} - e^{-\frac{E_{max}-2\mu_b}{2T_b}}\right), \quad \text{(MB)}\,. \tag{3.122}$$

The resulting expression depends on time via the toy-baryon temperature T_b and chemical potential μ_b. For the rest of this section we assume $|\mu_b| \ll T_b$, as usual in the phenomenological scenario, for the purpose of illustration[14]. The temperature- and momentum dependence of the medium correction in the range of typical momenta $|\mathbf{p}| \sim T_b$ is represented by the shaded areas in fig. 3.10 for the BE and MB cases, respectively. It is instructive to consider the non-relativistic regime ($T_b, |\mathbf{p}| \ll m_{\psi_1}$) and the ultra-relativistic regime ($T_b \gtrsim |\mathbf{p}| \gg m_{\psi_1}$). In the non-relativistic limit, the BE and MB cases coincide, and the medium correction is exponentially suppressed,

$$\epsilon_1^V(|\mathbf{p}|)/\epsilon_1^{V,vac} \to 1 + 2\,\exp\left(-\frac{m_{\psi_1}}{2T_b}\right). \tag{3.123}$$

Furthermore, it is independent of the momentum $|\mathbf{p}|$. In the ultra-relativistic limit, the medium correction in the BE and MB cases behave quite differently: In the MB case the medium correction saturates at $\epsilon_1^V/\epsilon_1^{V,vac} \lesssim 3$. In the BE case, it is logarithmically enhanced (see fig. 3.10):

$$\epsilon_1^V(|\mathbf{p}|)/\epsilon_1^{V,vac} \to 1 + \frac{2T_b}{r|\mathbf{p}|}\ln\left(\frac{4T_b|\mathbf{p}|}{m_{\psi_1}^2 + \frac{8\mathbf{p}^2 m_b^2}{m_{\psi_1}^2(1+r)}}\right). \tag{3.124}$$

[14] The usual motivation for this condition have been given in section 2.4. Within the toy model, due to the absence of gauge interactions, it is possible to have $|\mu_b| \simeq |\bar{\mu}_b| \sim T_b$ while the asymmetry remains small. It turns out that this is even necessary to obtain consistent numerical solutions within the present scenario, see section 5.

This effect is due to Bose-enhancement. Thus, we find that the quantum statistics is important for the size of the medium correction. In the following section, we will see that the logarithmic enhancement at high energies is also suppressed by the inclusion of sizable negative chemical potentials.

In order to get rid of the momentum dependence and to find out how large the medium corrections may be close to thermal equilibrium, we consider an thermally averaged CP-violating parameter. We define it by integrating the gain or loss term in the Boltzmann equation for the decay over the remaining free momentum:[15]

$$\langle \epsilon_i^V \rangle = \frac{\int d\Pi_{p_1}^3 d\Pi_{p_2}^3 d\Pi_{p_3}^3 w(p_1,p_2,p_3)\epsilon_i^V(p_1,p_2)}{\int d\Pi_{p_1}^3 d\Pi_{p_2}^3 d\Pi_{p_3}^3 w(p_1,p_2,p_3)}\,, \tag{3.125}$$

where the term w represents the gain or loss term of the decay processes:

$$w(p_1,p_2,p_3) = (2\pi)^4 \delta(E_{p_1}^{\psi_1} - E_{p_2}^b - E_{p_3}^b)\delta(\mathbf{p}_1 - \mathbf{p}_2 - \mathbf{p}_3)\big(1 + f_{|\mathbf{p}_1|}^{\psi_i}\big) f_{|\mathbf{p}_2|}^b f_{|\mathbf{p}_3|}^b\,. \tag{3.126}$$

This means that $\langle \epsilon_i^V \rangle$ measures the potential relative effect of the medium corrections in ϵ_1^V on the number densities and hence on the generated asymmetry. In the hierarchical limit $m_{\psi_1} \ll m_{\psi_2}$, the CP-violating parameter ϵ_1^V depends only on $|\mathbf{p}_1|$, see eqn. (3.120). In the ultra-relativistic limit $m_b = 0$ the integration over the momenta of the final states in eqn. (3.125) can be performed analytically and one finds:

$$\langle \epsilon_1^V \rangle = \frac{\int_0^\infty d|\mathbf{p}_1|\; \omega(|\mathbf{p}_1|)\epsilon_1^V(|\mathbf{p}_1|)}{\int_0^\infty d|\mathbf{p}_1|\; \omega(|\mathbf{p}_1|)}\,. \tag{3.127}$$

We consider again two cases which differ by the distributions used for the computation of $\omega(|\mathbf{p}_1|)$. Inserting Bose–Einstein distributions for f^b and f^{ψ_i} (with common temperature T and $\mu_b = \mu_{\bar{b}} = \mu_{\psi_1} = 0$) in (3.126) we obtain

$$w(|\mathbf{p}_1|) = \frac{2|\mathbf{p}_1|}{E_{p_1}^{\psi_1} \sinh^2\left(\frac{E_{p_1}^{\psi_1}}{2T}\right)} \ln\left(\frac{\sinh\left(\frac{E_{p_1}^{\psi_1}+|\mathbf{p}_1|}{4T}\right)}{\sinh\left(\frac{E_{p_1}^{\psi_1}-|\mathbf{p}_1|}{4T}\right)}\right)\,, \quad \text{(BE)}\,. \tag{3.128}$$

If we insert, on the other hand, Maxwell–Boltzmann distributions for f^b and neglect f^{ψ_i} in (3.126) the resulting expression for the weighting function reads

$$w(|\mathbf{p}_1|) = |\mathbf{p}_1|^2 \exp\left(-\frac{E_{p_1}^{\psi_1}}{T}\right)\,, \quad \text{(MB)}\,. \tag{3.129}$$

The numerical results for the remaining integral, i.e. the averaged CP-violating parameter in the BE and MB case are also shown in fig. 3.10. We observe that $\langle \epsilon_1^V \rangle \sim \epsilon_1^V(|\mathbf{p}| \sim T_b)$.

Before discussing the impact of the medium correction to the CP-violating parameter quantitatively by solving the Boltzmann equations in chapter 5, we comment on the relation between the top-down and the bottom-up approach. As has been mentioned before, in the zero-density limit, the top-down result eqn. (3.117) for the CP-violating parameter coincides with the canonical result eqn. (2.52). Nevertheless, the structure of the Boltzmann equations differs between the two

[15] Gain and loss term are equal in equilibrium.

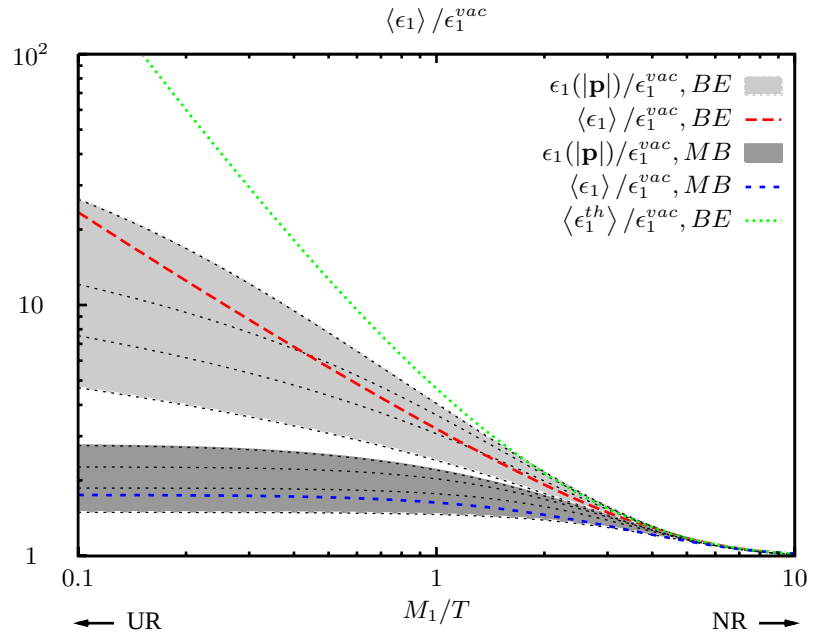

Figure 3.10: The CP-violating parameter $\epsilon_1^V(|\mathbf{p}|)$ with medium contributions for the toy model. The shaded areas correspond to the range $0.25 \leq |\mathbf{p}|/T \leq 4$ of momentum $|\mathbf{p}|$ of the decaying particle $\psi_1 \to bb/\bar{b}\bar{b}$ with respect to the rest-frame of the medium. Here we have assumed a thermal Bose-Einstein (BE) and Maxwell-Boltzmann (MB) distribution for $b/\bar{b}$ with vanishing chemical potential. In the non-relativistic limit (NR), the vacuum value is approached. In the ultra-relativistic limit (UR), the CP-violating parameter is strongly enhanced. The thermally averaged CP-violating parameter $\langle\epsilon_1^V\rangle$ for the BE (red line) and MB (blue line) cases and the result that would be obtained from thermal field theory (green dotted line), see chapter 4.

approaches, i.e. the quantum corrected ones are free of the "double-counting problem". Furthermore, we note again that the size of the medium correction differs between the top-down and the bottom-up approach supplemented by thermal quantum field theory. Within the latter, the medium corrections have been discussed by replacing $\epsilon_i^{V,vac} \to \epsilon_i^{V,th}$ in the canonical Boltzmann equations and $\epsilon_i^{V,th}$ was modified by the inclusion of thermal propagators in its calculation. It involves an additional term compared to the top-down result (3.117), which is quadratic in the particle distribution function. In fig. 3.10 we show that, within the toy model, the medium correction would be significantly over-estimated in the present thermal field theory approach. However, we show in the next chapter that the two approaches can be reconciled.

To conclude this chapter we summarize the results:

- By studying the toy model, we have obtained a network of quantum corrected Boltzmann equations which is similar to the one encountered in thermal leptogenesis in the hierarchical limit but exhibits important differences. They are applicable to systems of weakly coupled (quasi-)particles that have a width which is small compared to their mass and that evolves slowly compared to the microscopic interaction time scales. We expect that these conditions are satisfied in the given scenario of leptogenesis, where the deviations from equilibrium are moderate in general.

- The formalism is free of the "double-counting problem" typical for the canonical approach.

In other words the structure of the equations automatically ensures that the asymmetry vanishes in thermal equilibrium and no need for the RIS subtraction arises.

- The result for the vertex contribution to the CP-violating parameter differs from the literature result obtained in the framework of thermal quantum field theory. The medium corrections in our results are only linear in the particle number densities. Within the toy model the medium effects always increase the CP-violating parameter which, in turn, leads to an enhancement of the generated asymmetry.

- By comparing the CP-violating parameters obtained by using the Maxwell–Boltzmann and Bose–Einstein statistics, we find that quantum statistical effects play a considerable role. The medium effects increase the CP-violating parameter by a factor of at most two in the Maxwell–Boltzmann approximation. At high temperatures, the increase is up to an order of magnitude larger when Bose-enhancement is taken into account.

Chapter 4

Finite temperature field theory approach

In [14, 46, 47] expressions for the CP-violating parameter have been obtained in the framework of finite temperature field theory for the phenomenological scenario of thermal leptogenesis. These include higher order products in the distribution functions and therefore, by analogy, seem to contradict the results derived in the top-down approach in section 3.2. This discrepancy has first been demonstrated in the context of leptogenesis in [3]. Here, we use the finite temperature equivalent of the Cutkosky cutting rules [96–99] to derive thermal corrections to the expression for the imaginary part of the 3-point vertex function and the self-energy loop corrected vertex which can be used in the Boltzmann equation. We show that the apparent contradiction disappears if one considers retarded or advanced n-point functions.

In thermal quantum field theory the physical system is considered to be composed of two subsystems. One is given by the background plasma which forms a thermal reservoir at temperature $T = \beta^{-1}$ while the fields which are used in the computations live in the second system. These fields can interact with the reservoir via decays to or excitation from the reservoir. There are two main formulations of finite-temperature field theory [100]. Within the imaginary-time formalism (ITF), in the computation of an n-point function, continuous energy variables are replaced by discrete imaginary values. In this formulation the final result for real external energies is obtained by analytic continuation. This procedure becomes cumbersome for larger n or at higher loop levels. In contrast, in the real-time formalism (RTF) energies are real and no analytic continuation is necessary. However, in the straight-forward application of this formalism unphysical products of Dirac-delta functions with coinciding arguments appear in the computation of Feynman graphs. In order to cure this problem one usually introduces a further degree of freedom to cancel such irregular terms. In the "$1/2$-formalism" this is done by introducing two types of fields termed *type-1* and *type-2* fields.[1] Interactions do not mix these two fields but the vertices can be of either type, $g^1 = -ig$ and $g^2 = +ig$, for a generic (but real) coupling constant g, differing only by a relative minus sign. The propagators connecting the different types of vertices can be considered

[1] Historically this fields have been called *physical* and *ghost* fields respectively, because it was common belief that only one type-1 fields are physical and that type-2 fields are a auxiliary quantities which do not appear in external lines.

as components of a 2×2 propagator matrix[2][3]

$$G^{ab}(p) = \begin{pmatrix} G^{11}(p) & G^{12}(p) \\ G^{21}(p) & G^{22}(p) \end{pmatrix} = \begin{pmatrix} \Delta(p) & e^{\beta p_0/2}\Delta^-(p) \\ e^{-\beta p_0/2}\Delta^+(p) & \Delta^*(p) \end{pmatrix} .$$

For a scalar particle b the components are

$$\begin{aligned} \Delta(p) &= \frac{i}{p^2 - m_b^2 + i\epsilon} + 2\pi f^{b,eq}(p)\delta(p^2 - m_b^2) , \\ \Delta^{\pm}(p) &= 2\pi \left[\Theta(\pm p_0) + f^{b,eq}(p)\right] \delta(p^2 - m_b^2) . \end{aligned} \tag{4.1}$$

For a fermion f the components are

$$\begin{aligned} \Delta(p) &= (\gamma \cdot p + m_f) \left[\frac{i}{p^2 - m_f^2 + i\epsilon} - 2\pi f^{f,eq}(p)\delta(p^2 - m_f^2)\right] , \\ \Delta^{\pm}(p) &= 2\pi(\gamma \cdot p + m_f) \left[\Theta(\pm p_0) - f^{f,eq}(p)\right] \delta(p^2 - m_f^2) . \end{aligned} \tag{4.2}$$

Here, we denote by $f^{b,eq}(p)$ and $f^{f,eq}(p)$ the equilibrium distribution function for bosons and fermions respectively. They are functions of the Lorentz invariant product $p_\mu U^\mu$ of the particles' four-momentum and the four-velocity U of the plasma in a general frame. In the rest-frame of the plasma $U = (1, 0, 0, 0)$ we obtain the standard form which depends on p_0.[4] In the following we assume that it is sufficient to replace the different propagators in our toy model by their thermal field theory equivalents given in eqn. (4.1). This approach has been followed in previous works for the leptogenesis scenario [47]. Further thermal effects, such as thermal corrections to the masses and wave function renormalization are neglected here, as they are of higher order in the coupling constants.

Denoting vertices attached to external lines by x_i and those attached to internal lines only by z_j we can formally denote an amputated n-point graph by $F(x_1, \ldots, x_n; z_j)$. Here we assume that F is given in momentum space, writing the position space coordinates in order to identify the individual vertices. The contribution of this graph to the amplitude is $-iF(x_1, \ldots, x_n; z_j)$.

Physical amplitudes involve a sum over possible combinations of types of internal vertices:

$$\mathcal{F}(x_1, \ldots, x_n; z_j) = \sum_{\text{type } z_j} F(x_1, \ldots, x_n; z_j) .$$

For external vertices of fixed type it has been shown [96, 97] that this sum is equivalent to a sum over all ways of "circling" the internal vertices:[5]

$$\mathcal{F}(x_1, \ldots, x_n; z_j) = \sum_{\text{circling } z_j} F_{\gtrless}(x_1, \ldots, x_n; z_j) . \tag{4.3}$$

[2] In [47] and elsewhere resummed propagators have been used in this place amongst others to prevent the appearance of singularities. Since we are mainly interested in the structure of the thermal corrections we stick to the bare thermal propagators here.

[3] We adopt here the nomenclature used in thermal quantum field theory and do not comment on similarities between the quantities encountered here and in chapter 3.

[4] Compare the discussion below eqn. (3.117).

[5] The historic origin of this formula was that the external fields where considered to be all of type 1 (physical).

$F_>$ and $F_<$ with "circled" vertices represent graphs computed using the set of rules, given in fig. 4.1. These differ for the computation of $F_>$ and $F_<$ by interchange of the Δ^+ and Δ^- propagators. In $F^{\gtrless}(x_1,\ldots,x_n;z_j)$ we explicitly denote circling of a vertex α as $F^{\gtrless}(x_1,\ldots,\underline{x}_\alpha,\ldots,x_n;z_j)$. Note that the two ways of defining $\mathcal{F}$ in terms of $F_>$ and $F_<$ in eqn. (4.3) are in agreement only if the Kubo–Martin–Schwinger (KMS) boundary condition, in momentum space (in the rest-frame of the plasma) for bosons, $\Delta^-(p) = e^{-\beta p_0}\Delta^+(p)$, is satisfied.[6]

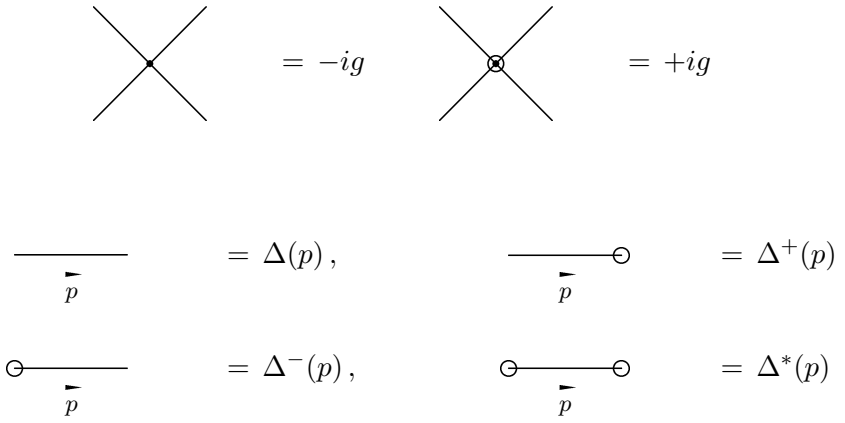

Figure 4.1: Circling rules for a generic theory used for the computation of $F_>$ in momentum space. The rules for the computation of $F_<$ differ by interchange of $\Delta^+(p)$ and $\Delta^-(p)$. The $\Delta^\pm$ propagators connecting circled and uncircled vertices may be interpreted as cut propagators. In vacuum they correspond to the cut propagators in the Cutkosky rules. The physical interpretation of the additional terms is that due interactions with the plasma in the reservoir energy flow is not restricted to a definite direction at finite temperature.

An obvious problem with the real-time formulation for the computation of n-point functions (in the $1/2$-formalism) is that there are in general 2^n such functions which differ in the types of the external vertices.

4.1 Physical and ghost fields

Historically the correct function was considered to be the one with all external vertices of type-1. In this case eqn. (4.3) leads to the following formula for the imaginary part of a graph's contribution to the amplitude, see appendix C:[7]

$$\Im\left\{i^{-1}\mathcal{F}(1,\ldots,1;z_j)\right\} = \frac{1}{2}\sum_{\text{circling }(x_i),\,z_j} F^{\gtrless}(x_1,\ldots,x_n;z_j)\,, \tag{4.4}$$

where the sum includes all possible circlings of the internal vertices z_j but only those circlings of external vertices x_i which include both, circled and uncircled vertices (indicated by the brackets

[6] The KMS relation holds in equilibrium. In this case it is easy to see that (the difference between $F^{\gtrless}$ being the usage of Δ^+ and Δ^-.) the graphs $F^{\gtrless}$ with either all or none of the external vertices and a fixed set of internal vertices circled differ by products of the form $\prod_i e^{\pm\beta(p_i)_0}$ which can be identified with each vertex, where i runs over all lines attached to this vertex. By energy conservation these terms are equal to 1.

[7] Note, that the vertex diagram does not involve any internal vertices. Since the external vertices are all of type 1 it is possible to compute its contribution using the G^{11} component of the propagator only [46]. Here we use a formula which can be compared to both the cutting rules in vacuum and, later, to the formula for the causal products.

around x_i). The six diagrams contributing to the imaginary part of the 3-point vertex function are shown in fig. 4.2.

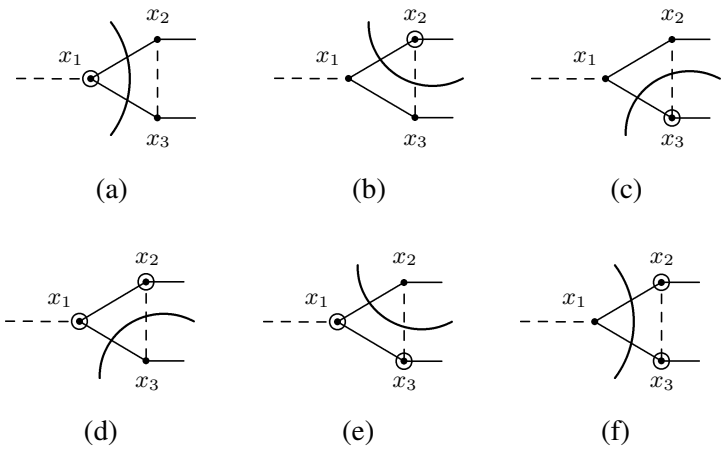

Figure 4.2: Circlings contributing to $\Im\left\{i^{-1}\mathcal{F}(1,1,1)\right\}$ for the vertex loop. The circlings can be interpreted as cuts, as indicated, by the lines separating circled from uncircled regions. The $\Delta^{\pm}$ propagators connecting these regions are proportional to mass-shell delta functions. In general (for diagrams involving internal vertices) not all diagrams contributing to the imaginary part can be interpreted as cut propagators in this approach [96]. For such cases a formula for the imaginary part was derived in [98] in which unconnected regions of circled vertices are canceled by the summation over field type indices, while this sum remains to be performed explicitly for the leftover terms. The equivalence of the two approaches has been shown in [99]. The contributions from diagrams involving cuts through the dashed internal line are suppressed relative to the others.

In this case we can write the imaginary part of the thermal vertex function as (using the rules for $F_<$)

$$\Im\left\{i^{-1}\mathcal{F}(1,1,1)\right\} = \frac{1}{2}\Big[F_<(\underline{x}_1,x_2,x_3) + F_<(x_1,\underline{x}_2,x_3) + F_<(x_1,x_2,\underline{x}_3) + \\ + F_<(\underline{x}_1,\underline{x}_2,x_3) + F_<(\underline{x}_1,x_2,\underline{x}_3) + F_<(x_1,\underline{x}_2,\underline{x}_3)\Big]. \tag{4.5}$$

The contributions from the diagrams in fig. 4.2(b)-(e), involving cuts through the ψ_j lines, are (exponentially) suppressed relative to the other graphs due to the large mass m_{ψ_j} in the hierarchical case. For this reason we consider the contributions from graphs fig. 4.2(a) and (f):[8]

$$\Im\left\{i^{-1}\mathcal{F}_{(a)+(f)}(1,1,1)\right\} = \frac{1}{2}\int\frac{d^4l}{(2\pi)^4}\Big[(+ig_1)(-ig_2)(-ig_3)\Delta^+(q+l)\Delta(q+l-k)\Delta^-(l) + \\ + (-ig_1)(+ig_2)(+ig_3)\Delta^-(q+l)\Delta^*(q+l-k)\Delta^+(l)\Big]. \tag{4.6}$$

We set the generic couplings g_1, g_2, g_3 to 1 now (to obtain directly the imaginary part of A_1 in

[8] Momenta are as defined in fig. 2.6.

eqn. (1.12)). and insert the explicit expressions for the different propagators:

$$\begin{aligned}\Im\Big\{i^{-1}\mathcal{F}_{(a)+(f)}(1,1,1)\Big\} = \\ -\frac{1}{2}\int\frac{d^4l}{(2\pi)^2}i\Big\{&\Big[\Theta(q_0+l_0)+f^{\bar{b},eq}_{q+l}\Big]\delta\big((q+l)^2-m^2_{\bar{b}}\big)\times\\ &\Big[\frac{i}{(q+l-k)^2-m^2_{\psi_j}+i\epsilon}+2\pi f^{\psi_j,eq}_{q+l-k}\delta\big((q+l-k)^2-m^2_{\psi_j}\big)\Big]\times\\ &\Big[\Theta(-l_0)+f^{\bar{b},eq}_{l}\Big]\delta\big(l^2-m^2_{\bar{b}}\big)-\\ -&\Big[\Theta(-(q_0+l_0))+f^{\bar{b},eq}_{q+l}\Big]\delta\big((q+l)^2-m^2_{\bar{b}}\big)\times\\ &\Big[\frac{-i}{(q+l-k)^2-m^2_{\psi_j}-i\epsilon}+2\pi f^{\psi_j,eq}_{q+l-k}\delta\big((q+l-k)^2-m^2_{\psi_j}\big)\Big]\times\\ &\Big[\Theta(l_0)+f^{\bar{b},eq}_{l}\Big]\delta\big(l^2-m^2_{\bar{b}}\big)\Big\}\,. \end{aligned}\tag{4.7}$$

Since ψ_j cannot simultaneously be on-shell with the two $\bar{b}$'s, we can drop the $i\epsilon$ prescription and the terms proportional to three mass-shell deltas:

$$\begin{aligned}\Im\Big\{i^{-1}\mathcal{F}_{(a)+(f)}(1,1,1)\Big\} = -\frac{1}{2}\int\frac{d^4l}{(2\pi)^2}i\delta\big((q+l)^2-m^2_{\bar{b}}\big)\delta\big(l^2-m^2_{\bar{b}}\big)\frac{i}{(q+l-k)^2-m^2_{\psi_j}}\\ \times\Big\{1+f^{\bar{b},eq}_{l}+f^{\bar{b},eq}_{q+l}+2f^{\bar{b},eq}_{l}f^{\bar{b},eq}_{q+l}\Big\}\,.\end{aligned}\tag{4.8}$$

The integration over $d\,|\mathbf{l}|\;dl_0$ proceeds along the same line as in the derivation of the CP-violating in the top-down approach. It leads to

$$\epsilon_i^{V,th} = -\frac{1}{8\pi}\frac{|g_j|^2}{m^2_{\psi_i}}\Im\left(\frac{g_ig_j^*}{g_i^*g_j}\right)\int\frac{d\Omega_l}{4\pi}\frac{1+f_1^{\bar{b},eq}+f_2^{\bar{b},eq}+2f_1^{\bar{b},eq}f_2^{\bar{b},eq}}{m^2_{\psi_j}/m^2_{\psi_i}+\frac{1}{2}(1+\cos\theta_l)}+\dots\,,\tag{4.9}$$

where the dots refer to the suppressed contributions corresponding to cuts through the ψ_j line. The indices on the distribution function mean that they are to be evaluated for the energies E_1 and E_2 given in eqn. (3.118). Equation (4.9) is quadratic in the distribution functions and can be compared to the literature result [46, 47] for the phenomenological scenario of thermal leptogenesis if one of the $\bar{b}$'s (and the corresponding distribution function) in the vertex loop is identified with the lepton and the other with the Higgs.

We can now repeat the same computation for the self-energy loop contribution to the CP-asymmetry. The circlings contributing in this case to eqn. (4.4) are shown in fig. 4.3.

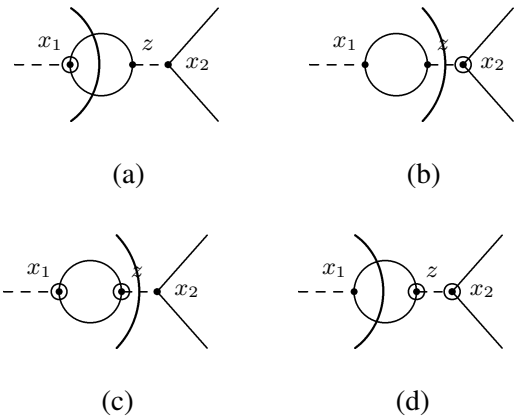

Figure 4.3: Circlings contributing to $\Im\left\{i^{-1}\mathcal{F}(1,1;z)\right\}$ for the self-energy loop. The graphs (b) and (c) vanish since ψ_i and ψ_j cannot be on-shell simultaneously. Note that we consider only the diagrams with ψ_i in the external and ψ_j in the internal line ($i \neq j$) because these are the only ones which contribute to ϵ_i.

$$\Im\left\{i^{-1}\mathcal{F}(1,1;z)\right\} = \frac{1}{2}\Big[F_<(\underline{x}_1, x_2, z) + F_<(x_1, \underline{x}_2, z) + \\ + F_<(\underline{x}_1, x_2, \underline{z}) + F_<(x_1, \underline{x}_2, \underline{z})\Big]\,. \tag{4.10}$$

The contributions from the diagrams in fig. 4.3(b) and (c), involving cuts through the ψ_j lines, vanish since ψ_j cannot simultaneously be on-shell with ψ_i:

$$\Im\left\{i^{-1}\mathcal{F}_{(a)+(d)}(1,1;z)\right\} = \frac{1}{2}\Big[(+ig_1)(-ig_2)(-ig_z)\Delta^-(q+l)\Delta^+(l)\Delta(q) + \\ + (-ig_1)(+ig_2)(+ig_z)\Delta^+(q+l)\Delta^-(l)\Delta^*(q)\Big]\,. \tag{4.11}$$

We set the generic couplings g_1, g_2, g_z to 1 again and insert the explicit expressions for the different propagators:

$$\Im\left\{i^{-1}\mathcal{F}_{(a)+(d)}(1,1;z)\right\} = \frac{1}{2\cdot 2!}\int \frac{d^4l}{(2\pi)^2}\delta\big((q+l)^2 - m_{\bar{b}}^2\big)\delta\big(l^2 - m_{\bar{b}}^2\big)\frac{1}{q^2 - m_{\psi_j}^2}\times \\ \Big\{1 + f_l^{\bar{b},eq} + f_{q+l}^{\bar{b},eq} + f_l^{\bar{b},eq} f_{q+l}^{\bar{b},eq}\Big\}\,, \tag{4.12}$$

where we included a symmetrization factor of $1/2!$. This leads to the self-energy contribution

$$\epsilon_i^{S,th} = -\frac{|g_j|^2}{16\pi}\Im\left(\frac{g_i g_j^*}{g_i^* g_j}\right)\frac{\sqrt{1 - 4m_{\bar{b}}^2/m_{\psi_i}^2}}{m_{\psi_j}^2 - m_{\psi_i}^2}\int\frac{d\Omega_l}{4\pi}\left\{1 + f_1^{\bar{b},eq} + f_2^{\bar{b},eq} + 2f_1^{\bar{b},eq} f_2^{\bar{b},eq}\right\}. \tag{4.13}$$

The results in eqn. (4.8) and eqn. (4.12) can easily be adapted to the phenomenological scenario of section 1.3, using the propagators in eqn. (4.2) for fermions for the Majorana neutrinos and leptons in the loop and eqn. (4.1) for the Higgs bosons. In this case the expressions for the asymmetries include spinor sums [47] which can be factored out, however. For the dependence on the distribution functions one obtains then the quadratic form

$$1 + f^{\phi,eq} - f^{\ell,eq} - 2f^{\phi,eq} f^{\ell,eq}\,. \tag{4.14}$$

This result was found in [46], but, by analogy, it obviously contradicts the result derived from non-equilibrium quantum field theory in the Boltzmann approximation (assuming that this derivation can be generalized to the phenomenological scenario) which does not include products of multiple distribution functions. This discrepancy becomes particular important as eqn. (4.14) implies cancellation of the leading effects since $f_p^{\phi,eq} - f_p^{\ell,eq} = 2 f_p^{\phi,eq} f_p^{\ell,eq}$. The remaining effect is due to the relative motion with respect to the plasma, because different momenta enter the distribution functions of leptons and Higgs particles in eqn. (4.14).

4.2 Causal n-point functions

We will now see how the finite temperature field theory approach can be reconciled with the results derived from non-equilibrium quantum field theory. In [101–103] it was shown that the combination

$$\mathcal{F}^{(\alpha)}_{R/A}(x_1,\ldots,x_n;z_j) = \sum_{\text{circling } x_i,z_j}^{i\neq\alpha} F_{\gtrless}(x_1,\ldots x_\alpha,\ldots,x_n;z_j)\,, \tag{4.15}$$

referred to as the retarded (advanced) product, has the distinguishing property that the time component $(x_\alpha)_0$ is singled out as being the largest (smallest). This becomes clear when we consider the so-called largest (smallest) time equation

$$F_{\gtrless}(x_1,\ldots,x_\alpha,\ldots,x_n) + F_{\gtrless}(x_1,\ldots,\underline{x}_\alpha,\ldots,x_n) = 0\,, \quad \text{if } (x_\alpha)_0 \text{ largest/smallest}\,, \tag{4.16}$$

which implies pairwise cancellation of the terms in eqn. (4.15) if any external vertex x_i with $i \neq \alpha$ has the largest (smallest) time component. Furthermore, it has been shown that the causal products agree with the results of the calculation in imaginary-time formalism analytically continued to real energies, at least in a few examples including the 3-point vertex. It is reasonable to use such causal combinations in Boltzmann collision terms since, for example, the products created in the decay of some particle should always have larger time components than the decaying particle.

The imaginary part of the causal sum was shown in [102] to obey

$$\begin{aligned}\Im\big\{i^{-1}\mathcal{F}^{(\alpha)}_{R/A}(x_1,\ldots,x_\alpha,\ldots,x_n;z_j)\big\} = \\ \mp\frac{1}{2}\sum_{\text{circling } x_i}^{\text{not all}}\sum_{\text{circling } z_j}\Im\Big\{&i^{-1}F_{>}(x_1,\ldots,\underline{x}_\alpha,\ldots,x_n;z_j) - \\ &-i^{-1}F_{<}(x_1,\ldots,\underline{x}_\alpha,\ldots,x_n;z_j)\Big\}\,,\end{aligned} \tag{4.17}$$

where "not all" means that not all x_i should be circled at the same time and the imaginary part is taken of the causal product in momentum space. Here, the vertex x_α with largest or smallest time is always circled.

We can now compute the imaginary part of the advanced product $\Im\big\{\mathcal{F}^{(1)}_A(x_1,x_2,x_3)\big\}$ for the 3-point vertex with smallest time component $(x_1)_0$ of the decaying particle. The relevant circlings are shown in fig. 4.4.

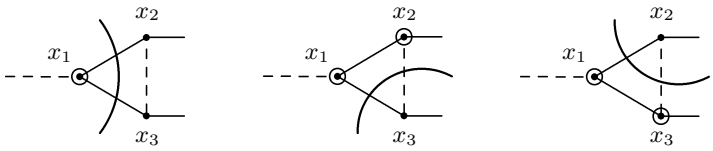

(a) (b) (c)

Figure 4.4: Circlings contributing to $\Im\{\mathcal{F}_A^{(1)}(x_1,x_2,x_3)\}$ for the vertex loop. The sum involves both, $F_>$ and $F_<$ contributions. These differ only by a relative sign and the replacement $\Delta^\pm \leftrightarrow \Delta^\mp$ in the circling rules. Since the finite temperature contributions (terms proportional to $f^{,eq}$) to the latter are the same, all contributions of order higher than one in the distribution functions cancel.

As before the contributions fig. 4.4(b) and (c) are suppressed due to the cut through the ψ_j propagator line. In addition these contributions cancel exactly in the framework of the toy model in the integrated equations. To see this we write the contributions from fig. 4.4(b) to the sum as

$$\begin{aligned}\{F_>(\underline{x}_1,\underline{x}_2,x_3)-F_<(\underline{x}_1,\underline{x}_2,x_3)\}\delta^{(4)}(q-k-p)\\ \propto\int d^4l_1\int d^4l_2\int d^4l_3(+ig_1)(+ig_2)(-ig_3)\\ \times\delta^{(4)}(q+l_3-l_1)\delta^{(4)}(l_1-l_2-k)\delta^{(4)}(l_2-l_3-p)\\ \times\Delta^*(l_1)\Big[\Delta^-(l_2)\Delta^+(l_3)-\Delta^+(l_2)\Delta^-(l_3)\Big]\,.\end{aligned}\tag{4.18}$$

Similarly the contributions from fig. 4.4(c) can be written as

$$\begin{aligned}\{F_>(\underline{x}_1,x_2,\underline{x}_3)-F_<(\underline{x}_1,x_2,\underline{x}_3)\}\delta^{(4)}(q-k-p)\\ \propto\int d^4l_1\int d^4l_2\int d^4l_3(+ig_1)(-ig_2)(+ig_3)\\ \times\delta^{(4)}(q+l_3-l_1)\delta^{(4)}(l_1-l_2-k)\delta^{(4)}(l_2-l_3-p)\\ \times\Delta^*(l_3)\Big[\Delta^-(l_1)\Delta^+(l_2)-\Delta^+(l_1)\Delta^-(l_2)\Big]\,.\end{aligned}\tag{4.19}$$

In the integrated Boltzmann equations we can perform the combined transformation $q\to -q$, $k\to -p$, $p\to -k$ without changing anything if the final state particles (with momentum k and p) in the decay have same quantum statistics and identical distribution functions as is the case in the toy model. Simultaneously exchanging the dummy variables l_1 and l_3 in eqn. (4.19) we find that the contributions in eqns. (4.18) and (4.19) are just equal with opposite sign. Hence the contributions to the integrated Boltzmann equations cancel. Note that the same result was found in the top-down treatment of the vertex contribution, see the discussion below eqn. (3.114).

Now, we compute the remaining contribution from fig. 4.4(a):

$$\begin{aligned}\Im\{i^{-1}\mathcal{F}_A^{(1)}(x_1,x_2,x_3)\}=&\frac{1}{2}\Im\{i^{-1}F_>(\underline{x}_1,x_2,x_3)-i^{-1}F_<(\underline{x}_1,x_2,x_3)\}\\ =&\frac{1}{2}\Im\Big\{i^{-1}\int\frac{d^4l}{(2\pi)^4}\Big[(+ig_1)(-ig_2)(-ig_3)\Delta^-(q+l)\Delta(q+l-k)\Delta^+(l)-\\ &-(+ig_1)(-ig_2)(-ig_3)\Delta^+(q+l)\Delta(q+l-k)\Delta^-(l)\Big]\Big\}\,.\end{aligned}\tag{4.20}$$

Again dropping the $i\epsilon$ prescription in the ψ_j propagators and the respective Dirac-deltas we get

$$\begin{aligned}\Im\{i^{-1}\mathcal{F}_A^{(1)}(x_1,x_2,x_3)\} = -\frac{1}{2}\Im\int\frac{d^4l}{(2\pi)^2}\delta\big((q+l)^2-m_b^2\big)\delta\big(l^2-m_b^2\big)\frac{i}{(q+l-k)^2-m_{\psi_j}^2}\times\\ \Big\{\Big[\Theta(-(q_0+l_0))\Theta(l_0)-\Theta(q_0+l_0)\Theta(-l_0)\Big]\\ +\Big[\Theta(-(q_0+l_0))-\Theta(q_0+l_0)\Big]f_l^{\bar{b},eq}+\\ +\Big[\Theta(l_0)-\Theta(-l_0)\Big]f_{q+l}^{\bar{b},eq}\Big\},\end{aligned} \tag{4.21}$$

which becomes

$$\begin{aligned}&\Im\{i^{-1}\mathcal{F}_A^{(1)}(x_1,x_2,x_3)\} =\\ &=+\frac{1}{2}\int\frac{d^4l}{(2\pi)^2}\delta\big((q+l)^2-m_b^2\big)\delta\big(l^2-m_b^2\big)\frac{1}{(q+l-k)^2-m_{\psi_j}^2}\Big\{1+f_l^{\bar{b},eq}+f_{q+l}^{\bar{b},eq}\Big\}.\end{aligned} \tag{4.22}$$

Performing the integration over $d|\mathbf{l}|\,dl_0$, this indeed leads to the result for the CP-violating parameter obtained in th top-down approach eqn. (3.117). The same computation can be performed for the self-energy loop. The possible circlings are shown in fig. 4.5.

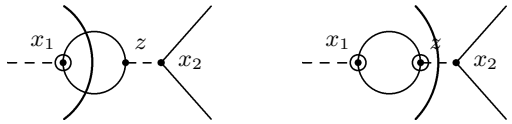

(a) (b)

Figure 4.5: Circlings contributing to $\Im\{\mathcal{F}_A^{(1)}(x_1,x_2;z)\}$ for the self-energy loop. Graph (b) vanishes since ψ_i and ψ_j cannot be on-shell simultaneously.

$$\begin{aligned}\Im\{i^{-1}\mathcal{F}_A^{(1)}(x_1,x_2;z)\} =&\frac{1}{2}\Im\{i^{-1}F_>(\underline{x}_1,x_2,x_3)-i^{-1}F_<(\underline{x}_1,x_2,z)\}\\ =&-\frac{1}{2\cdot 2!}\Im\Big\{\int\frac{d^4l}{(2\pi)^4}\Big[(+ig_1)(-ig_z)(-ig_3)\Delta^-(q+l)\Delta(q)\Delta^+(l)-\\ &-(+ig_1)(-ig_z)(-ig_3)\Delta^+(q+l)\Delta(q)\Delta^-(l)\Big]\Big\},\end{aligned} \tag{4.23}$$

which becomes

$$\begin{aligned}&\Im\{i^{-1}\mathcal{F}_A^{(1)}(x_1,x_2;z)\} =\\ &=\frac{1}{4}\int\frac{d^4l}{(2\pi)^2}\delta\big((q+l)^2-m_b^2\big)\delta\big(l^2-m_b^2\big)\frac{1}{q^2-m_{\psi_j}^2}\Big\{1+f_l^{\bar{b},eq}+f_{q+l}^{\bar{b},eq}\Big\},\end{aligned} \tag{4.24}$$

This corresponds to the result for the self-energy contribution in the hierarchical limit in the top-down approach [4] if the equilibrium distribution functions are replaced with non-equilibrium ones. In the vacuum limit it leads to the expression for $\epsilon_i^{S,vac}$ eqn. (2.62). Thus, we have shown

that the CP-violating parameter ϵ^{th} obtained with help of thermal quantum field theory coincides with the one obtained in the top-down approach (in the approximately symmetric case) when one uses causal products instead of the usual ones which assume type-1 external vertices. The generalization to a (symmetric) non-equilibrium configuration for the toy model can be performed by the canonical replacement of the equilibrium distribution functions with non-equilibrium ones $f^{eq} \to f$.

We are now in the position to infer the form of the thermal corrections to the CP-violating parameter in the phenomenological scenario by drawing the analogy to the toy model. The reasoning here is that the findings for the toy model in the top-down approach result in expressions for the contributions to the CP-violating parameter which can be reproduced in the equilibrium limit by the use of causal products in the thermal field theory approach. (The use of causal products for the computation of amplitudes appearing in Boltzmann equations is also suggested by previous results within thermal field theory.) By this observation we are encouraged to reconsider the thermal computations for the phenomenological theory based on causal functions for vertex and self-energy loop. In the phenomenological scenario the computation of the loop integrals is just a little more involved than in the scalar toy model, but the proceeding is well-known and the same as in [47, 104] so that it is sufficient to consider the dependence on the distribution functions. Replacing one of the scalar thermal lines in the loops (vertex and self-energy loop) by a thermal fermion propagator we find that the dependence on the distribution functions is given by

$$1 - f_1^{\ell,eq} + f_2^{\phi,eq} = 1 + 2 f_1^{\ell,eq} f_2^{\phi,eq} \,,$$

which, in contrast to previous findings, does not vanish but leads to an enhancement of the CP-violating parameter (the right-hand side of this equation applies in the ultra-relativistic limit). We can then, a little more courageously, assume in addition that the structure of the Boltzmann equations for the phenomenological scenario is analogous to the one given in eqn. (3.108) with appropriate quantum statistical factors for bosons and fermions respectively and appropriate symmetrization factors. This defines the full set of Boltzmann equations including medium corrections to the CP-violating parameter for the phenomenological scenario presented in the introduction.[9] We note here that this result should be treated with care, because additional new effects could arise when the phenomenological scenario is investigated in the top-down approach. In addition, the applicability of the quasi-particle picture can not be tested in the framework of thermal field theory. In particular the results presented above will only apply in the hierarchical case [4].

[9] Of course, there are different particle species and further interactions including additional $2-2$ scattering processes in the phenomenological theory. But from the results obtained here and in the research papers [3, 4] it is obvious how consistent equations for decays and inverse decays can be constructed which include quantum statistical terms and guarantee that no asymmetry is produced in equilibrium.

Chapter 5

Numerical results

In this section we solve the Boltzmann equations derived in the top-down approach for the toy model in the hierarchical limit, eqns. (3.108), numerically. To stay consistent within our model we keep the quantum statistical factors for bosons (which would be different in the phenomenological scenario). In order to study the effect of the quantum corrections, we compare the results obtained by integrating the network of Boltzmann equations with quantum corrected $\epsilon_1(|\mathbf{p}|)$ to those which are obtained after replacing $\epsilon_1(|\mathbf{p}|)$ with ϵ_1^{vac}. This means that we keep here the new structure of the Boltzmann equations and study corrections which arise from the quantum corrected ϵ_1 only. The computations have initially been performed for the vertex contributions only [3] but, because of the findings in chapter 4, it is clear that the self-energy contributions are just the half of the vertex ones. As outlined above, this is consistent with the results obtained for the self-energy contributions in the top-down approach [4]. We can therefore use $\epsilon_1(|\mathbf{p}|) = \frac{3}{2}\epsilon_1^V(|\mathbf{p}|)$ in the hierarchical limit. Since the plots presented in this section are relative with respect to the very small ϵ_1^{vac} they remain the same.

We work with a spatially flat and radiation dominated FRW universe with $g_* = 106.75$ effective relativistic degrees of freedom and choose parameters which are typical for the scenario of thermal leptogenesis (see chapter 1): $\epsilon_1^{vac} = 10^{-5}$ and $m_{\psi_1} = 10^{10}\,\text{GeV}$. In both, the corrected ϵ_1 and the vacuum ϵ_1^{vac} case, we start at the same sufficiently high temperature so that all species, including ψ_1, have relativistic initial abundances. We choose thermal initial conditions for all species. Because of the presence of the statistical factors we need to start with sufficiently negative chemical potentials as to avoid Bose–Einstein condensation of the different species during their evolution.[1] We choose them such that they are related by $\mu_{\psi_1} = 2\mu_b = 2\mu_{\bar{b}}$, i.e. the system is in chemical equilibrium.

The coupling λ can be adjusted such that the rates of the $2-2$ interactions (3.109) are much larger than those of the decays and inverse decays (3.110)-(3.111) at all times.[2] This keeps b and $\bar{b}$ close to kinetic equilibrium, just as Higgs particles and leptons are kept in equilibrium by rapid gauge interactions in the standard scenario. The distribution functions for these species are therefore given by their equilibrium form throughout the entire evolution. This means that they

[1] In this regime it would not be appropriate to describe the system by conventional Boltzmann kinetic equations. Since we are interested in scenarios that are qualitatively similar to realistic models of leptogenesis here, we do not consider this case.

[2] As we will show in this case there is no need to compute the collision integrals for $2-2$ scattering explicitly and we can use perturbative values for λ for most of the relevant range of $|g|^2$ assuming that it is sufficient to demand that the rate for $b\bar{b} \leftrightarrow b\bar{b}$ is at least 10^3 times larger than that of $bb \leftrightarrow \psi_1$.

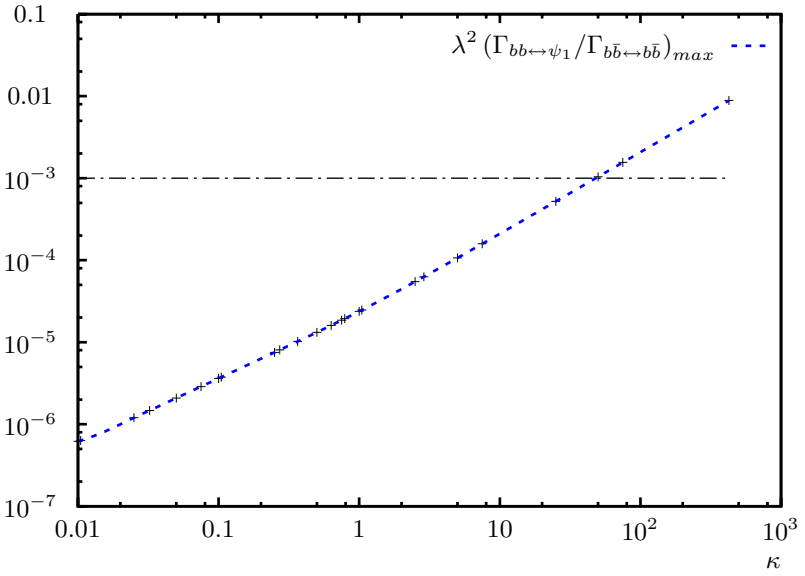

Figure 5.1: The maximum value of the ratio of the rates for $bb \leftrightarrow \psi$ and $b\bar{b} \leftrightarrow b\bar{b}$ over washout factor κ.

can be described in terms of four parameters μ_b, T_b and $\mu_{\bar{b}}$, $T_{\bar{b}}$. Interactions (3.109) enforce the relation $T_{\bar{b}} = T_b$ between the parameters. Therefore, it is sufficient to study the evolution of f^b and $f^{\bar{b}}$ in terms of the remaining three parameters. The evolution of ψ_1, however, is studied in terms of the complete distribution function discretized on a grid with 400 momentum modes. Our computation, therefore, includes classical non-equilibrium effects in the decay of ψ_1. Such effects have been studied recently in [105–107]. All integrals are evaluated numerically including all quantum statistical factors for stimulated emission.

5.1 Numerical method

Along with this thesis a numerical method has been developed for the solution of networks of Boltzmann equations, part of which is presented in appendix D which is based on [1]. Concerning Boltzmann equations, which are integro-differential equations, the crucial problem is to compute the collision terms on the right-hand side in an efficient manner, since this has to be repeated in every time step. At the same time the result for these integrations should be accurate, because deficient approximations add to the problem of numerical stiffness which is inherent in the Boltzmann equations. Based on analytic expressions for an integral over three spherical Bessel functions [108] it was shown how homogeneity and isotropy can be exploited to simplify the collision integrals significantly. In particular it has been shown how the various collision terms for decays, inverse decays and $2 - 2$ scattering can be reduced to lower dimensional integrals in general. Since these studies constituted a large part of this thesis it seems reasonable to present the following in the main part, even though we are concerned here with a simple special case, where the new results coincide with previous findings. At the same time this section serves to present the parameters which enter the computations on the numerical side.

To solve the system of Boltzmann equations (3.108), we introduce the transformed variables

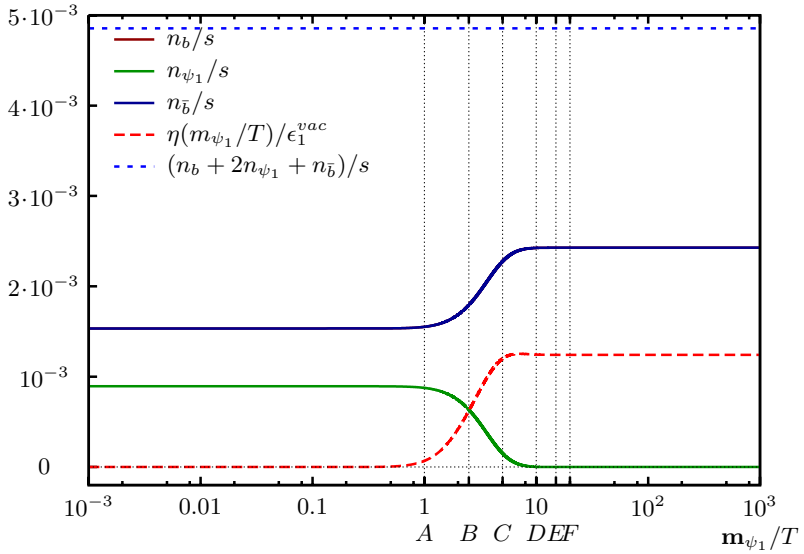

Figure 5.2: Number densities of the various species and the generated asymmetry η as functions of m_{ψ_1}/T for $\kappa \simeq 0.366$ (case c). The total number density is approximately conserved.

$x = a(t)$ and $k_i = Sa(t)|\mathbf{p}_i|$ for time and momentum. The constant factor S is chosen such that $Sx = T^{-1} = (2 \cdot 1.66\sqrt{g_*}/M_{\rm Pl}t)^{\frac{1}{2}}$. The distributions as functions of the transformed momenta are then well represented, in some sense, in the range $k_i \simeq 0.025 - 50.0$.[3] In addition, we introduce the transformed on-shell energies and masses, $m_i = SxM_i$ and $k_i^0 = ({k_i}^2 + {m_i}^2)^{\frac{1}{2}} = Sx(|\mathbf{p}_i|^2 + {M_i}^2)^{\frac{1}{2}}$. In this coordinates the Liouville operator for the FRW space-time takes the form $L[f](|\mathbf{k}|) \to S^{-1}Hk_1^0\,\partial\tilde{f}^b(k_1)/\partial x$, where $\tilde{f}^b(k_1)$ is the transformed one-particle distribution function dependent on k_1 and x. Defining $\tilde{L}[\tilde{f}^b](k_1) \equiv \partial\tilde{f}^b(k_1)/\partial x$, the Boltzmann equations can be written in the form $\tilde{L}[\tilde{f}^b](k_1) = \tilde{C}[.\tilde{f}^b.](k_1)$ with transformed collision integral $C[.\tilde{f}^b.]$.

We transform the integrals to the new coordinates at the same time. In particular, the collision integrals for a scattering process $12 \leftrightarrow 34$ (here $b\bar{b} \leftrightarrow b\bar{b}$, $bb \leftrightarrow bb$ and $\bar{b}\bar{b} \leftrightarrow \bar{b}\bar{b}$) can be reduced to a twofold integral, compare appendix D:

$$\begin{aligned}\tilde{C}^{12\leftrightarrow 34}_{k_1}[.\tilde{f}^b.] = \frac{1}{SHx^2}\frac{1}{64\pi^3 k_1^0}\int\int\frac{k_3\,dk_3}{k_3^0}\frac{k_4\,dk_4}{k_4^0}\Theta\big(k_2^0 - m_2\big)D_{12\leftrightarrow 34}\\ \times\Big[\big(1+\tilde{f}^b(k_1)\big)\big(1+\tilde{f}^b(k_2)\big)\tilde{f}^b(k_3)\tilde{f}^b(k_4) -\\ \tilde{f}^b(k_1)\tilde{f}^b(k_2)\big(1+\tilde{f}^b(k_3)\big)\big(1+\tilde{f}^b(k_4)\big)\Big],\end{aligned} \tag{5.1}$$

where $k_2^0 = k_3^0 + k_4^0 - k_1^0$ and $k_2 = \sqrt{(k_2^0)^2 - {m_2}^2}$. The integrated scattering kernel $D_{12\leftrightarrow 34}$ for a constant (momentum independent) amplitude $\mathcal{A}$ and for massless species 1, 2, 3 and 4 is given

[3] In particular we require that the approximate numerical value of the moments (5.7) are close to their true values for close-to-equilibrium distributions. Also we demand that particles created in decays are not produced with momenta outside of this range to a significant extent so that total number densities show the expected behavior.

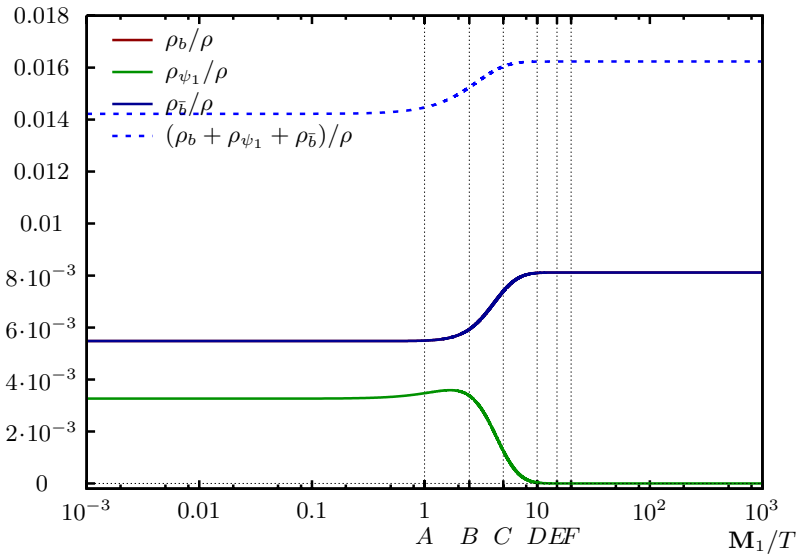

Figure 5.3: Energy densities of the various species as functions of m_{ψ_1}/T for $\kappa \simeq 0.366$ (case c). The ratio of the total energy density $\rho_b + \rho_{\bar{b}} + \rho_\psi$ and the total cosmological energy density ρ is not constant. This feature is due to the different scaling behavior of relativistic and non-relativistic species. For this reason the ratio ρ_ψ/ρ increases slightly before the particles start to decay. This is more pronounced for smaller washout factors (see fig. 5.7).

by

$$D_{12\leftrightarrow 34}(k_1,k_2,k_3,k_4) = \frac{\mathcal{A}}{2k_1}\Theta(k_3+k_4-|k_1-k_2|) \times \Theta(k_1+k_2-|k_3-k_4|)(k_3+k_4-|k_3-k_1|-|k_4-k_1|)\,. \quad (5.2)$$

Similarly, the collision integrals for a particle created in inverse decays, $1 \leftrightarrow 23$ (here $\psi_1 \leftrightarrow bb$ and $\psi_1 \leftrightarrow \bar{b}\bar{b}$), can be reduced to a single integral:

$$\tilde{C}^{1\leftrightarrow 23}_{k_1}[.\tilde{f}^b.] = \frac{S}{H}\frac{1}{32\pi k_1^0}\int \frac{k_3\,dk_3}{k_3^0}\Theta\big(k_2^0-m_2\big)D_{1\leftrightarrow 23}\times \Big[\big(1+\tilde{f}^{\psi_1}(k_1)\big)\tilde{f}^b(k_2)\tilde{f}^b(k_3) - \tilde{f}^{\psi_1}(k_1)\big(1+\tilde{f}^b(k_2)\big)\big(1+\tilde{f}^b(k_3)\big)\Big]\,, \quad (5.3)$$

where $k_2^0 = k_1^0 - k_3^0$ and $k_2 = \sqrt{(k_2^0)^2 - {m_2}^2}$. The integrated scattering kernel $D_{1\leftrightarrow 23}$ is given by

$$D_{1\leftrightarrow 23}(k_1,k_2,k_3) = \frac{2\mathcal{A}}{k_1}\Theta(k_1-|k_2-k_3|)\Theta((k_2+k_3)-k_1)\,. \quad (5.4)$$

Finally, the collision integrals for a particle created in decays, $12 \leftrightarrow 3$ (here $bb \leftrightarrow \psi_1$ and $\bar{b}\bar{b} \leftrightarrow$

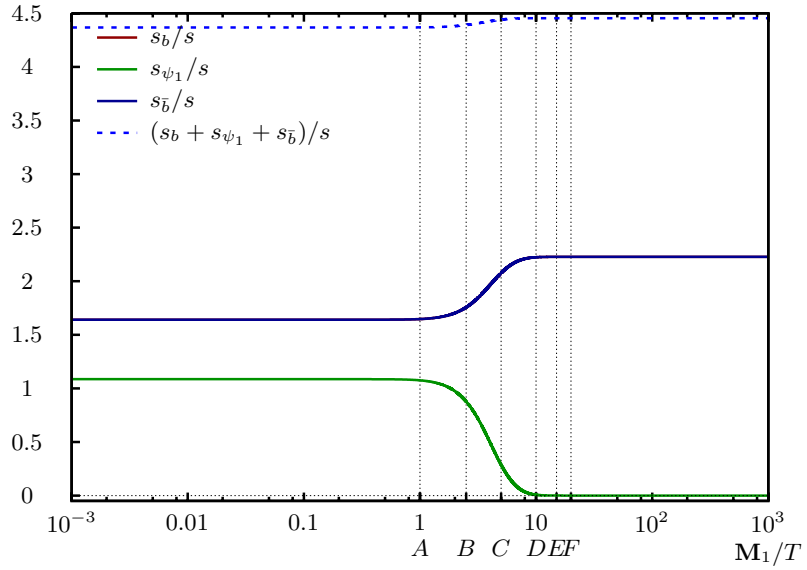

Figure 5.4: Entropy densities of the various species and the total entropy density $(s_b + s_{\bar{b}} + s_\psi)/s$ as functions of m_{ψ_1}/T for $\kappa \simeq 0.366$ (case c).

ψ_1), can be reduced to the single integral

$$\tilde{C}^{12\leftrightarrow 3}_{k_1}[.\tilde{f}^b.] = \frac{S}{H}\frac{1}{32\pi k_1^0}\int \frac{k_3\, dk_3}{k_3^0}\Theta\big(k_2^0 - m_2\big) D_{12\leftrightarrow 3}\times \\ \Big[\big(1+\tilde{f}^b(k_1)\big)\big(1+\tilde{f}^b(k_2)\big)\tilde{f}^{\psi_1}(k_3) - \\ -\tilde{f}^b(k_1)\tilde{f}^b(k_2)\big(1+\tilde{f}^{\psi_1}(k_3)\big)\Big]\,, \tag{5.5}$$

where $k_2^0 = k_3^0 - k_1^0$ and $k_2 = \sqrt{(k_2^0)^2 - m_2{}^2}$. The integrated scattering kernel $D_{12\leftrightarrow 3}$ is given by

$$D_{12\leftrightarrow 3}(k_1,k_2,k_3) = \frac{2\mathcal{A}}{k_1}\Theta(k_3 - |k_1 - k_2|)\Theta((k_1+k_2) - k_3)\,. \tag{5.6}$$

Number density and energy density corresponding to the distribution $\tilde{f}^b$ in transformed coordinates read

$$n[\tilde{f}^b] = \frac{1}{2\pi^2}\left(\frac{1}{Sx}\right)^3 \int (k_1)^2 \tilde{f}^b(k_1) dk_1\,, \\ \rho[\tilde{f}^b] = \frac{1}{2\pi^2}\left(\frac{1}{Sx}\right)^4 \int (k_1)^2 k_1^0 \tilde{f}^b(k_1) dk_1\,. \tag{5.7}$$

For massless particles these are the second and third moment of the distribution, respectively. As outlined in section 5, we assume that the interactions $bb \leftrightarrow bb$, $\bar{b}\bar{b} \leftrightarrow \bar{b}\bar{b}$ and $b\bar{b} \leftrightarrow b\bar{b}$ are rapid enough to keep the distribution functions of b and $\bar{b}$ very close to their equilibrium distributions, parametrized by $a_0, a_1, \bar{a}_0$ and $\bar{a}_1$:

$$f_a^{\bar{b},eq}(k_1) = [\exp(a_0 + a_1 k_1) - 1]^{-1}\,, \\ f_a^{b,eq}(k_1) = [\exp(\bar{a}_0 + \bar{a}_1 k_1) - 1]^{-1}\,. \tag{5.8}$$

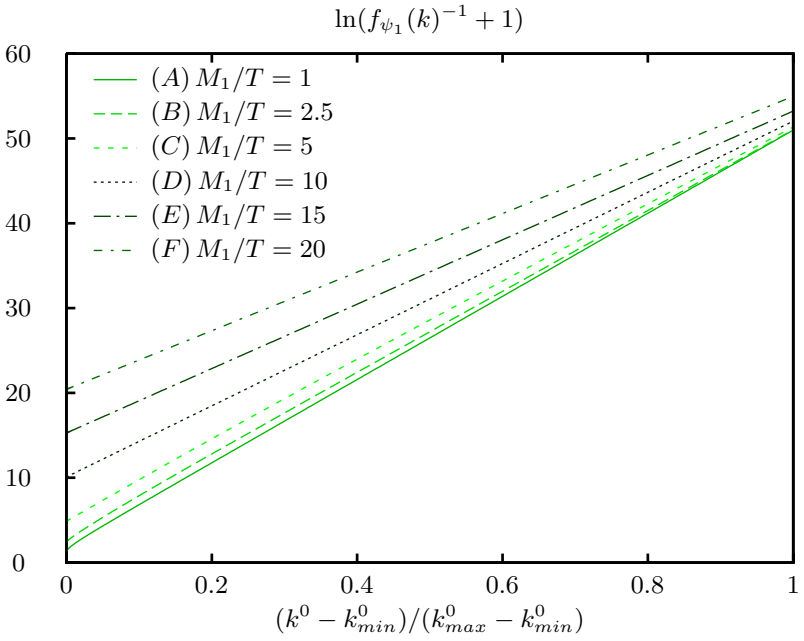

Figure 5.5: Deviation of the distribution function f_{ψ_1} from equilibrium for washout factor $\kappa \simeq 0.366$ (case c).

Assuming that $b\bar{b} \leftrightarrow b\bar{b}$ alone is much faster than the inverse decays into ψ_1, the evolution of f^b and $f^{\bar{b}}$ can therefore be described by means of three parameters a_0, $\bar{a}_0$ and a_1. The equations for the evolution of these parameters are obtained by forming the moments $n[.]$ of eqn. (3.108b) and (3.108c):[4]

$$\begin{aligned} n\left[\tilde{L}[f_a^{b,eq}]\right] =& \frac{da_0}{dx} n\left[\frac{\partial f_a^{b,eq}}{\partial a_0}\right] + \frac{da_1}{dx} n\left[\frac{\partial f_a^{b,eq}}{\partial a_1}\right] = n\left[\tilde{C}^{bb\leftrightarrow\psi_1}\right] , \\ n\left[\tilde{L}[f_a^{\bar{b},eq}]\right] =& \frac{d\bar{a}_0}{dx} n\left[\frac{\partial f_a^{\bar{b},eq}}{\partial \bar{a}_0}\right] + \frac{da_1}{dx} n\left[\frac{\partial f_a^{\bar{b},eq}}{\partial a_1}\right] = n\left[\tilde{C}^{\bar{b}\bar{b}\leftrightarrow\psi_1}\right] . \end{aligned} \tag{5.9}$$

Here, we used $n\left[\tilde{C}^{bb\leftrightarrow bb}[f^b]\right] = n\left[\tilde{C}^{\bar{b}\bar{b}\leftrightarrow\bar{b}\bar{b}}[f^{\bar{b}}]\right] = 0$ and $n\left[\tilde{C}^{b\bar{b}\leftrightarrow b\bar{b}}[f^b, f^{\bar{b}}]\right] = n\left[\tilde{C}^{\bar{b}b\leftrightarrow\bar{b}b}[f^{\bar{b}}, f^b]\right] = 0$. The third equation is obtained by forming the moment $\rho[.]$ of the sum of eqn. (3.108b) and (3.108c), i.e.

$$\begin{aligned} \rho\left[\tilde{L}[f_a^{b,eq}]\right] + \rho\left[\tilde{L}[f_a^{\bar{b},eq}]\right] =& \frac{da_0}{dx}\rho\left[\frac{\partial f_a^{b,eq}}{\partial a_0}\right] + \frac{d\bar{a}_0}{dx}\rho\left[\frac{\partial f_a^{\bar{b},eq}}{\partial a_0}\right] + \\ &+ \frac{da_1}{dx}\rho\left[\frac{\partial f_a^{b,eq}}{\partial a_1}\right] + \frac{da_1}{dx}\rho\left[\frac{\partial f_a^{\bar{b},eq}}{\partial a_1}\right] \\ =& \rho\left[\tilde{C}^{bb\leftrightarrow\psi_1}\right] + \rho\left[\tilde{C}^{\bar{b}\bar{b}\leftrightarrow\psi_1}\right] , \end{aligned} \tag{5.10}$$

[4]Here and in the following we use the abbreviations $C^{bb\leftrightarrow\psi_1}[] = \tilde{C}^{bb\leftrightarrow\psi_1}[f_a^{b,eq}, \tilde{f}^{\psi_1}]$ and $C^{\bar{b}\bar{b}\leftrightarrow\psi_1}[] = \tilde{C}^{\bar{b}\bar{b}\leftrightarrow\psi_1}[f_a^{\bar{b},eq}, \tilde{f}^{\psi_1}]$. Also note that f^b, $f^{\bar{b}}$ and f^{ψ_1} are functions of the transformed coordinates, here.

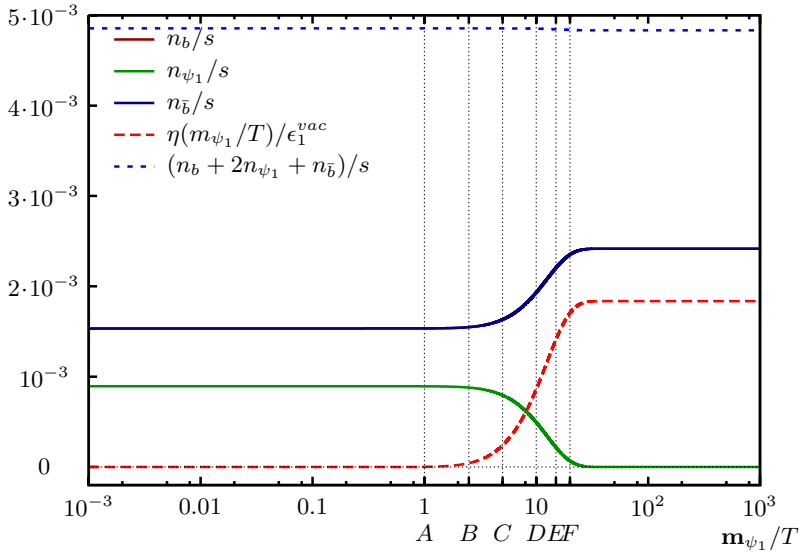

Figure 5.6: Number densities of the various species and the generated asymmetry η as functions of m_{ψ_1}/T for $\kappa \simeq 0.01$ (case a).

where we used $\rho\left[\tilde{C}^{b\bar{b}\leftrightarrow b\bar{b}}[f^b, f^{\bar{b}}]\right] + \rho\left[\tilde{C}^{\bar{b}b\leftrightarrow \bar{b}b}[f^{\bar{b}}, f^b]\right] = 0$. The derivatives of $f_a^{b,eq}$ with respect to the parameters a_i can be rewritten as

$$\frac{\partial f_a^{b,eq}(k_1)}{\partial a_i} = -(k_1^0)^i[1 + f_a^{b,eq}(k_1)]f_a^{b,eq}(k_1)\,, \quad i = 0, 1\,. \tag{5.11}$$

An analogous relation holds for the derivatives of $f_a^{\bar{b},eq}$ with respect to $\bar{a}_0$ and a_1. Solving eqns. (5.9) and (5.10) for da_0/dx, $d\bar{a}_0/dx$ and da_1/dx, we find the differential equations for the three parameters:

$$\begin{aligned}
\frac{da_0}{dx} &= -\frac{\dot{a}_1 n\left[k_1^0(1 + f_a^{b,eq})f_a^{b,eq}\right] + n\left[\tilde{C}^{bb\leftrightarrow\psi_1}\right]}{n\left[(1 + f_a^{b,eq})f_a^{b,eq}\right]}\,,\\
\frac{d\bar{a}_0}{dx} &= -\frac{\dot{a}_1 n\left[k_1^0(1 + f_a^{\bar{b},eq})f_a^{\bar{b},eq}\right] + n\left[\tilde{C}^{\bar{b}\bar{b}\leftrightarrow\psi_1}\right]}{n\left[(1 + f_a^{\bar{b},eq})f_a^{\bar{b},eq}\right]}\,,\\
\frac{da_1}{dx} &= -\Big(\left(n\left[\tilde{C}^{bb\leftrightarrow\psi_1}\right]\rho_f + n\left[k_1^0(1 + f_a^{b,eq})f_a^{b,eq}\right]\rho_C\right)\times\\
&\qquad n\left[(1 + f_a^{\bar{b},eq})f_a^{\bar{b},eq}\right]\rho\left[(1 + f_a^{b,eq})f_a^{b,eq}\right]\\
&\quad + \left(n\left[\tilde{C}^{\bar{b}\bar{b}\leftrightarrow\psi_1}\right]\rho_f + n\left[k_1^0(1 + f_a^{\bar{b},eq})f_a^{\bar{b},eq}\right]\rho_C\right)\times\\
&\qquad n\left[(1 + f_a^{b,eq})f_a^{b,eq}\right]\rho\left[(1 + f_a^{\bar{b},eq})f_a^{\bar{b},eq}\right]\Big)/h + \rho_C/\rho_f\,,
\end{aligned} \tag{5.12}$$

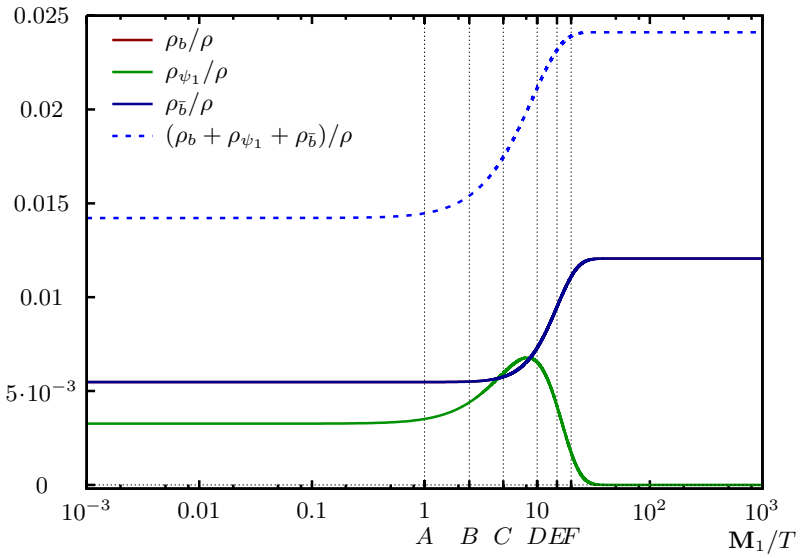

Figure 5.7: Energy densities of the various species and the total energy density $(\rho_b + \rho_{\bar{b}} + \rho_\psi)/\rho$ as functions of m_{ψ_1}/T for $\kappa \simeq 0.01$ (case a).

where we have defined

$$\begin{aligned} h \;=\; & \rho_f \Big(n\big[(1+f_a^{b,eq})f_a^{b,eq}\big] n\big[(1+f_a^{\bar{b},eq})f_a^{\bar{b},eq}\big] \rho_f + \\ & n\big[k_1^0(1+f_a^{\bar{b},eq})f_a^{\bar{b},eq}\big] n\big[(1+f_a^{b,eq})f_a^{b,eq}\big] \rho\big[(1+f_a^{\bar{b},eq})f_a^{\bar{b},eq}\big] + \\ & n\big[k_1^0(1+f_a^{b,eq})f_a^{b,eq}\big] n\big[(1+f_a^{\bar{b},eq})f_a^{\bar{b},eq}\big] \rho\big[(1+f_a^{b,eq})f_a^{b,eq}\big] \Big) , \end{aligned} \tag{5.13}$$

as well as

$$\begin{aligned} \rho_f =& -\rho\big[k_1^0(1+f_a^{b,eq})f_a^{b,eq}\big] - \rho\big[k_1^0(1+f_a^{\bar{b},eq})f_a^{\bar{b},eq}\big] , \\ \rho_C =& \rho\big[\tilde{C}^{bb\leftrightarrow\psi_1}\big] + \rho\big[\tilde{C}^{b\bar{b}\leftrightarrow\psi_1}\big] . \end{aligned} \tag{5.14}$$

As stated in the main text, we need to start with finite chemical potentials as to avoid the occurrence of Bose–Einstein condensation. We choose the minimal acceptable value $a_0 = \bar{a}_0 = 0.5$, corresponding to $\mu_b = \mu_{\bar{b}} = -0.5\,T_0$ and $\mu_{\psi_1} = 2\mu_b$. The initial value $a_1 = 1$ corresponds to the initial cosmological temperature T_0 which is assumed to be the same for all species. We checked that the results do not depend on T_0 as long as $T_0 \gg m_{\psi_1}$. The heavy species ψ_1 is subject to relatively weak interactions only, so that its distribution function can deviate from kinetic equilibrium. Therefore, we solve the full Boltzmann equation for ψ_1,

$$\tilde{L}[f^{\psi_1}](k_1) = \tilde{C}_{k_1}^{\psi_1\leftrightarrow bb}[f^{\psi_1}, f^b] + \tilde{C}_{k_1}^{\psi_1\leftrightarrow b\bar{b}}[f^{\psi_1}, f^{\bar{b}}] , \tag{5.15}$$

along with the integrated ones for b and $\bar{b}$.

Because of the integration of the equations for the massless species all collision terms for $2-2$ scattering drop out of the system. In order to verify that the rates for these processes are much larger than the ones of the decays and inverse decays we have computed the rates for these processes numerically. The maximum (during the full evolution) of the ratio of $\Gamma_{bb\leftrightarrow\psi_1}$ and $\Gamma_{b\bar{b}\leftrightarrow b\bar{b}}$

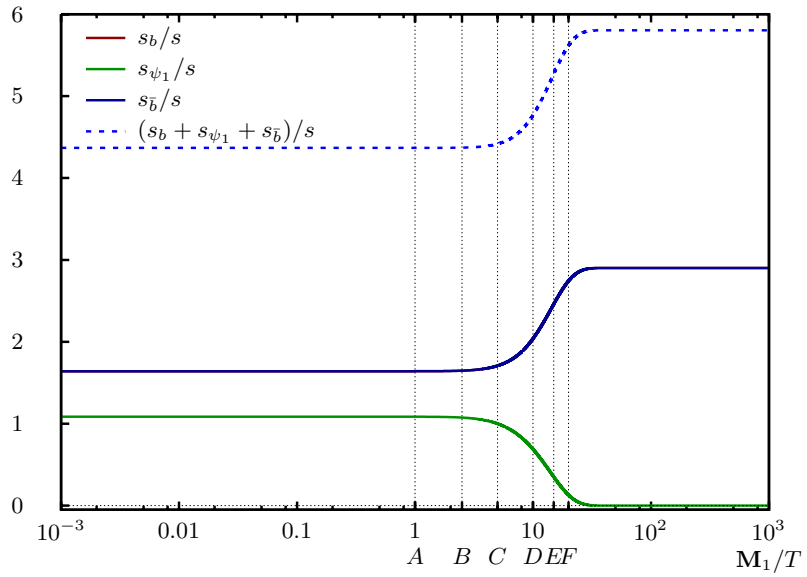

Figure 5.8: Entropy densities of the various species and the total entropy density $(s_b + s_{\bar{b}} + s_\psi)/s$ as functions of m_{ψ_1}/T for $\kappa \simeq 0.01$ (case a).

is exemplarily presented in fig. 5.1 (the rates for the other $2-2$ processes are similar). It shows that we can choose $\lambda \sim 1$ or smaller for most of the relevant range of $|g|^2$ if we demand that $\Gamma_{b\bar{b}\leftrightarrow b\bar{b}}/\Gamma_{bb\leftrightarrow\psi_1} \gtrsim 10^3$ as criterion that b and $\bar{b}$ are in kinetic equilibrium at all times. Here the equilibrium shape of f^b and $f^{\bar{b}}$ is not distorted by the expansion since we are dealing with massless particles. In addition, it can be argued that the $2-2$ processes are meant to model rapid gauge interactions with different particles which would have the same effect of equilibrating b and $\bar{b}$. In this sense we could even formally tolerate non-perturbative values of λ.

To turn the equations into a system of ODE's the distribution functions were discretized on a grid of dimension 400 with linearly increasing spacings in the range $k_1 \simeq 0.025 \ldots 50.0$ to account for the characteristic behavior of close-to-equilibrium distributions at small and large momenta. All integrals were approximated by Riemann sums on this grid. The system of Boltzmann equations behaves numerically stiff. This means that it is advisable to use an implicit method for its numerical solution to achieve acceptable step sizes (and hence acceptable execution times and numerical errors). Here CVODE with its backward differentiation formula with Newton iteration was used as ODE solver. The full Jacobian was computed analytically in every external step. A relative tolerance of 10^{-8} was attributed to every momentum mode. Due to the implicit method all solutions were computed in $\mathcal{O}(10^3)$ steps.

Since the global systematic error due to the discretization cannot be computed within the method the proper behavior of the system was tested by successive refinement of the grid and comparison of some of the macroscopic quantities with the theory predictions. For this purpose, we present two examples of the number densities n_x, the energy densities ρ_x and the entropy densities for the washout factors $\kappa \simeq 0.366$ (case c in fig. 5.2-5.4) and $\kappa \simeq 0.01$ (case a in fig. 5.6-5.8). The total number density $(n_b + 2n_{\psi_1} + n_{\bar{b}})/s$ is almost conserved (as discussed in section 5). The ratio $(\rho_b + \rho_{\psi_1} + \rho_{\bar{b}})/\rho$ is not constant (see fig. 5.3). This behavior is expected for a system involving non-relativistic massive particles and is also observed for the bottom-up equations. The ratio is much smaller than one so that it is justified to neglect the backreaction on the curvature. Finally,

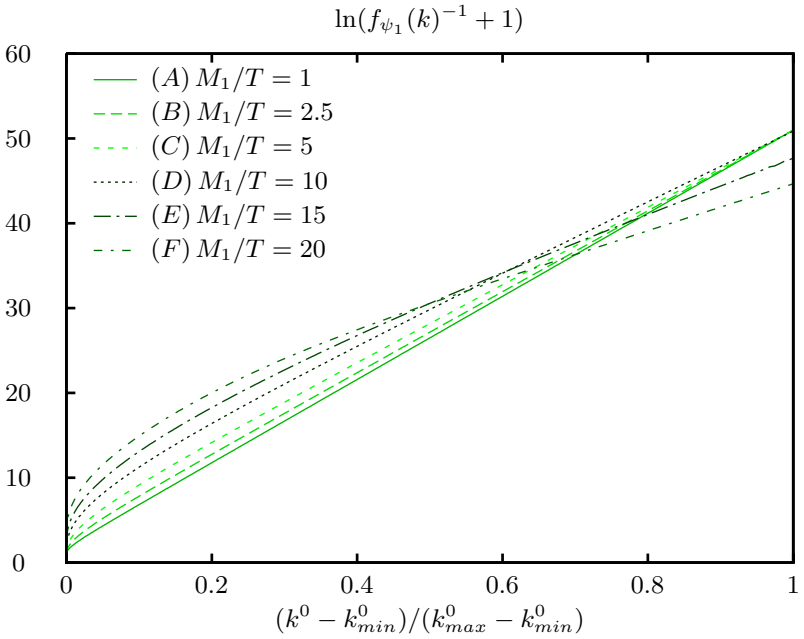

Figure 5.9: Deviation of the distribution function f_{ψ_1} from equilibrium for washout factor $\kappa \simeq 0.01$ (case a).

the total entropy density is steadily increasing as it should. fig. 5.5 and fig. 5.9 show the deviation of the distribution function f_{ψ_1} from kinetic equilibrium ones for which the curves would be straight lines. The deviation from equilibrium is larger for smaller values of κ and increases at late times, as expected.

5.2 Numerical results

We define the generated toy-baryon asymmetry as

$$\eta(m_{\psi_1}/T) = \frac{n_b(m_{\psi_1}/T) - n_{\bar{b}}(m_{\psi_1}/T)}{s(m_{\psi_1}/T)}\,. \tag{5.16}$$

Here n_b and $n_{\bar{b}}$, the number densities of species b and $\bar{b}$ respectively (compare (5.7)), are computed in the presence of the quantum corrected ϵ_1, and s is the standard entropy density [5]. The analogous asymmetry computed with ϵ_1^{vac} is denoted by $\eta^{vac}(m_{\psi_1}/T)$.

Fig. 5.10 shows the numerical value of the ratio $\langle\epsilon_1\rangle/\epsilon_1^{vac}$ for various values of the washout parameter $\kappa \equiv \Gamma/H(m_{\psi_1}) = |g_1|^2 m_{pl}/(4.5\cdot 16\pi\sqrt{g_*}m_{\psi_1}^3)$. The flattening for small m_{ψ_1}/T as compared to the thermal equilibrium result in fig. 3.10 is due to the finite chemical potential of $\bar{b}$. This shows that larger corrections could be obtained if additional interactions for b and $\bar{b}$ are introduced which would allow to start with smaller chemical potentials and hence would lead to a stronger enhancement.

The buildup of the asymmetry with and without quantum corrections as a function of the inverse temperature is depicted in fig. 5.11 and fig. 5.12. Comparing these figures one can verify the enhancement of the asymmetry at intermediate stages for larger washout factors (case d). Note

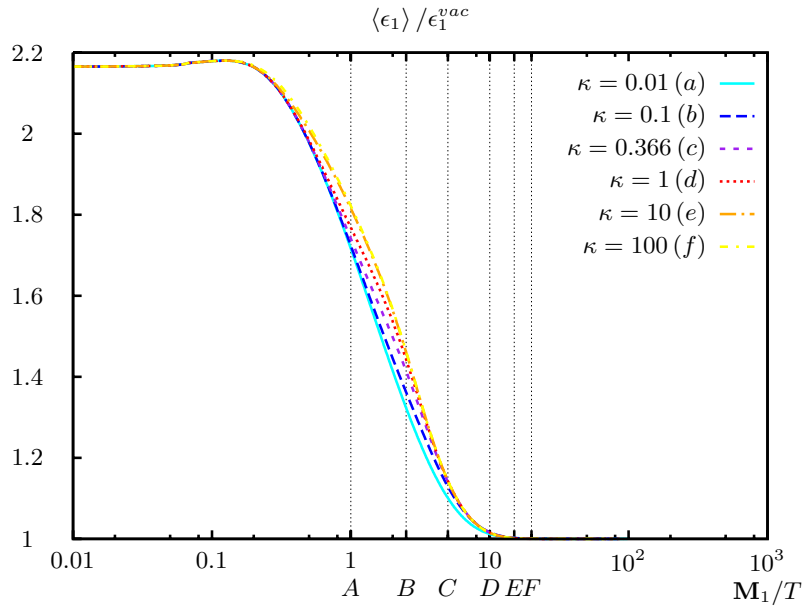

Figure 5.10: The ratio $\langle\epsilon_1\rangle/\epsilon_1^{vac}$. The shape of the curves differs from that of the corresponding graph in fig. 3.10, mainly because its computation involves a finite chemical potential (which depends on m_{ψ_1}/T) here. Similar graphs can be obtained by including a finite chemical potential in eqn. (3.121).

also that due to the medium contribution to the CP-violating parameter the generated asymmetry is not a monotonous function of the washout parameter κ.

The dependence of the resulting final asymmetries $\eta = \eta(m_{\psi_1}/T \to \infty)$ and $\eta^{vac} = \eta^{vac}(m_{\psi_1}/T \to \infty)$ as well as the dependence of the ratio $(\eta - \eta^{vac})/\eta^{vac}$ on the washout parameter is presented in fig. 5.13. The asymmetry is always larger when quantum corrections are taken into account compared to the results without corrections (compare section 3.2.3). The asymmetry η has a maximum for moderate washout factors $\kappa \simeq 0.059$ in contrast to the usual result which has its maximum in the limit of zero washout factor. Our interpretation of this effect is as follows: For large washout factors the enhancement of ϵ_1 due to the quantum corrections enhances the asymmetry generated by the decays only at intermediate stages, because the same processes diminish the asymmetry in particular at late times where the averaged asymmetry drops to smaller values (compare fig. 5.10). For small κ the particles decay late, and the backreaction is largely suppressed so that the washout is ineffective. However the interval of integration in eqn. (3.120) is located at relatively large momenta since the mass increasingly dominates $E_p^{\psi_1}$ as the momenta are red-shifted to smaller values. This means that the integration is over an interval in which the distribution $f^{\bar{b}}$ becomes smaller and smaller. This explains why the quantum corrections tend to zero for small κ. For the same reasons the relative effect of the quantum corrections peaks at a moderate $\kappa \simeq 0.34$ with about 26%. We note again that the size and the sign of the corrections depend on the quantum statistics of the particles in the vertex loop and will be different in a phenomenological scenario.

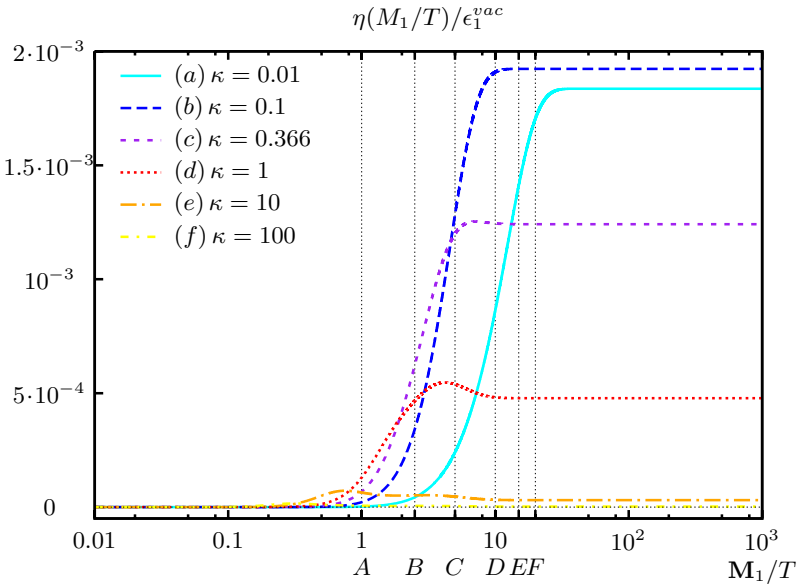

Figure 5.11: The asymmetry $\eta(m_{\psi_1}/T)$ with quantum corrections included. In the weak washout regime (case a) the asymmetry is produced at smaller temperatures and it is not necessarily larger than for larger washout factors (compare a and b).

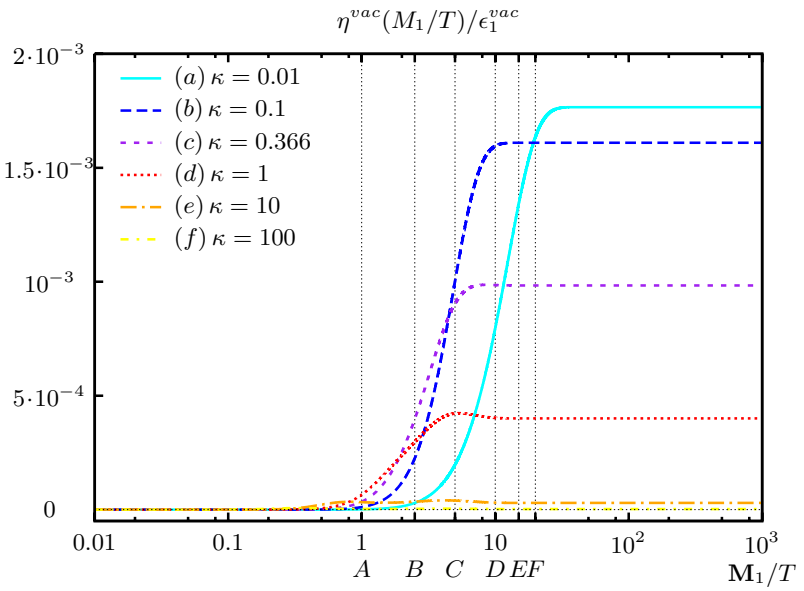

Figure 5.12: The asymmetry $\eta^{vac}(m_{\psi_1}/T)$ without quantum corrections.

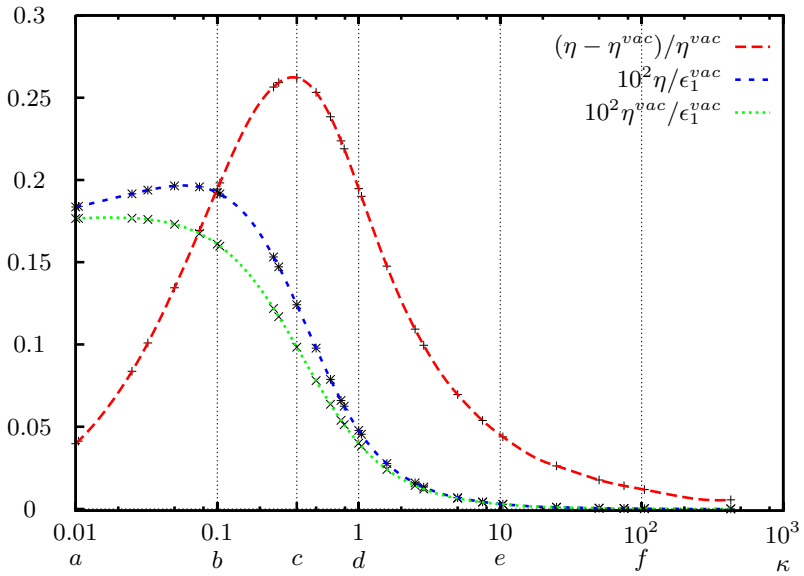

Figure 5.13: The final asymmetries and the ratio $(\eta - \eta^{vac})/\eta^{vac}$ over washout factor κ. The cases a, b, c, d, e, f correspond to washout factors 0.01, 0.1, 0.366, 1, 10, 100. Case c is close to the maximum relative excess of the quantum corrected results at $\kappa \simeq 0.34$. In contrast to the usual results the final asymmetry does not take its maximum value for the smallest washout factor. Instead, the asymmetry η peaks at $\kappa \simeq 0.059$.

Chapter 6

Conclusion

The dynamic generation of the matter-antimatter asymmetry of the universe, which is observed in experiments, is one of the most interesting problems at the intersection of cosmology and particle physics. It can be solved by postulating the existence of some weakly interacting heavy species which undergoes baryon and/or lepton number and CP violating out-of-equilibrium decays in the early universe. The need for a heavy particle candidate and the requirement for a theoretical explanation of the small neutrino masses, the only certain physics beyond the standard model known today, can be satisfied in a unified manner by virtue of the see-saw mechanism. Such extensions result in leptogenesis scenarios in which a $B - L$ asymmetry is generated and then converted to the observed baryon asymmetry.

In this thesis we focused on an aspect which is common to many scenarios of baryogenesis and leptogenesis, namely the kinetic description of the out-of-equilibrium decay scenario. While it is obvious that a top-down derivation is desirable, in which implicit assumptions can be tested, state-of-the-art calculations are essentially still based on the classical bottom-up approach. With respect to quantum effects different issues can arise in different scenarios, such as the case where quasi-degenerate heavy Majorana neutrino masses are assumed or when flavour effects are taken into account. Here we studied a simple toy model consisting of one complex and two real scalar fields, which can be matched to the scenario of (unflavoured) thermal leptogenesis, in the hierarchical regime. First, the model was studied within the bottom-up approach, which is based on generalized Boltzmann equations with S-matrix elements computed in vacuum and parallels the usual discussion for phenomenological theories. The "double-counting problem" in the presence of the quantum statistical terms for blocking or stimulated emission was illuminated in this context.

The same model was then reconsidered in a top-down approach using the Schwinger–Keldysh/ Kadanoff–Baym formalism in a covariant generalization as starting point. This ansatz, based on non-equilibrium quantum field theory, allows for a systematic description and has important advantages in comparison to the bottom-up approach. In particular, the full Kadanoff–Baym equations do not rely on the concept of quasi-particles and their collisions in the plasma. If the quasi-particle picture is applicable, as we have assumed here, the formalism permits to derive a system of "Boltzmann-like" kinetic equations which we refer to as quantum corrected Boltzmann equations. These have two major advantages. Firstly, their structure automatically ensures that no asymmetry is produced in thermal equilibrium i.e. the formalism is free of the "double-counting problem". This means that there is no need for the subtraction of real intermediate states as in the bottom-up approach. Therefore, it answers the question how the quantum statistical terms can be taken into account in a consistent manner. Secondly, they account for the dependence of the quasi-particles'

properties as well as scattering and decay rates on the state of the surrounding medium. It was found that the medium contributions to the CP-violating parameter depend linearly on the particle number densities and that it agrees with the bottom-up result in the vacuum limit. The reason for the linear dependence is that only one of the internal lines in the vertex loop is "thermal". This was apparently in conflict with the results obtained earlier in the framework of thermal field theory by replacing the zero temperature propagators in the computation of the three-point function with their finite temperature equivalents. The thermal field theory approach was then reconsidered in order to reconcile it with the new results from the top-down approach. It turned out that this is in fact possible when so-called causal products are used for the computation of the CP-violating parameter. Thereby it was shown that the conflict was due to an ambiguity in the computation of n-point functions which exists in the real-time formulation of thermal quantum field theory.

It is well-known that there are self-energy and vertex contributions to the CP-violating parameter. Here, we have concentrated on the latter ones. When the ambiguity in thermal quantum field theory is resolved, the medium corrections to the CP-violating parameter, obtained in the top-down approach in the given approximation, can be obtained by a canonical replacement of the equilibrium distribution functions with non-equilibrium ones. We exploited this observation to postulate the form of medium contributions for the self-energy loop. In fact this result is confirmed by the results published in [4] where these contributions are considered in the top-down approach (this applies to the hierarchical case only). By analogy, we were then in the position to conclude which form the medium corrections take for the phenomenological scenario, because the thermal field theory approach differs only by the use of fermionic thermal propagators for the lepton in the loops. Here we assumed that no additional new effects need to be considered when the top-down approach is extended to the phenomenological case. However, currently, this assumption is motivated solely by the concordance between the results obtained in the top-down and bottom-up approaches for the toy model in the given limiting case.

Within the scalar toy model the medium effects increase the CP-violating parameter by up to an order of magnitude. It asymptotically approaches the vacuum value as the temperature decreases. This behaviour is partly due to a Bose-enhancement of the vertex loop correction. If Maxwell–Boltzmann distributions are used in this computation, the corresponding CP-violating parameter increases by a factor two at maximum. Finally an appropriate method for the solution of Boltzmann equations was presented and the system of the quantum corrected Boltzmann equations was solved numerically. Due to the medium corrections to the CP-violating parameter the asymmetry reaches its maximum value at a small but finite value of the washout parameter κ, rather than for $\kappa \to 0$. To avoid the regime of Bose–Einstein-condensation we have to assume that the species have rather large chemical potentials initially. This effectively decreases the medium correction to the CP-violating parameter. In this setup the generated asymmetry differs from its value in the canonical formalism by approximately 26%. In a phenomenological scenario additional interactions keep the chemical potentials close to zero so that the deviation could take larger values.

With respect to the phenomenological scenario the new results exhibit the qualitative difference that the medium corrections do not vanish (in the ultra-relativistic limit) as was the case for the literature results. For this reason such contributions are exceeded by different thermal effects in the state-of-the-art calculations. This situation could change now so that it will be interesting to study it numerically. Additionally, the thermal masses can also consistently be described within the Kadanoff–Baym formalism. As, so far, only the case of an approximately symmetric background medium has been studied in the top-down approach it will be interesting to investigate the influence of a nonzero asymmetry on the medium corrections to the CP-violating parameter. Moreover, it

will be very interesting to study the quantitative effects of the modified Boltzmann equations for the quasi-degenerate case obtained in [4] for an intermediate regime of the mass degeneracy. This case corresponds to the interesting scenario of resonant leptogenesis. In the extremely degenerate case, where the mass-splitting is comparable to the decay width, it turned out that the quasi-particle approximation cannot be applied. Especially then it will be interesting to investigate the full set of Kadanoff–Baym equations numerically without further approximations as some of their properties cannot be included in Boltzmann-like equations for principle reasons.

Acknowledgements

At this place I like to express my gratitude to all those who have contributed to the success of my Ph.D. studies.

First of all, I wish to thank Prof. Dr. Manfred Lindner, who welcomed me as Ph.D. student in his group at the Max-Planck-Institute for Nuclear Physics and who supervised this work. It was supported by the "Sonderforschungsbereich" TR27.

Since it is almost impossible to list all people who I have met during these times, as fellows and friends, and who have contributed indirectly to this work, I shall not make the mistake to try it. Let me just underline the major ones. Markus Michael Müller who awakened my interest in non-equilibrium aspects of leptogenesis during the time of my diploma-thesis. Most notably there are Alexander Kartavtsev and Mathias Garny who began to share this interest in the subject and contributed significantly to the important publications which this work is based upon. Furthermore, they did proofread large parts of this thesis (not the acknowledgements, in case I make mistakes as I allways do). Michael Schmidt, Claudia Hagedorn and Thomas Schwetz-Mangold and all the other fellows who shared their office with me or who I have met in private.

Then I like to express my gratitude to my family and to my friends.

Ludwig Boltzmann, in case you wonder, developed together with James Clerk Maxwell the celebrated Boltzmann equation in order to prove the existence of fundamental constituents of matter (atoms). In the absence of computers, it must have seemed impossible to derive observable consequences at first, thus the argument remained incomplete. Presumable after a lot of hard work (done by Boltzmann and maybe Maxwell), Maxwell then found a solution ("Put $n = 5$"). This might explain Boltzmann's euphoric sentence. Solving the Boltzmann equation for arbitrary interactions in its full generality (numerically) is still a major problem.

Appendix A

Kadanoff–Baym formalism for complex scalars

In this appendix, we derive the Kadanoff–Baym and quantum corrected Boltzmann equations for the complex scalar field. It is included for the readers convenience and follows quite closely the presentation given in [3] which generalizes the one of section 3.1 for the scalar φ^4-theory. Results from [65, 69, 70, 76, 77, 109, 110] are employed.

Schwinger–Dyson equation

Again, the starting point is the generating functional for Green's functions:

$$\mathcal{Z}[J,K] = \int \mathscr{D}b\mathscr{D}\bar{b}\exp[i(S + J\bar{b} + \bar{J}b + \bar{b}Kb)]\,. \tag{A.1}$$

The fields and external sources are defined on the the positive and negative branches of the Schwinger-Keldysh closed real-time contour shown in fig. 3.1. As before we suppress branch-indices. The compact notation of for contour integrals over the closed real-time path is used and the scalar products of the local and bi-local sources $J(x)$ and $K(x,y)$ and the fields are defined as invariant configuration space integrals, see eqn. (3.4). In contrast to the previous case the sources are now complex functions. The requirement that the last term in eqn. (A.1) must be real implies that $K(x,y) = K^*(y,x)$. We work in covariant notation which is implicit in the path-integral measures and in $\mathscr{D}^4z$.

The generating functional for connected Green's functions is given by

$$\mathcal{W}[J,K] = -i\ln\mathcal{Z}[J,K]\,. \tag{A.2}$$

and the functional derivatives with respect to the external sources read

$$\frac{\partial\mathcal{W}[J,K]}{\partial J(x)} = \bar{b}(x)\,, \quad \frac{\partial\mathcal{W}[J,K]}{\partial K(x,y)} = \frac{1}{2}\big[D(y,x) + \bar{b}(x)B(y)\big]\,, \tag{A.3}$$

where B and D denote the expectation value and the propagator of the field respectively. The derivative of $\mathcal{W}$ with respect to $\bar{J}$ is just the complex conjugate of (A.3).

The 2PI effective action is again obtained by a functional Legendre transform of the generating functional for connected Green's functions $\mathcal{W}$:

$$\Gamma[D,B] \equiv \mathcal{W}[J,K] - J\bar{b} - \bar{J}B - \mathrm{Tr}[KD] - \bar{b}KB. \tag{A.4}$$

One finds for the functional derivatives of the effective action, with help of the chain-rule:

$$\frac{\delta\Gamma[D,B]}{\delta\bar{b}(x)} = -J(x) - \int \mathscr{D}^4 z\, K(x,z)B(z)\,, \tag{A.5a}$$

$$\frac{\delta\Gamma[D,B]}{\delta D(x,y)} = -K(y,x)\,. \tag{A.5b}$$

Next, we shift the complex field by its expectation value $b \to b + B$. Exploiting the invariance of the path integral measure under this transformations, the effective action can be rewritten in the form

$$\Gamma[D,B] = -\,i\ln\int \mathscr{D}b\mathscr{D}\bar{b}\exp[i(S + \bar{J}b + J\bar{b} + \bar{b}Kb)] + S_{cl}[B] - \mathrm{Tr}[KD]\,. \tag{A.6}$$

Now, we tentatively write the effective action in the form

$$\Gamma[D,B] \equiv S_{cl}[B] + i\ln\det\left[D^{-1}\right] + i\,\mathrm{Tr}\left[\mathscr{D}^{-1}D\right] + \Gamma_2[D,B]\,, \tag{A.7}$$

which defines the 2PI functional Γ_2.

The third term on the right-hand side of eqn. (A.7) is given by a convolution of the field propagator D and the free inverse propagator $\mathscr{D}^{-1}$. Its differentiation with respect to $D(y,x)$ gives

$$\mathscr{D}^{-1}(x,y) = i(\Box_x + m_b^2)\,\delta^g(x,y)\,. \tag{A.8}$$

The definition of the generalized Dirac-delta $\delta^g(x,y)$ can be found in section 3.1. The functional derivative of the second term on the right-hand side of eqn. (A.7) is given by $-iD^{-1}(y,x)$ which be obtained upon use of

$$\int \mathscr{D}^4 z\, D^{-1}(x,z)D(z,y) = \delta^g(x,y)\,. \tag{A.9}$$

Therefore, we find

$$\begin{aligned}\frac{\delta\Gamma[D,B]}{\delta D(x,y)} &= -\,iD^{-1}(y,x) + i\,\mathscr{D}^{-1}(y,x) + \frac{\delta\Gamma_2[D,B]}{\delta D(x,y)} \\ &= -\,K(y,x)\,.\end{aligned} \tag{A.10}$$

We are interested in physical situations which correspond to vanishing sources. To be precise, within non-equilibrium field theory, this is only true for times $x^0, y^0 > t_{init}$. The local and bi-local sources supported at $x^0 = y^0 = t_{init}$ formally encode the information about the (Gaussian) initial state, see e.g. [78]. However, these sources do not appear explicitly in the Kadanoff-Baym equations, and therefore we omit them here. It follows that eqn. (A.10) can be rewritten in the form

$$D^{-1}(x,y) = \mathscr{D}^{-1}(x,y) - \Sigma(x,y)\,, \tag{A.11}$$

where the self-energy is defined in complete analogy to eqn. (3.27) by

$$\Sigma(x,y) \equiv i\frac{\delta\Gamma_2[D,B]}{\delta D(y,x)}\,. \tag{A.12}$$

Note that the factor two in the definition of the self-energy is absent.

Kadanoff–Baym equations

Convolving the Schwinger–Dyson eqn. (A.11) with D from the right and using eqn. (A.9), we obtain

$$i[\Box_x + m_b^2]D(x,y) = \delta^g(x,y) + \int \mathscr{D}^4 z\, \Sigma(x,z)D(z,y)\,. \tag{A.13}$$

Next, following the usual procedure, we represent the time-ordered propagator as a linear combination of the statistical propagator and spectral function:

$$D(x,y) = D_F(x,y) - \frac{i}{2}\mathrm{sgn}_{\mathcal{C}}(x^0 - y^0)D_\rho(x,y)\,, \tag{A.14}$$

where $\mathrm{sgn}_{\mathcal{C}}$ denotes the signum function with respect to time-ordering along the closed time path, and

$$D_F(x,y) \equiv \frac{1}{2}\langle[b(x),\bar{b}(y)]_+\rangle\,, \tag{A.15a}$$

$$D_\rho(x,y) \equiv i\langle[b(x),\bar{b}(y)]_-\rangle\,. \tag{A.15b}$$

To find out how D_F and D_ρ behave under complex conjugation let us introduce

$$D_>(x,y) \equiv \langle b(x)\bar{b}(y)\rangle = \mathrm{Tr}[\mathscr{P}\, b(x)\bar{b}(y)]\,, \tag{A.16a}$$

$$D_<(x,y) \equiv \langle \bar{b}(y)b(x)\rangle = \mathrm{Tr}[\mathscr{P}\, \bar{b}(y)b(x)]\,. \tag{A.16b}$$

Using the Hermiticity of the density matrix $\mathscr{P}$ and the cyclic invariance of the trace, we obtain

$$D_>^*(x,y) = D_>(y,x), \quad D_<^*(x,y) = D_<(y,x)\,. \tag{A.17}$$

Consequently

$$D_F^*(x,y) = D_F(y,x), \quad D_\rho^*(x,y) = -D_\rho(y,x)\,. \tag{A.18}$$

Analogous relations also hold for the spectral and statistical components of the self-energy.

The local part of the self-energy is proportional to the Dirac-delta and can be absorbed in the effective mass of the field, $m_b^2(x) \equiv m_b^2 + \Sigma^{loc}(x,x)$, whereas the remaining part of the self-energy can be split into a spectral part Σ_ρ and a statistical part Σ_F in a complete analogy to eqn. (A.14).

Because of the sgn-function, the action of the Laplace–Beltrami operator on eqn. (A.14) gives rise to the product $g^{00}\delta(x^0,y^0)\nabla_0^x D_\rho(x,y)$. Upon use of the definition of the spectral function and canonical commutation relations for a complex scalar field this product reduces to the generalized Dirac-delta $\delta^g(x,y)$, which cancels the Dirac-delta on the right-hand side of eqn. (A.13).

Separating spectral and statistical components in eqn. (A.13), we obtain the system of Kadanoff–Baym equations:

$$\big[\Box_x + m_b^2(x)\big]D_F(x,y) = \int_0^{y^0} \mathscr{D}^4 z\, \Sigma_F(x,z)D_\rho(z,y) - \int_0^{x^0} \mathscr{D}^4 z\, \Sigma_\rho(x,z)D_F(z,y), \tag{A.19a}$$

$$\big[\Box_x + m_b^2(x)\big]D_\rho(x,y) = \int_{x^0}^{y^0} \mathscr{D}^4 z\, \Sigma_\rho(x,z)D_\rho(z,y)\,. \tag{A.19b}$$

It is very similar to that for the real scalar field, see section 3.1. An important difference is that the functions in eqns. (A.19a) and (A.19b) are complex. This means that one gets four equations for the real and imaginary components of the spectral function and the statistical propagator.

Quantum kinetic equations

The Kadanoff–Baym equation (for the statistical propagator and the spectral function) can be rewritten in terms of advanced and retarded propagators, D_R and D_A:

$$\begin{aligned}\left[\Box_x + m_b^2(x)\right] D_{F(\rho)}(x,y) &= \\ &= -\int \mathscr{D}^4 z \theta(z^0)\left[\Sigma_{F(\rho)}(x,z) D_A(z,y) + \Sigma_R(x,z) D_{F(\rho)}(z,y)\right].\end{aligned} \tag{A.20}$$

Because of (A.18), the retarded and advanced propagators are related by

$$D_R(x,y) \equiv \theta(x^0 - y^0) D_\rho(x,y) = -\theta(x^0 - y^0) D_\rho^*(y,x) = D_A^*(y,x)\,. \tag{A.21}$$

Interchanging x and y in (A.20) and performing a complex conjugation of the resulting equation, we find

$$\begin{aligned}\left[\Box_y + m_b^2(y)\right] D_{F(\rho)}(x,y) &= \\ &= -\int \mathscr{D}^4 z \theta(z^0)\left[D_R(x,z) \Sigma_{F(\rho)}(z,y) + D_{F(\rho)}(x,z) \Sigma_A(z,y)\right].\end{aligned} \tag{A.22}$$

The sum of original eqn. (A.20) and transformed eqn. (A.22) is referred to as constraint equation while the difference is the quantum kinetic equation. Since the latter has been obtained from the former by reversible transformations, a solution of eqn. (A.20) is also a solution of eqn. (A.22) and hence of the constraint and quantum kinetic equations.

For the reasons given in section 3.1, it is convenient to introduce the covariantly generalized (see section 3.1) center and relative coordinates, X and s. In terms of these coordinates eqns. (A.18) can be rewritten in the form

$$D_F^*(X,s) = D_F(X,-s), \quad D_\rho^*(X,s) = -D_\rho(X,-s)\,.$$

The Winger transforms of the spectral function and statistical propagator are defined, as before, by:

$$D_F(X,p) = \sqrt{-g}_X \int d^4 s\, e^{ips} D_F(X,s)\,, \tag{A.23a}$$

$$D_\rho(X,p) = -i\sqrt{-g}_X \int d^4 s\, e^{ips} D_\rho(X,s)\,. \tag{A.23b}$$

Consequently, the Wigner transformed statistical propagator and spectral function are again real-valued functions. The Wigner transforms of the retarded and advanced propagators are defined analogously. From eqn. (A.21) it then follows that the relation

$$D_A(X,p) = D_R^*(X,p) \tag{A.24}$$

between the advanced and retarded components also holds for a complex scalar field. Combining eqns. (A.21) and (A.23) and using $\theta(s^0) + \theta(-s^0) = 1$ one finds:

$$D_R(X,p) - D_A(X,p) = i D_\rho(X,p)\,. \tag{A.25}$$

Equations (A.24) and (A.25) imply, that

$$D_{R(A)}(X,p) = D_h(X,p) \pm \frac{i}{2} D_\rho(X,p), \tag{A.26}$$

where $D_h(X,p) \equiv \Re\{D_R(X,p)\}$ has been introduced. An analogous relation holds for the retarded and advanced self-energies.

As announced, by subtracting eqn. (A.22) from eqn. (A.20) and Wigner transforming both sides of the result we obtain the quantum kinetic equations. In addition, we need to send the initial time to the infinite past, $t_{init} \to -\infty$, which means that we drop the functions $\theta(z^0)$ on the right-hand sides of eqns. (A.20) and (A.22), and to perform a gradient expansion with respect to X. Proceeding as in section 3.1, in particular dropping terms beyond the linear order in the gradients, we obtain a kinetic equation for the spectral function.

$$\{\omega(X,p), D_\rho(X,p)\}_{PB} = \{\Sigma_\rho(X,p), D_h(X,p)\}_{PB}, \tag{A.27}$$

where we have introduced

$$\omega(X,p) \equiv g^{\mu\nu} p_\mu p_\nu - m_b^2(X) - \Sigma_h(X,p)\,, \tag{A.28}$$

and the Poisson brackets are as in eqn. (3.63).

Wigner-transforming the sum of eqns. (A.22) and (A.20), we obtain the constraint equation for the spectral function. To linear order in the gradients it is an algebraic equation:

$$\omega(X,p) D_\rho(X,p) = \Sigma_\rho(X,p) D_h(X,p)\,. \tag{A.29}$$

To close the system and to analyze the spectrum, we also need the equations for the retarded and advanced propagators. They can be obtained from (A.20) and (A.22) upon use of the definitions of D_R and D_A and the canonical commutation relations:

$$[\Box_x + m_b^2(x)] D_{R(A)}(x,y) = \delta^g(x,y) - \int \mathscr{D}^4 z\, \Sigma_{R(A)}(x,z) D_{R(A)}(z,y)\,, \tag{A.30}$$

$$[\Box_y + m_b^2(y)] D_{A(R)}(x,y) = \delta^g(x,y) - \int \mathscr{D}^4 z\, D_{A(R)}(x,z) \Sigma_{A(R)}(z,y)\,. \tag{A.31}$$

Wigner-transforming the difference of eqns. (A.30) and (A.31) and subtracting eqn. (A.27), we obtain the kinetic equation for real part of the retarded and advanced propagators:

$$\{\omega(X,p), D_h(X,p)\}_{PB} = -\frac{1}{4}\{\Sigma_\rho(X,p), D_\rho(X,p)\}_{PB}\,. \tag{A.32}$$

Wigner-transforming the sum of eqns. (A.30) and (A.31) and subtracting eqn. (A.29), we obtain the second constraint equation:

$$\omega(X,p) D_h(X,p) = -1 - \frac{1}{4}\Sigma_\rho(X,p) D_\rho(X,p)\,. \tag{A.33}$$

The solution of the system of constraint eqns. (A.29) and (A.33) reads

$$D_\rho(X,p) = \frac{-\Sigma_\rho(X,p)}{\omega^2(X,p) + \frac{1}{4}\Sigma_\rho^2(X,p)}\,, \tag{A.34a}$$

$$D_h(X,p) = \frac{\omega(X,p)}{\Sigma_\rho(X,p)} D_\rho(X,p)\,. \tag{A.34b}$$

As can be checked by substitution, solution (A.34) is also solution of the kinetic eqns. (A.27) and (A.32). In other words, to linear order in the gradients we have analytic expressions for the spectral function and retarded (advanced) propagators. The spectral function has a sharp peak on the mass shell, i.e. for $\omega(X,p)=0$. The height and exact shape of the peak are time-dependent.

Proceeding in a similar way, we can derive the kinetic and the constraint equations for the statistical propagator:

$$\begin{aligned}\{\omega(X,p),D_F(X,p)\}_{PB} = &\{\Sigma_F(X,p),D_h(X,p)\}_{PB}\\ &+D_F(X,p)\Sigma_\rho(X,p)-\Sigma_F(X,p)D_\rho(X,p)\,,\end{aligned} \tag{A.35}$$

$$\begin{aligned}\omega(X,p)D_F(X,p) =&\frac{1}{4}\{\Sigma_F(X,p),D_\rho(X,p)\}_{PB}\\ &+\frac{1}{4}\{D_F(X,p),\Sigma_\rho(X,p)\}_{PB}+\Sigma_F(X,p)D_h(X,p)\,.\end{aligned} \tag{A.36}$$

The constraint equation is no longer algebraic and can not be solved analytically in general. However, if the system is in thermal equilibrium, then all the quantities are constant in time and space and the Poisson brackets in (A.36) vanish identically. The solution of the resulting equation reads

$$D_F^{eq}(p)=\frac{\Sigma_F(p)}{\Sigma_\rho(p)}D_\rho^{eq}(p)\,. \tag{A.37}$$

That is, we have obtained the fluctuation-dissipation relation from the constraint eqn. (A.36). As can be checked by substitution, in equilibrium (A.37) is indeed a solution of (A.35). Furthermore, using (A.14) and the KMS periodicity condition we find [78]

$$D_F^{eq}(p)=\left[f^{b,eq}(p)+\frac{1}{2}\right]D_\rho^{eq}(p)\,, \tag{A.38}$$

where $f^{b,eq}$ denotes the Bose–Einstein distribution function.

Boltzmann kinetic equations

Neglecting the Poisson brackets on the right-hand side of (A.35), we obtain the Boltzmann equation for the statistical propagator:

$$p^\alpha\mathcal{D}_\alpha D_F(X,p)=\frac{1}{2}\big[D_F(X,p)\Sigma_\rho(X,p)-\Sigma_F(X,p)D_\rho(X,p)\big]\,. \tag{A.39}$$

Motivated by the fluctuation-dissipation relation (A.38), we trade the statistical propagator for the one-particle number density:

$$D_F(X,p)=\left[f^b(X,p)+\frac{1}{2}\right]D_\rho(X,p)\,. \tag{A.40}$$

By the same arguments as those given in section 3.1, we can also apply the quasi-particle approximation:

$$D_\rho(X,p)=2\pi\,\mathrm{sgn}(p_0)\,\delta\left(g_{\mu\nu}p^\mu p^\nu-m_b^2\right)\,. \tag{A.41}$$

We can then rewrite eqn. (A.39) as an equation for the phase-space distribution function $f^b(X,p)$:

$$[p^\alpha \mathcal{D}_\alpha f^b(X,p)] D_\rho(X,p) = \frac{1}{2}\big[\Sigma_>(X,p) D_<(X,p) - D_>(X,p)\Sigma_<(X,p)\big]\,,$$

where we have introduced

$$D_{\gtrless}(X,p) = D_F(X,p) \pm \frac{1}{2} D_\rho(X,p)\,. \tag{A.42}$$

eqn. (A.42) is very similar to the Boltzmann equation for a real scalar field in section 3.1. There is, however, an important difference. For negative values of p_0 the distribution function f^b describes anti-particles:

$$f^b(X,-p) \equiv -[f^{\bar{b}}(X,p) + 1]\,. \tag{A.43}$$

In other words, eqn. (A.42) describes the time evolution of both particles and anti-particles. One can obtain an explicit equation for $f^{\bar{b}}$ by changing the sign of p_0:

$$[p^\alpha \mathcal{D}_\alpha f^{\bar{b}}(X,p)] D_\rho(X,p) = \frac{1}{2}\big[\bar{\Sigma}_>(X,p) \bar{D}_<(X,p) - \bar{D}_>(X,p)\bar{\Sigma}_<(X,p)\big]\,,$$

where we have introduced $\bar{\Sigma}_{\gtrless}(X,p) \equiv \Sigma_{\lessgtr}(X,-p)$ and taken into account that in the quasi-particle approximation $D_\rho(X,-p) = -D_\rho(X,p)$.

Appendix B

Calculation of the self-energies

The 2PI effective action is given by the sum of all 2PI diagrams with vertices as given by the interaction lagrangian and internal lines representing the complete connected propagators [78]. The structure of the terms of the effective action can be read off the diagrams in fig. 3.6:

$$i\Gamma_2^{(a)} = -\frac{i}{2}\lambda \int_x D^2(x,x)\,, \tag{B.1a}$$

$$i\Gamma_2^{(b)} = -\frac{1}{8}\lambda^2 \int_{xy} D^2(x,y)D^2(y,x)\,, \tag{B.1b}$$

$$i\Gamma_2^{(c)} = -\frac{1}{4}\, g_m g_n^* \int_{xy} G^{mn}(x,y)D^2(x,y) - \frac{1}{4}\, g_m^* g_n \int_{xy} G^{mn}(x,y)D^2(y,x)\,, \tag{B.1c}$$

$$i\Gamma_2^{(d)} = \frac{1}{4} g_i g_j g_m^* g_n^* \int_{xyvu} G^{ij}(x,y)G^{mn}(v,u)D(y,v)D(x,v)D(y,u)D(x,u)\,, \tag{B.1d}$$

where, to shorten the notation, we have introduced

$$\int_{x_1 \ldots x_n} \equiv \int \mathscr{D}^4 x_1 \ldots \mathscr{D}^4 x_n\,.$$

The self-energies of the complex scalar field are obtained by functional differentiation of the effective action with respect to the two-point correlation function:

$$\Sigma(x,y) \equiv i\frac{\delta\Gamma_2[D,G]}{\delta D(y,x)}\,. \tag{B.2}$$

Differentiating the individual contributions to the effective action, we obtain

$$\Sigma^{(a)}(x,y) = -i\delta^g(x,y)\lambda D(x,x)\,, \tag{B.3a}$$

$$\Sigma^{(b)}(x,y) = -\frac{1}{2}\lambda^2 D^2(x,y)D(y,x)\,, \tag{B.3b}$$

$$\Sigma^{(c)}(x,y) = -g_i g_j^* G^{ij}(y,x)D(y,x)\,, \tag{B.3c}$$

$$\Sigma^{(d)}(x,y) = g_i g_j g_m^* g_n^* \int_{vu} G^{mn}(x,v)G^{ij}(y,u)D(y,v)D(u,v)D(u,x)\,. \tag{B.3d}$$

The components of the self-energy of the system of real scalar fields are obtained upon functional differentiation of the effective action with respect to the components of the correlation function:

$$\Pi^{ij}(x,y) \equiv 2i\frac{\delta\Gamma_2[D,G]}{\delta G^{ji}(y,x)}\,. \tag{B.4}$$

The result of the differentiation reads

$$\Pi^{(c)}_{ij}(x,y) = -\frac{1}{2} g_i g_j^* D^2(x,y) - \frac{1}{2} g_i^* g_j D^2(y,x)\,, \tag{B.5a}$$

$$\Pi^{(d)}_{ij}(x,y) = \frac{1}{2}\int_{vu} G^{mn}(v,u)\big[g_i g_j g_m^* g_n^* D(x,v)D(x,u)D(y,v)D(y,u) + \\ + g_i^* g_j^* g_m g_n D(v,x)D(u,x)D(v,y)D(u,y)\big]\,. \tag{B.5b}$$

The next step is to derive the spectral and statistical components of the self-energies eqns. (B.3) and (B.5). Upon use of the decomposition (A.14) and of the analogous decomposition of the propagators of the real scalar field, one easily obtains a corresponding decomposition of the self-energies $\Sigma^{(b)}$, $\Sigma^{(c)}$ and $\Pi^{(c)}$ into the statistical and spectral components. Linear combinations of the resulting expressions are presented in eqns. (3.98a), (3.98b), and (3.99a). The calculation of the spectral and statistical components of $\Sigma^{(d)}$ and $\Pi^{(d)}$, which contain two integrations over space-time, is more involved (see also [75]). Decomposing the two-point correlation functions in eqn. (B.3d) into the statistical and spectral components, we get 32 terms. Each of the terms must be integrated over the closed time path $\mathcal{C}$. It is useful to use relations like

$$\int_{\mathcal{C}} du^0\, \mathrm{sgn}_{\mathcal{C}}(x^0-u^0)\,\mathrm{sgn}_{\mathcal{C}}(u^0-y^0)\, D_\rho(x,u)D_\rho(u,y) = \\ = 2\,\mathrm{sgn}_{\mathcal{C}}(x^0-y^0)\int_{y^0}^{x^0} du^0\, D_\rho(x,u)D_\rho(u,y)\,. \tag{B.6}$$

One then finds that ten terms vanish upon integration over the contour: one term which does not contain any $\mathrm{sgn}_{\mathcal{C}}$ functions; five terms which contain only one $\mathrm{sgn}_{\mathcal{C}}$ function; two terms which contain a product of two $\mathrm{sgn}_{\mathcal{C}}$ functions both depending only on one of the integration variables, u or v; and finally two terms which contain a product of three $\mathrm{sgn}_{\mathcal{C}}$ functions but depend only on one of the "external" arguments, x or y. For the remaining terms the integration over the contour

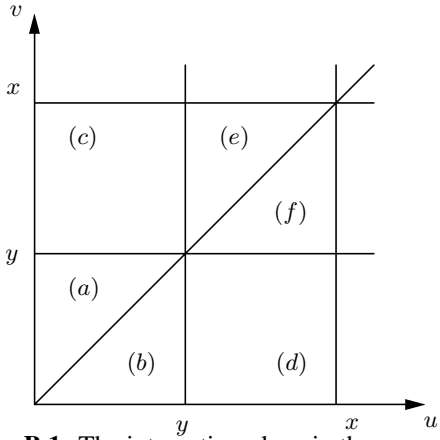

Figure B.1: The integration plane in the case $x^0 > y^0$.

$\mathcal{C}$ reduces to a "single time" integration over a combination of the six regions in fig. B.1. Note that the upper limits of the integration never exceed the largest time argument (x^0 in fig. B.1) which ensures the causality of the Kadanoff–Baym equations. In most cases integration over a part of the uv plane can be easily represented as integration over the whole plane, $0 < u, v < \infty$, if two of the spectral functions are replaced by the corresponding retarded and (or) advanced propagators. There are, however, two exceptions: if the resulting integral is only over region (e) or region (f)

in fig. B.1. Using the identities

$$\int_{(e)} = \int_{(a+c+e)} + \int_{(b)} - \int_{(a+b+c)} , \tag{B.7a}$$

$$\int_{(f)} = \int_{(b+d+f)} + \int_{(a)} - \int_{(a+b+d)} , \tag{B.7b}$$

and the definitions of the retarded and advanced propagators, we can represent the corresponding contributions as combinations of integrals over the whole uv plane. Collecting all the terms, we obtain expressions presented in eqns. (3.98c) and (3.99b).

Wigner transformation

To calculate the self-energies entering the Boltzmann equations, we have to Wigner-transform products of several two-point functions. Using the definitions (A.23), we obtain for the Wigner-transform of a product of n functions of the same arguments, see eqn. (3.57):

$$f_1(x,y)\dots f_n(x,y) \to \int d\Pi^4_{p_1}\dots d\Pi^4_{p_n}(2\pi)^4\delta^g(p-p_1-\dots p_n)f(X,p_1)\dots f(X,p_n)\,. \tag{B.8}$$

Equation (B.8) allows us to Wigner-transform the self-energies (3.98a), (3.98b) and (3.99a). The self-energy (3.98c) has a more complicated structure:

$$f(x,y) = \int_{vu} f_1(y,v)f_2(u,v)f_3(u,x)f_4(y,u)f_5(x,v)\,. \tag{B.9}$$

We will now calculate the Wigner-transform of eqn. (B.9) in the Boltzmann approximation. That is, in each f_n we will neglect the deviation of the corresponding center coordinate from $X \equiv X_{xy}$. For instance:

$$f_1(y,v) \to f_1(X_{yv}, s_{yv}) \to f_1(X_{xy}, s_{yv})\,. \tag{B.10}$$

In this approximation the integration over u and v induces two conditions on the momenta: $p_v = p_u = 0$, where $p_u = p_2 + p_3 - p_4$ and $p_v = p_1 + p_2 + p_5$. Integration over the relative coordinate s, see eqn. (A.23a), induces an additional constraint: $p = p_s$, where $p_s = \frac{1}{2}(p_5 - p_4 - p_3 - p_1)$. Thus, in the Boltzmann approximation the Wigner transform of eqn. (B.9) takes the form:

$$\begin{aligned} f(X,p) = \int d\Pi^4_{p_1}\dots\, d\Pi^4_{p_5}(2\pi)^4\delta^g(p_u)(2\pi)^4\delta^g(p_v) \\ \times(2\pi)^4\delta^g(p-p_s)\, f_1(X,p_1)\dots\, f_5(X,p_5) \end{aligned} \tag{B.11}$$

As far as decays are concerned, two of the momenta in eqn. (B.11) correspond to the initial and final states, whereas three of the momenta correspond to the internal lines of the loop. The Dirac Dirac-deltas in eqn. (B.11) ensure conservation of four-momentum in each vertex of the loop.

The self-energy (3.99b) has the structure

$$f(x,y) = \int_{vu} f_1(v,u)f_2(x,v)f_3(x,u)f_4(y,v)f_5(y,u)\,. \tag{B.12}$$

Proceeding in the same way, we again obtain eqn. (B.11) but now with $p_v = p_1 - p_2 - p_4$, $p_u = p_1 + p_3 + p_5$ and $p_s = \frac{1}{2}(p_2 + p_3 - p_4 - p_5)$. This completes the calculation of the Winger-transforms of the self-energies.

Appendix C

Generalized optical theorem and cutting rules

The generalized optical theorem is a direct consequence of the unitarity of the S-matrix (i.e. it expresses the conservation of probability) [61, 111]. It can be generalized to unstable particles by means of the Cutkosky cutting rules for the computation of the discontinuities of Feynman graphs [61].

$$-i\Big[\mathcal{M}_{a\to b}(\{k_i\},\{p_i\}) - \mathcal{M}^*_{b\to a}(\{p_i\},\{k_i\})\Big] = \\ = \sum_i \left(\prod_{i_l}\int d\Pi_{i_l}\right)(2\pi)^4\delta^{(4)}(\sum_j k_j - \sum_{i_l} p_{i_l})\mathcal{M}_{a\to i}(\{k_i\},\{q_{i_l}\})\mathcal{M}^*_{b\to i}(\{p_i\},\{q_{i_l}\}) \tag{C.1}$$

The amplitudes $\mathcal{M}_{a\to b}$ include all contributing diagrams (at a given order of perturbation theory) and the sum on the right-hand side is over all possible *real* intermediate states i which contribute to $\mathcal{M}_{a\to b}$. The intermediate state momenta are integrated over their invariant phase space.

The generalized optical theorem can also be seen as a consequence of the Cutkosky cutting rules [112–114] for the computation of the imaginary part of the diagrams in the perturbative expansion.

(i) Cut through the diagram in all possible ways such that the cut propagators can simultaneously be put on shell.

(ii) For each cut, replace $1/(p^2 - m^2 + i\epsilon) \to -2\pi i\Theta(p_0)\delta(p^2 - m^2)$ in each cut propagator, then perform the loop integrals.

(iii) Sum the contributions of all possible cuts.

With certain restrictions, related to the notion of cutting [99], the Cutkosky rules can be generalized to thermal quantum field theory. Due to the second degree of freedom in RTF in general a large number of diagrams, with different types of the vertices, has to be taken into account. Different formulas have been derived to reduce the number of relevant diagrams by performing sums partially by using the "largest/smallest time equation" eqn. (4.16).

In [96] a formula for the absorptive (imaginary) part of the amplitude was derived. Starting from eqn. (4.16) one can derive the "circling relation"

$$\sum_{\text{circling } x_i, z_j} F_{\gtrless}(x_1, \ldots, x_n; z_j) = \sum_{\text{circling } x_i} \mathcal{F}(x_1, \ldots, x_n; z_j) = 0\,, \tag{C.2}$$

since there is always a vertex with largest time component. From the circling rules it can be shown that the complex conjugate of a function $F_<$ with all external vertices uncircled and a fixed set of internal vertices circled is just $F_>$ with all external vertices and the conjugate set of internal vertices circled:

$$F_<(x_1, \ldots, x_n; z_j, \underline{z}_k) = F_>(\underline{x}_1, \ldots, \underline{x}_n; \underline{z}_j, z_k)\,. \tag{C.3}$$

Assuming that the KMS boundary condition holds we have the relations

$$\begin{aligned} F_<(x_1, \ldots, x_n; z_j, \underline{z}_k) &= F_>(x_1, \ldots, x_n; \underline{z}_j, z_k)\,, \\ F_<(\underline{x}_1, \ldots, \underline{x}_n; z_j, \underline{z}_k) &= F_>(\underline{x}_1, \ldots, \underline{x}_n; \underline{z}_j, z_k)\,. \end{aligned} \tag{C.4}$$

With help of eqn. (C.3) one finds

$$\begin{aligned} \Im\{i^{-1}\mathcal{F}(x_1, \ldots, x_n; z_j)\} &= \frac{1}{2i}\Big(\{i^{-1}\mathcal{F}(x_1, \ldots, x_n; z_j)\} - \{i^{-1}\mathcal{F}(x_1, \ldots, x_n; z_j)\}^*\Big) \\ &= \frac{1}{2i}\Big(i^{-1}\sum_{\text{circling } z_j} F_<(x_1, \ldots, x_n; z_j) + i^{-1}\Big(\sum_{\text{circling } z_j} F_<(x_1, \ldots, x_n; z_j)\Big)^*\Big) \\ &= -\frac{1}{2}\Big(\sum_{\text{circling } z_j} F_<(x_1, \ldots, x_n; z_j) + \sum_{\text{circling } z_j} F_>(\underline{x}_1, \ldots, \underline{x}_n; z_j)\Big)\,. \end{aligned}$$

To this one can add $1/(2)$ times the sum in eqn. (C.2) without changing anything:

$$\begin{aligned} \Im\{i^{-1}\mathcal{F}(x_1, \ldots, x_n; z_j)\} =& \frac{1}{2}\sum_{\text{circling } (x_i), z_j} F_<(x_1, \ldots, x_n; z_j) \\ & \frac{1}{2}\sum_{\text{circling } z_j} F_<(\underline{x}_1, \ldots, \underline{x}_n; z_j) - \frac{1}{2}\sum_{\text{circling } z_j} F_>(\underline{x}_1, \ldots, \underline{x}_n; z_j)\,, \end{aligned}$$

where the brackets indicate that in this sum either none or all of x_i are circled. The last two terms in this equation cancel due to eqn. (C.4). We arrive at the final result

$$\Im\{i^{-1}\mathcal{F}(x_1, \ldots, x_n; z_j)\} = \frac{1}{2}\sum_{\text{circling } (x_i), z_j} F_<(x_1, \ldots, x_n; z_j)\,.$$

Appendix D

Reduction of the collision integral

In order to be able to perform the integration of the collision integral accurately and effectively it is necessary to perform the angular integration analytically. Omitting the superscripts denoting the particle species[1] in we can write a collision integral for $2-2$ scattering as (see eqn. (2.12)):

$$\begin{aligned} C^{kp\leftrightarrow qr}[f](k) &= \frac{1}{2E_k}\int (2\pi)^4\delta(E_k+E_p-E_q-E_r)\delta^3(\mathbf{k}+\mathbf{p}-\mathbf{q}-\mathbf{r})\,|\mathcal{M}|^2 \\ &\quad \times F^{kp\leftrightarrow qr}[f]\,\frac{d^3p}{(2\pi)^3 2E_p}\frac{d^3q}{(2\pi)^3 2E_q}\frac{d^3r}{(2\pi)^3 2E_r}\,, \end{aligned} \tag{D.1}$$

where we have introduced

$$F^{kp\leftrightarrow qr}[f] = (1-\xi^k f_k)(1-\xi^p f_p)f_q f_r - f_k f_p(1-\xi^q f_q)(1-\xi^r f_r)\,. \tag{D.2}$$

We write the 3-dimensional Dirac-delta as the Fourier transform of unity and switch to spherical coordinates:

$$\delta^3(\mathbf{k}+\mathbf{p}-\mathbf{q}-\mathbf{r}) = \int e^{i\lambda(\mathbf{k}+\mathbf{p}-\mathbf{q}-\mathbf{r})}\frac{d^3\lambda}{(2\pi)^3}\,,$$

The collision term eqn. (D.1) then becomes

$$C^{kp\leftrightarrow qr}[f](k) = \frac{1}{64\pi^3 E_k}\int \delta(E_k+E_p-E_q-E_r)F^{kp\leftrightarrow qr}[f]\,D(k,p,q,r)\frac{p\,dp}{E_p}\frac{q\,dq}{E_q}\frac{r\,dr}{E_r}\,. \tag{D.3}$$

Here D was defined as

$$\begin{aligned} D(k,p,q,r) &= D^{kp\leftrightarrow qr}(k,p,q,r) \\ &= \frac{pqr}{8\pi^2}\int d\Omega_p\int d\Omega_q\int d\Omega_r\;\delta^3(\mathbf{k}+\mathbf{p}-\mathbf{q}-\mathbf{r})\,|\mathcal{M}|^2 \\ &= \frac{pqr}{64\pi^5}\int \lambda^2\,d\lambda\int e^{i\lambda\mathbf{k}}\,d\Omega_\lambda\int e^{i\lambda\mathbf{p}}\,d\Omega_p\int e^{-i\lambda\mathbf{q}}\,d\Omega_q\int e^{-i\lambda\mathbf{r}}\,d\Omega_r\,|\mathcal{M}|^2\,. \end{aligned} \tag{D.4}$$

Note, that this definition renders $D(k,p,q,r)$ a dimensionless quantity. Due to the presence of the Dirac-delta we expect that the result is non-zero only if $q+r>|k-p|$ and $k+p>|q-r|$,

[1] From here on we will always use the momenta k, p, q and r in connection with only one particle species, such that it serves as a label for the species at the same time. We also use the convention $v=|\mathbf{v}|$ to denote the modulus of the three-momenta.

because the equation $\mathbf{k}+\mathbf{p}=\mathbf{q}+\mathbf{r}$ does not have a solution otherwise, for whatever combination of the solid angles Ω_p, Ω_q, Ω_r. Therefore, the result will be proportional to

$$\begin{aligned}\Theta\left(k,p,q,r\right) &\equiv \Theta(q+r-|k-p|)\,\Theta(k+p-|q-r|)\\ &= \Theta(\min\left(k+p,q+r\right)-\max\left(|k-p|\,,|q-r|\right))\,. \end{aligned} \tag{D.5}$$

After computing $D(k,p,q,r)$ we can proceed with the integration of the remaining energy Dirac-delta in eqn. (D.3):

$$C^{kp\leftrightarrow qr}[f](k)=\frac{1}{64\pi^3 E_k}\int\int\Theta(E_p-m_p)F[f]D(k,p,q,r)\frac{q\,dq}{E_q}\frac{r\,dr}{E_r}\,, \tag{D.6}$$

where $p=\sqrt{E_p^2-m_p^2}$ with $E_p=E_q+E_r-E_k$ is given by energy conservation. The Heaviside-function prevents integration over combinations of q and r which are kinematically forbidden. Note, that the choice to integrate eqn. (D.3) over p is not unique. The integration over q and r leads to analytically equivalent expressions for C.

Thus, the collision integral is reduced to a two-dimensional one, suitable for numerical integration. However, all the work is now hidden in the definition of $D=D(k,p,q,r)$ which is characteristic for the scattering model, i.e. for the matrix element of the underlying theory for the scattering process under consideration.

The computation of D is easily carried out for matrix elements squared with simple angular dependence such as the constant ($|\mathcal{M}|^2=\text{const}$), for matrix elements in the Fermi approximation ($|\mathcal{M}|^2\propto(k\cdot p)(q\cdot r),(k\cdot p)$, including re-namings of the momenta therein) and for resonant processes in the narrow width approximation ($|\mathcal{M}|^2\propto\delta(s-m_X^2)$, where m_X is the mass of the particle in the intermediate state).

In general, the spin averaged matrix element $|\mathcal{M}|^2$ will depend on Lorentz-invariant combinations of the four-momenta of the in- and outgoing particles, usually the Mandelstam variables s, t, u,

$$\begin{aligned} s &= (k+p)^2\,,\\ t &= (k-q)^2=m_k^2+m_q^2-2E_kE_q+2\,|\mathbf{k}|\,|\mathbf{q}|\cos\left(\theta_{kq}\right)\,,\\ u &= (k-r)^2=m_k^2+m_r^2-2E_kE_r+2\,|\mathbf{k}|\,|\mathbf{r}|\cos\left(\theta_{kr}\right)\,. \end{aligned} \tag{D.7}$$

In the following we take t and u as the two independent variables and s is expressed by

$$s=\sum_{i=k,p,q,r}m_i^2\;-t-u\,. \tag{D.8}$$

In [1] it has been shown that D can be written as

$$D(k,p,q,r)=\frac{qr}{\pi}\int_A\frac{|\mathcal{M}|^2}{\sqrt{F(\theta_q,\theta_r)}}\,d\cos\theta_{\mathbf{q}}\,d\cos\theta_{\mathbf{r}}\,, \tag{D.9}$$

with

$$\begin{aligned} &F(\theta_q,\theta_r) \;=\\ &\quad=(2qr\sin\theta_{\mathbf{q}}\sin\theta_{\mathbf{r}})^2-\left[(k-q\cos\theta_{\mathbf{q}}-r\cos\theta_{\mathbf{r}})^2+(q\sin\theta_{\mathbf{q}})^2+(r\sin\theta_{\mathbf{r}})^2-p^2\right]^2\,. \end{aligned} \tag{D.10}$$

The domain of integration A is given by $-1 \leq \cos\theta_q,\ \cos\theta_r \leq 1$ and $F(\theta_q, \theta_r) > 0$.

The expression (D.9) for D has only a two-dimensional integral and is by far superior to the original expression with respect to numerical integration. The integrand may have singular points at the boundary of A. Hence the routines for numerical integration must be chosen adequately. Usually, for a numerical method, it is sufficient to know $D(k, p = \sqrt{(E_q + E_r - E_k)^2 - m_p^2}, q, r)$ for a finite set of momenta $\{k_i, q_j, r_l\}$ on a grid. Therefore it is possible, in principle, to tabulate D through numerical integration of eqn. (D.9). For applications in cosmology, this relation is only of restricted use, since the momenta or, equivalently, the particle masses are scaled in each step of the time evolution, so that the values of $D(k_i, p, q_j, r_l)$ need to be recomputed permanently.

In order to evaluate eqn. (D.4) in a numerical efficient way, one can expand $|\mathcal{M}|^2$ in terms of $\cos(\theta_{kq})$ and $\cos(\theta_{kr})$:

$$|\mathcal{M}|^2 = \sum_{n=0}^{\infty}\sum_{m=0}^{\infty} A_{nm} (\cos\theta_{kq})^n (\cos\theta_{kr})^m \ , \tag{D.11}$$

Note that the coefficients A_{nm} can depend on the magnitudes of the momenta. Upon integration of eqn. (D.4) we can then write

$$D(k, p, q, r) = \sum_{n=0}^{\infty}\sum_{m=0}^{\infty} A_{nm}(k, p, q, r) D^{nm}(k, p, q, r) \, , \tag{D.12}$$

assuming that the series converges for all relevant k, p, q and r (the momenta are still restricted by energy conservation).

In order to give a meaning to eqn. (D.12) we need to compute the integral

$$D^{nm}(k, p, q, r) \quad = \quad \frac{pqr}{8\pi^2} \int d\Omega_p \int d\Omega_q \int d\Omega_r \ \delta^3(\mathbf{k} + \mathbf{p} - \mathbf{q} - \mathbf{r}) (\cos\theta_{kq})^n (\cos\theta_{kr})^m \, . \tag{D.13}$$

In [1] it has been shown, that the results for $D^{nm}(k, p, q, r)$ can always be written in the form

$$D^{n,m}(k, p, q, r) = A \frac{\Theta(k, p, q, r)}{k^{n+m+1} q^n r^m} \left(B_1 R_1 + B_2 R_2 + B_3 R_3 + C\right) . \tag{D.14}$$

A is a numeric prefactor. The coefficients B_i and C are multivariate polynomials in the momenta k, p, q, r.

$$\begin{aligned} & c_1 = k + p - q - r, \quad c_2 = k - p + q - r, \quad c_3 = k - p - q + r \\ & \text{and} \quad R_1 = R(c_1), \quad R_2 = R(c_2), \quad R_3 = R(c_3) \, , \end{aligned} \tag{D.15}$$

where $R(x) = x\Theta(x)$ is the ramp function. D^{nm} with $n \leq m$ ($D^{n,m}$ with $n > m$ can be derived from $D^{m,n}$ by interchanging q and r. The expressions B_2 (B_3) are found by substituting in B_1 the term c_1 by c_2 (c_3) and f_i by ${f_i}^{q\to -q}$ (${f_i}^{r\to -r}$) for all i.

For the lowest orders the coefficients are given by:

$$D^{0,0}(k, p, q, r) : \tag{D.16}$$

$$A = 1/2\,,\ C = 2\,k\,,$$
$$B_1 = -1\,,$$

$$D^{0,1}(k,p,q,r): \tag{D.17}$$
$$A = -1/12\,,\ C = -4\,k^3\,,$$
$$B_1 = f_2 c_1 - {c_1}^2 + f_1\,,$$
$$[\ f_1 = 6\,kr, f_2 = 3\,k - 3\,r]$$

$$D^{0,2}(k,p,q,r): \tag{D.18}$$
$$A = \frac{1}{120}\,,\ C = 8\,k^3\big(2\,k^2 + 5\,r^2\big)\,,$$
$$B_1 = f_2 c_1 + f_3 {c_1}^2 + f_4 {c_1}^3 - 3\,{c_1}^4 + f_1\,,$$
$$[\ f_1 = -60\,k^2 r^2, f_2 = -60\,kr\big(k - r\big), f_3 = -20\,r^2 - 20\,k^2 + 60\,kr, f_4 = -15\,r + 15\,k]$$

$$D^{1,1}(k,p,q,r): \tag{D.19}$$
$$A = \frac{1}{120}\,,\ C = 4\,k^3\big(3\,k^2 + 5\,p^2 - 5\,q^2 - 5\,r^2\big)\,,$$
$$B_1 = f_2 c_1 + f_3 {c_1}^2 + f_4 {c_1}^3 - {c_1}^4 + f_1\,,$$
$$[\ f_1 = -60\,k^2 qr, f_2 = -30\,k\big(-2\,qr + kq + kr\big), f_3 = 20\,kq + 20\,kr - 20\,qr - 10\,k^2,$$
$$f_4 = -5\,q - 5\,r + 5\,k]$$

For the numerical computations in this thesis only the lowest order coefficients for $D^{0,0}$ were needed needed. Some higher-order D^{nm}'s can be found in [1].

Bibliography

[1] A. Hohenegger, *Solving the homogeneous Boltzmann equation with arbitrary scattering kernel*, Phys. Rev. D **79** (2009), no. 6, 063502, 0806.3098.

[2] A. Hohenegger, A. Kartavtsev, and M. Lindner, *Deriving Boltzmann Equations from Kadanoff-Baym Equations in Curved Space-Time*, Phys. Rev. D **78** (2008), no. 8, 085027, 0807.4551.

[3] M. Garny, A. Hohenegger, A. Kartavtsev, and M. Lindner, *Systematic approach to leptogenesis in nonequilibrium QFT: vertex contribution to the CP-violating parameter*, Phys. Rev. D **80** (2009), 125027, .

[4] M. Garny, A. Hohenegger, A. Kartavtsev, and M. Lindner, *Systematic approach to leptogenesis in nonequilibrium QFT: self-energy contribution to the CP-violating parameter*, in preparation, 2009.

[5] E. W. Kolb and M. S. Turner, *The Early Universe*, Addison-Wesley, Redwood City, CA, 1990.

[6] G. Steigman, *Big bang nucleosynthesis: Probing the first 20 minutes*, (2003), astro-ph/0307244.

[7] P. D. Serpico et al., *Nuclear Reaction Network for Primordial Nucleosynthesis: A Detailed Analysis of Rates, Uncertainties and Light Nuclei Yields*, Journal of Cosmology and Astroparticle Physics **0412** (2004), 010, astro-ph/0408076.

[8] WMAP, G. Hinshaw et al., *Five-Year Wilkinson Microwave Anisotropy Probe (WMAP) Observations: Data Processing, Sky Maps, & Basic Results*, Astrophys. J. Suppl. **180** (2009), 225–245, 0803.0732.

[9] WMAP, E. Komatsu et al., *Five-Year Wilkinson Microwave Anisotropy Probe (WMAP) Observations: Cosmological Interpretation*, Astrophys. J. Suppl. **180** (2009), 330–376, 0803.0547.

[10] A. D. Sakharov, *Violation of CP invariance, C asymmetry, and baryon asymmetry of the universe*, Pisma Zh. Eksp. Teor. Fiz. **5** (1967), 32–35.

[11] M. Fukugita and T. Yanagida, *Barygenesis without grand unification*, Physics Letters B **174** (1986), no. 1, 45–47.

[12] G. 't Hooft, *Symmetry breaking through Bell-Jackiw anomalies*, Phys. Rev. Lett. **37** (1976), 8–11.

[13] V. A. Kuzmin, V. A. Rubakov, and M. E. Shaposhnikov, *On the anomalous electroweak baryon number nonconservation in the early universe*, Phys. Lett. B **155** (1985), 36.

[14] S. Davidson, E. Nardi, and Y. Nir, *Leptogenesis*, Physics Reports **466** (2008), no. 4-5, 105–177, 0802.2962.

[15] M. A. Luty, *Baryogenesis via leptogenesis*, Phys. Rev. D **45** (1992), no. 2, 455–465.

[16] E. Nardi, Y. Nir, E. Roulet, and J. Racker, *The importance of flavor in leptogenesis*, Journal of High Energy Physics **01** (2006), 164–164, hep-ph/0601084.

[17] R. Barbieri, P. Creminelli, A. Strumia, and N. Tetradis, *Baryogenesis through leptogenesis*, Nucl. Phys. B **575** (2000), 61–77, hep-ph/9911315.

[18] A. Abada et al., *Flavour matters in leptogenesis*, Journal of High Energy Physics **09** (2006), 010, hep-ph/0605281.

[19] S. Blanchet and P. Di Bari, *Flavor effects on leptogenesis predictions*, Journal of Cosmology and Astroparticle Physics **0703** (2007), 018, hep-ph/0607330.

[20] A. Pilaftsis, *CP violation and baryogenesis due to heavy Majorana neutrinos*, Phys. Rev. D **56** (1997), no. 9, 5431–5451, hep-ph/9707235.

[21] A. Pilaftsis and T. E. J. Underwood, *Resonant leptogenesis*, Nucl. Phys. B **692** (2004), 303–345, hep-ph/0309342.

[22] A. Pilaftsis and T. E. J. Underwood, *Electroweak-scale resonant leptogenesis*, Phys. Rev. D **72** (2005), no. 11, 113001, hep-ph/0506107.

[23] A. De Simone and A. Riotto, *On Resonant Leptogenesis*, Journal of Cosmology and Astroparticle Physics **0708** (2007), 013, 0705.2183.

[24] A. De Simone, *Quantum Boltzmann equations in resonant leptogenesis*, (2008), 0805.2354.

[25] J. Bernstein, *Kinetic Theory in the Expanding Universe*, Cambridge University Press, Cambridge [u.a.], 1988.

[26] S. R. de Groot, W. A. van Leeuwen, and C. G. van Weert, *Relativistic Kinetic Theory*, North-Holland Publ. Comp., Amsterdam, 1980.

[27] C. Cercignani and G. M. Kremer, *The Relativistic Boltzmann Equation: Theory and Applications*, Birkhäuser, Basel, Boston, 2002.

[28] R. L. Liboff, *Kinetic Theory*, 3. ed., Springer, New York, 2003.

[29] M. Escobedo, S. Mischler, and M. A. Valle, *Homogeneous Boltzmann Equation in Quantum Relativistic Kinetic Theory*, Texas State University, Department of Mathematics, 2003.

[30] D. Benedetto, F. Castella, R. Esposito, and M. Pulvirenti, *A short review on the derivation of the nonlinear quantum Boltzmann equations*, Commun. Math. Sci. **suppl. 1** (2007), 55–7.

[31] L. Erdös, M. Salmhofer, and H.-T. Yau, *On the Quantum Boltzmann Equation*, Journal of Statistical Physics **116** (2004), 367–380.

[32] L. P. Kadanoff and G. Baym, *Quantum Statistical Mechanics*, Benjamin, New York, 1962.

[33] J. Berges, *Controlled nonperturbative dynamics of quantum fields out of equilibrium*, Nucl. Phys. A **699** (2002), 847–886, hep-ph/0105311.

[34] G. Aarts and J. Berges, *Nonequilibrium time evolution of the spectral function in quantum field theory*, Phys. Rev. D **64** (2001), 105010, hep-ph/0103049.

[35] M. Lindner and M. M. Müller, *Comparison of Boltzmann Equations with Quantum Dynamics for Scalar Fields*, Phys. Rev. D **73** (2006), 125002, hep-ph/0512147.

[36] M. Lindner and M. M. Müller, *Comparison of Boltzmann Kinetics with Quantum Dynamics for a Chiral Yukawa Model Far From Equilibrium*, Phys. Rev. D **77** (2008), 025027, 0710.2917.

[37] J. Berges, S. Borsanyi, and C. Wetterich, *Isotropization far from equilibrium*, Nucl. Phys. B **727** (2005), 244, hep-ph/0505182.

[38] S. Juchem, W. Cassing, and C. Greiner, *Nonequilibrium quantum-field dynamics and off-shell transport for ϕ^4-theory in 2+1 dimensions*, Nucl. Phys. A **743** (2004), 92–126, nucl-th/0401046.

[39] W. Buchmüller and S. Fredenhagen, *Quantum mechanics of baryogenesis*, Phys. Lett. B **483** (2000), no. 1-3, 217–224, hep-ph/0004145.

[40] A. De Simone and A. Riotto, *Quantum Boltzmann Equations and Leptogenesis*, Journal of Cosmology and Astroparticle Physics **0708** (2007), 002, hep-ph/0703175.

[41] E. Calzetta and B. L. Hu, *Closed Time Path Functional Formalism in Curved Space- Time: Application to Cosmological Back Reaction Problems*, Phys. Rev. D **35** (1987), 495.

[42] E. Calzetta, S. Habib, and B. L. Hu, *Quantum kinetic field theory in curved space-time: covariant Wigner function and Liouville-Vlasov equation*, Phys. Rev. D **37** (1988), 2901.

[43] S. A. Ramsey and B. L. Hu, *O(N) quantum fields in curved spacetime*, Phys. Rev. D **56** (1997), 661–677, gr-qc/9706001.

[44] A. Tranberg, *Quantum field thermalization in expanding backgrounds*, Journal of High Energy Physics **11** (2008), 037, 0806.3158.

[45] A. Anisimov, W. Buchmüller, M. Drewes, and S. Mendizabal, *Nonequilibrium Dynamics of Scalar Fields in a Thermal Bath*, Annals of Physics **324** (2008), no. 6, 1234–1260, 0812.1934.

[46] L. Covi, N. Rius, E. Roulet, and F. Vissani, *Finite temperature effects on CP-violating asymmetries*, Phys. Rev. D **57** (1998), no. 1, 93–99, hep-ph/9704366.

[47] G. F. Giudice, A. Notari, M. Raidal, A. Riotto, and A. Strumia, *Towards a complete theory of thermal leptogenesis in the SM and MSSM*, Nucl. Phys. B **685** (2004), no. 1-3, 89 – 149, hep-ph/0310123.

[48] O. Adriani et al., *A new measurement of the antiproton-to-proton flux ratio up to 100 GeV in the cosmic radiation*, Phys. Rev. Lett. **102** (2009), 051101, 0810.4994.

[49] A. G. Cohen, A. De Rujula, and S. L. Glashow, *A matter-antimatter universe?*, Astrophys. J. **495** (1998), 539–549, astro-ph/9707087.

[50] WMAP, D. N. Spergel et al., *Three-Year Wilkinson Microwave Anisotropy Probe (WMAP) Observations: Implications for Cosmology*, The Astrophysical Journal Supplement Series **170** (2007), no. 2, 377–408, astro-ph/0603449.

[51] A. D. Sakharov, *Violation of CP Invariance, C Asymmetry, and Baryon Asymmetry of the Universe*, Soviet Physics Journal of Experimental and Theoretical Physics (JETP) **5** (1967), 24–27.

[52] G. 't Hooft, *Symmetry Breaking Through Bell-Jackiw Anomalies*, Phys. Rev. Lett. **37** (1976), 8–11.

[53] A. Riotto and M. Trodden, *Recent progress in baryogenesis*, Annual Review of Nuclear and Particle Science **49** (1999), no. 1, 35–75, hep-ph/9901362.

[54] G. C. Branco, R. Gonzalez Felipe, F. R. Joaquim, and M. N. Rebelo, *Leptogenesis, CP violation and neutrino data: What can we learn?*, Nucl. Phys. B **640** (2002), 202–232, hep-ph/0202030.

[55] B. Kayser, *Neutrino mass, mixing, and flavor change*, (2002), hep-ph/0211134.

[56] L. Covi, E. Roulet, and F. Vissani, *CP violating decays in leptogenesis scenarios*, Phys. Lett. B **384** (1996), no. 1-4, 169–174, hep-ph/9605319.

[57] W. Buchmüller, R. D. Peccei, and T. Yanagida, *Leptogenesis as the origin of matter*, Annual Review of Nuclear and Particle Science **55** (2005), no. 1, 311–355, hep-ph/0502169.

[58] W. Buchmüller, P. Di Bari, and M. Plümacher, *Cosmic microwave background, matter-antimatter asymmetry and neutrino masses*, Nucl. Phys. B **643** (2002), 367–390, hep-ph/0205349.

[59] E. K. Akhmedov, M. Frigerio, and A. Y. Smirnov, *Probing the seesaw mechanism with neutrino data and leptogenesis*, Journal of High Energy Physics **09** (2003), 021, hep-ph/0305322.

[60] A. Kartavtsev and D. Besak, *Baryogenesis via Leptogenesis in an inhomogeneous Universe*, Phys. Rev. D **78** (2008), 083001, 0803.2729.

[61] M. E. Peskin and D. V. Schroeder, *An Introduction to Quantum Field Theory*, Perseus Books, Reading, USA, 1995.

[62] E. W. Kolb and S. Wolfram, *Baryon number generation in the early universe*, Nucl. Phys. B **172** (1980), 224–284.

[63] G. 't Hooft and M. Veltman, *Scalar one-loop integrals*, Nucl. Phys. B **153** (1979), 365–401.

[64] G. J. van Oldenborgh and J. A. M. Vermaseren, *New algorithms for one-loop integrals*, Zeitschrift für Physik C Particles and Fields **46** (1990), 425–437.

[65] P. Danielewicz, *Quantum Theory of Nonequilibrium Processes. 1*, Annals of Physics **152** (1984), 239–304.

[66] Y. B. Ivanov, J. Knoll, and D. N. Voskresensky, *Resonance Transport and Kinetic Entropy*, Nucl. Phys. **A672** (2000), 313–356, nucl-th/9905028.

[67] J. Knoll, Y. B. Ivanov, and D. N. Voskresensky, *Exact Conservation Laws of the Gradient Expanded Kadanoff-Baym Equations*, Annals of Physics **293** (2001), 126–146, nucl-th/0102044.

[68] J.-P. Blaizot and E. Iancu, *The quark-gluon plasma: Collective dynamics and hard thermal loops*, Physics Reports **359** (2002), no. 5-6, 355–528, hep-ph/0101103.

[69] J. S. Schwinger, *Brownian motion of a quantum oscillator*, Journal of Mathematical Physics **2** (1961), 407–432.

[70] L. V. Keldysh, *Diagram technique for nonequilibrium processes*, Zh. Eksp. Teor. Fiz. **47** (1964), 1515–1527.

[71] M. Basler, *Functional methods for arbitrary densities in curved space-time*, Fortschr. Phys. **41** (1993), 1–43.

[72] D. J. Toms, *Functional measure for quantum field theory in curved spacetime*, Phys. Rev. D **35** (1987), no. 12, 3796–3803.

[73] S. Weinstock, *Boltzmann collision term*, Phys. Rev. D **73** (2006), no. 2, 025005, hep-ph/0510417.

[74] F. Fillion-Gourdeau, J.-S. Gagnon, and S. Jeon, *All orders Boltzmann collision term from the multiple scattering expansion of the self-energy*, Phys. Rev. D **74** (2006), 025010, hep-ph/0603212.

[75] M. E. Carrington and S. Mrowczynski, *Transport theory beyond binary collisions*, Phys. Rev. D **71** (2005), no. 6, 065007.

[76] K. Chou, Z. Su, B. Hao, and L. Yu, *Equilibrium and Nonequilibrium Formalisms Made Unified*, Physics Reports **118** (1985), 1.

[77] J. M. Cornwall, R. Jackiw, and E. Tomboulis, *Effective action for composite operators*, Phys. Rev. D **10** (1974), no. 8, 2428–2445.

[78] J. Berges, *Introduction to nonequilibrium quantum field theory*, AIP Conf. Proc. **739** (2005), 3–62, hep-ph/0409233.

[79] C. J. Isham, *Twisted Quantum Fields in a Curved Space-Time*, Proceedings of the Royal Society of London. Series A, Mathematical and Physical Sciences **362** (1978), no. 1710, 383–404.

[80] L. D. Landau and E. M. Lifshitz, *Course of Theoretical Physics 2: The Field Theory*, Pergamon Press, Oxford, 1981.

[81] J. Berges and S. Borsanyi, *Nonequilibrium quantum fields from first principles*, Eur. Phys. J. **A29** (2006), 95, hep-th/0512010.

[82] H. van Hees and J. Knoll, *Renormalization in self-consistent approximations schemes at finite temperature. I: Theory*, Phys. Rev. **D65** (2001), 025010, hep-ph/0107200.

[83] J.-P. Blaizot, E. Iancu, and U. Reinosa, *Renormalizability of Phi-derivable approximations in scalar ϕ^4 theory*, Phys. Lett. **B568** (2003), 160–166, hep-ph/0301201.

[84] J. Berges, S. Borsanyi, U. Reinosa, and J. Serreau, *Nonperturbative renormalization for 2PI effective action techniques*, Annals of Physics **320** (2005), 344–398, hep-ph/0503240.

[85] A. Arrizabalaga, J. Smit, and A. Tranberg, *Equilibration in ϕ^4 theory in 3+1 dimensions*, Phys. Rev. **D72** (2005), 025014, hep-ph/0503287.

[86] S. Borsanyi and U. Reinosa, *Renormalised nonequilibrium quantum field theory: scalar fields*, (2008), 0809.0496.

[87] M. Garny and M. M. Müller, *Kadanoff-Baym Equations with Non-Gaussian Initial Conditions: The Equilibrium Limit*, (2009), 0904.3600.

[88] P. Danielewicz, *Quantum theory of nonequilibrium processes. II. Application to nuclear collisions*, Annals of Physics **152** (1984), 305–326.

[89] J. Berges and J. Cox, *Thermalization of quantum fields from time-reversal invariant evolution equations*, Phys. Lett. **B517** (2001), 369–374, hep-ph/0006160.

[90] G. Aarts and J. Berges, *Classical aspects of quantum fields far from equilibrium*, Phys. Rev. Lett. **88** (2002), 041603, hep-ph/0107129.

[91] J. Berges, S. Borsanyi, and J. Serreau, *Thermalization of Fermionic Quantum Fields*, Nucl. Phys. **B660** (2003), 51–80, hep-ph/0212404.

[92] S. Juchem, W. Cassing, and C. Greiner, *Quantum dynamics and thermalization for out-of-equilibrium ϕ^4-theory*, Phys. Rev. **D69** (2004), 025006, hep-ph/0307353.

[93] J. Winter, *Wigner transformation in curved space-time and the curvature correction of the Vlasov equation for semiclassical gravitating systems*, Phys. Rev. D **32** (1985), no. 8, 1871–1888.

[94] J. Bernstein, *The Physics of Phase Space*, Springer–Verlag, Berlin, 1987.

[95] J. Berges and S. Borsanyi, *Range of validity of transport equations*, Phys. Rev. **D74** (2006), 045022, hep-ph/0512155.

[96] R. L. Kobes and G. W. Semenoff, *Discontinuities of green functions in field theory at finite temperature and density*, Nucl. Phys. B **260** (1985), no. 3-4, 714 – 746.

[97] R. L. Kobes and G. W. Semenoff, *Discontinuities of green functions in field theory at finite temperature and density (II)*, Nucl. Phys. B **272** (1986), no. 2, 329 – 364.

[98] P. F. Bedaque, A. K. Das, and S. Naik, *Cutting rules at finite temperature*, Mod. Phys. Lett. A **12** (1997), 2481–2496, hep-ph/9603325.

[99] F. Gelis, *Cutting rules in the real-time formalisms at finite temperature*, Nucl. Phys. B **508** (1997), 483–505, hep-ph/9701410.

[100] R. J. Rivers, *Path Integral Methods in Quantum Field Theory*, Cambridge University Press, 1988.

[101] R. Kobes, *Correspondence between imaginary-time and real-time finite-temperature field theory*, Phys. Rev. D **42** (1990), no. 2, 562–572.

[102] R. Kobes, *Retarded functions, dispersion relations, and Cutkosky rules at zero and finite temperature*, Phys. Rev. D **43** (1991), no. 4, 1269–1282.

[103] M. A. van Eijck and C. G. van Weert, *Finite-temperature retarded and advanced Green functions*, Physics Letters B **278** (1992), no. 3, 305 – 310.

[104] L. Covi, N. Rius, E. Roulet, and F. Vissani, *Finite temperature effects on CP violating asymmetries*, Phys. Rev. **D57** (1998), 93–99, hep-ph/9704366.

[105] A. Basbøll and S. Hannestad, *Decay of heavy Majorana neutrinos studied using the full Boltzmann equation, including its implications for leptogenesis*, Journal of Cosmology and Astroparticle Physics **2007** (2007), no. 0701, 003 hep-ph/0609025.

[106] F. Hahn-Woernle, M. Plümacher, and Y. Y. Y. Wong, *Full Boltzmann equations for leptogenesis including scattering*, (2009), 0907.0205.

[107] J. Garayoa, S. Pastor, T. Pinto, N. Rius, and O. Vives, *On the full Boltzmann equations for Leptogenesis* 0905.4834.

[108] R. Mehrem, J. T. Londergan, and M. H. Macfarlane, *Analytic Expressions for Integrals of Products of Spherical Bessel Functions*, Journal of Physics A: Mathematical and General **24** (1991), no. 7, 1435–1453.

[109] P. M. Bakshi and K. T. Mahanthappa, *Expectation Value Formalism in Quantum Field Theory I and II*, Journal of Mathematical Physics **4** (1963), 1–16.

[110] E. Calzetta and B. L. Hu, *Nonequilibrium Quantum Fields: Closed Time Path Effective Action, Wigner Function and Boltzmann Equation*, Phys. Rev. **D37** (1988), 2878.

[111] S. Weinberg, *The Quantum Theory of Fields*, vol. 1, Cambridge Univ. Press, Cambridge [u.a.], 1995.

[112] R. E. Cutkosky, *Singularities and Discontinuities of Feynman Amplitudes*, Journal of Mathematical Physics **1** (1960), no. 5, 429–433.

[113] R. J. Eden, P. V. Landshoff, D. I. Olive, and J. C. Polkinghorne, *The Analytic S-Matrix*, Cambridge University Press, 2002.

[114] M. Le Bellac, *Quantum and Statistical Field Theory*, Oxford University Press, 1992.